



MEASUREMENT OF PURE LIQUID MOLAR HEAT CAPACITIES USING A DUAL PURPOSE DIFFERENTIAL FLOW CALORIMETER

By

WELCOME TSHUMA

BEng. (Honours) Chemical

National University of Science and Technology

This dissertation is in fulfillment of the academic requirements for the degree of Master of Science in Chemical Engineering at the School of Engineering, University of KwaZulu-Natal

Supervisor: Prof. Deresh Ramjugernath

Co-Supervisor: Prof. David Raal

June 2016

Declaration

I, Welcome Tshuma, declare that:

- I. The research reported in this thesis, except where otherwise indicate, is my original work
- II. This thesis has not been submitted for any degree or examination at any other university
- III. This thesis does not contain other persons' data, pictures, graphs or other information, unless specifically acknowledged as being sourced from other persons
- IV. This thesis does not contain other persons' writing, unless specifically acknowledged as being sourced from other researchers. Where other written sources have been quoted, then:
 - a) their words have been re-written but the general information attributed to them has been referenced; b) where their exact words have been used, their writing has been placed inside quotation marks and referenced
- V. Where I have reproduced a publication of which I am an author, co-author or editor, I have indicated in detail which part of the publication was actually written by myself alone and fully referenced such publications
- VI. This thesis does not contain text, graphics or tables copied and pasted from the internet, unless specifically acknowledged, and the source being detailed in the thesis and in the reference sections

Welcome Tshuma

Date

As the candidate's supervisor I agree/ do not agree to the submission of this thesis

Prof. Ramjugernath

Date

Abstract

A dual purpose differential flow calorimeter has been designed and constructed for low temperature and pressure measurement of both endothermic excess enthalpies and liquid heat capacities of pure liquids and binary mixtures. The equipment is a modification of a previous heat-of-mixing calorimeter model. In order to eliminate or reduce heat loss from heater lead-in-wires, the new design features a novel looped arrangement of the heater-mixer ribbon. This was suggested by solutions of the exact differential equation governing heat transfer in a flow calorimeter. Flow-rate and physical property-dependent conductive heat loss is the principal problem in heat capacity flow calorimetry. Pt-100 temperature sensors - in specially machined sheaths - were installed, projecting into the inflowing streams to eliminate conductive errors. Overall convective heat losses (as $U_i A_i$ for no energy input), were measured separately from the conductive heat loss experiments. Extensive data are presented for heat losses and heat capacities, as functions of flow rates and heater inputs, for water, toluene and n-butanol. The conductive heat losses, reduced by the novel heater arrangement, were correlated satisfactorily (after much effort). This was undertaken with a new universal equation in terms of dimensionless groups involving fluid flow rate, energy input, density, viscosity, heat capacity and thermal conductivity. Dimensionless groups, arising from the abovementioned differential equation in dimensionless variables, provided a useful starting point for the correlation. The accuracy of the measured C_p^L values was influenced mostly by the accuracy of measurement of conductive heat leaks. Measured heat capacities were in excellent agreement with the best (recommended) values from literature. It is recommended that measurements be made on additional fluids (e.g. halogenated hydrocarbons) to confirm or extend the universal correlation for conductive heat losses. It is also recommended that the REGLO Z-181 pump heads be replaced with the more powerful Z-1830 ones, particularly for excess enthalpy measurements.

Acknowledgements

Firstly I would like to thank the Lord Almighty for the gift of life and the abundance of blessings that I have witnessed in my life.

I am deeply grateful to my supervisors, Professor Deresh Ramjugernath and Professor David Raal, who read every word written in this work. The author would like to acknowledge the DST/NRF South African Research Chairs Initiative (SARChI) for the support of this research. I acknowledge the unwavering support rendered by Mr. Leon Augustine and Mr. Ayanda Khanyile during mechanical equipment construction and maintenance. Additionally, I would like to extend sincere thanks to Mr. Sanjay Deera and Mr. Markus Nowotny (CheckIt Systems) for their contributions during automation of the equipment.

I would also like to acknowledge the continued support of my family throughout the course of the project as well as members of the Thermodynamics Research Group. Their companionship contributed immensely to the success of this project.

Table of Contents

Declaration.....	ii
Abstract.....	iii
Acknowledgements.....	iv
Table of Contents.....	v
Notation.....	ix
Chapter 1.....	1
1.0 Introduction	1
1.1 Importance of heat capacity and heat of mixing	1
1.2 Sources of motivation and objectives of project	1
Chapter 2.....	3
2.0 Introduction to Excess Enthalpy and Heat Capacity	3
2.1 Excess Enthalpy (H^E)	3
2.2 Heat Capacity (C_p)	5
2.2.1 Isochoric.....	5
2.2.2 Saturation.....	5
2.2.3 Isobaric.....	5
2.3.0 Prediction procedures.....	6
2.3.1 Prediction procedures and correlations for excess enthalpy	6
2.3.2 Empirical methods	6
2.3.3 Solution theory-based methods	7
2.3.4 Prediction procedures and correlations for heat capacity	8
2.3.4.1 Prediction methods for pure liquid heat capacity	8
2.3.4.1.1 QPPR methods	8
2.3.4.1.1.1 Corresponding state theorem (CST) methods	8
2.3.4.1.1.2 Thermodynamic methods.....	9
2.3.4.1.3 Empirical methods	9
2.3.4.1.2 QSPR methods	9
2.3.4.2 Prediction procedures for liquid mixtures	10
Chapter 3.....	11
3.1 Calorimetry	11
3.2 Classification of calorimeters.....	11
3.3 Description of Calorimeters	11

3.4	Adiabatic calorimetry	12
3.5	Diathermal calorimetry	14
3.6	Construction principle	15
3.7	Description of calorimeters based on the nature of their vessels	15
3.7.1	Batch calorimeters	15
3.7.2	Displacement (Titration) calorimeters	15
3.7.3	Flow calorimetry	16
3.7.3.1	Flow Calorimetry for Excess Enthalpy	17
3.7.3.1.1	Purity and flow rates of influent stream	17
3.7.3.1.2	Temperature equilibration	17
3.7.3.1.3	Fluid mixing	18
3.7.3.1.4	Determination of heat effect of mixing	19
3.7.3.1.5	Separation of heat of mixing from frictional heating	19
3.7.3.1.6	Determination of downstream composition using the refractive index method	20
3.7.3.1.7	Heinz and Lichtenthaler High Pressure Isothermal Flow calorimeter	21
3.7.3.2	Flow calorimetry for heat capacity	24
3.7.3.2.1	Heat losses through conduction	24
3.7.3.2.2	Heat losses through convection	27
3.7.3.2.3	Evaluation of C_p	28
3.7.3.2.4	Design features to reduce conductive heat losses	28
3.7.3.2.5	Prominent heat capacity flow calorimeter designs	29
Chapter 4	30
4.0	Equipment Design and Operation Procedure	30
4.1.1	The liquid flow path	35
4.2	Details of construction	37
4.2.1	Ismatec microgear pumps	37
4.2.2	Temperature equilibration	38
4.2.2.1	Design and performance of coils	38
4.2.3	Design and performance of water baths	39
4.2.3.1	Water bath 1	39
4.2.3.2	Water bath 2	40
4.2.4	Polypropylene housing	40
4.2.5	Calorimeter modules	42
4.2.5.1	Mixing module	42

4.2.5.2 Reference module.....	48
4.2.6 The heating circuit	49
4.2.7 Detection system	50
4.2.7.1 Temperature sensors.....	50
4.2.7.2 Pressure sensors	51
4.2.7.3 Data acquisition unit.....	51
4.2.7.3.1 Compact RIO (cRIO) system	51
4.2.7.3.2 Reconfigurable NI cRIO 9073 chassis.....	51
4.2.7.3.3 NI C series analog input modules.....	52
4.2.7.3.4 DC power supply	52
4.2.7.3.5 Host PC	52
Chapter 5.....	54
5.0 Experimental procedure.....	54
5.1 Calibrations.....	54
5.1.1 Pump calibration.....	54
5.1.2 RTD calibration	55
5.1.2.1 Characterization calibration.....	55
5.1.2.2 Tolerance testing.....	56
5.1.3 Pressure transmitter calibration	56
5.1.3.1 Tolerance testing.....	57
5.2 Procedure for measuring pure liquid Heat Capacity.....	58
5.2.1 Development of conductive heat leak correlation.....	58
5.2.2 Determination of exponents n_1 , n_4 and calorimeter properties λ	60
5.2.3 Development of universal heat leak correlation.....	61
5.2.2.1 Measurement of heats of mixing.....	62
Chapter 6.....	63
6.0 Results and discussions	63
6.1 Experimental fluid: De-ionized water	64
6.2 Experimental Liquid: 1-Butanol.....	70
6.3 Experimental fluid: Toluene.....	76
6.4 Predicting capabilities of the conductive heat leak correlation	82
6.5 Measured Molar Heat Capacities	85
6.6 Discussions	88
Chapter 7.....	92

Conclusions	92
References	94
Appendix A	99
Experimental fluid: De-Ionized water	99
Appendix B	105
Experimental fluid: n-Butanol	105
Appendix C	111
Experimental fluid: Toluene	111
Appendix D	117
Equipment specifications	117
Appendix E	120
Pump 1 calibrations experimental data	120
Appendix F	121
Pt-100 sensor calibrations	121
Appendix G	123
Pt-100 sensor tolerance testing	123
Appendix H	124
Pressure transmitter calibration	124
Appendix I	125
Pressure transmitter tolerance testing	125

Notation

Variables and meanings

A – tube surface heat transfer area (m^2)

a – wire cross-sectional area (m^2)

B – wire circumference (m)

C – heat capacity (J/mol K)

D – tube diameter (m)

E – internal energy (J)

EOS – equation of state

f – wire coiling correction factor

G – Gibbs free energy (J)

g – gravitational acceleration constant (m/s^2)

H – enthalpy (J)

h – film heat transfer coefficient ($\text{W/m}^2\text{K}$)

$I. D$ – internal diameter (m)

i – electrical current (Amps)

k – thermal conductivity ($\text{W/m}^2\text{K}$)

L – length of tubing (m)

M – extensive thermodynamic property

\dot{m} – mass flowrate (g/s)

\dot{n} – molar flowrate (mol/s)

$O. D$ – outside diameter (m)

P – Pressure (kPa)

Q – heat energy (W)

q – heat loss (W)

R – electrical resistance (ohms)

\mathfrak{R} – universal gas constant (J/ K mol)

S – entropy (J/mol K)

T – fluid temperature ($^{\circ}\text{C}$)

t – time (s)

U – overall heat transfer coefficient ($\text{W/m}^2\text{K}$)

u – fluid velocity (m/s)

V – volume (m^3)

\dot{V} – fluid volumetric flowrate (ml/s)

VLE – vapour-liquid equilibrium

W – mechanical work (J)

X – heater length along the horizontal coordinate (m)

x_i – mole fraction of component *i* in solution

Z – height above datum level (m)

Greek alphabet

α – thermal diffusivity i.e. $[k/\rho C_p]$ (m^2s^{-1})

β – isothermal compressibility i.e. $[-V^{-1}(\partial V/\partial P)_T]$ (atm^{-1})

γ – isochoric pressure coefficient i.e. $[(\partial P/\partial T)_V]$ (atm K^{-1})

μ – fluid viscosity (Pa.s)

θ – nichrome wire/heater temperature ($^{\circ}\text{C}$)

σ – isobaric expansivity i.e. $[V^{-1}(\partial V/\partial T)_P]$ (K^{-1})

ρ – fluid density (g/ml)

τ – residence time (s)

λ – calorimeter properties/characteristics ($^{\circ}\text{C}$)

ω – acentric factor (dimensionless)

Ω – ohm

Subscripts

a – at ambient state

b – value of property bulk fluid temperature

c – critical thermodynamic property

CV – heat loss through convection

e – at environmental temperature

eq – equivalent

f – friction work

gained – heat transfer into a material

gen – property generated

HL – conductive heat loss

L – liquid property

m – metal property

o – pure solvent property

P – at constant pressure

r – reduced thermodynamic property

T – at constant temperature

V – at constant volume

Superscripts

E – excess property

g – gaseous phase

$i. d$ – ideal gas property

L – liquid phase

$_$ – normalised property

$"$ – property flux (i.e. per unit area)

Dimensionless groups

Nu – Nusselt number

Pe – Peclet number

Pr – Prandtl number

Re – Reynolds number

Chapter 1

1.0 Introduction

1.1 Importance of heat capacity and heat of mixing

Heat capacity data are essential in determining the heat loads of streams in enthalpy balance calculations, in the design of heat transfer equipment, design and analysis of refrigeration cycles and so on. Although moderately precise data may be suitable in certain applications, some applications do require very high quality data e.g. differential ebulliometry. Heats of mixing (excess enthalpy) data, on the other hand, provide information about the energy content of a mixture, the type of interaction between molecules, and are of importance in many process design calculations. Furthermore, H^E data are required, as a function of temperature, for thermodynamic consistency tests of isobaric equilibrium data and can be used in the prediction of vapour-liquid equilibrium data.²³

1.2 Sources of motivation and objectives of project

The heat capacity of a substance is a function of the temperature and pressure conditions to which it is subjected. Most of the data in the literature was obtained either at a fixed temperature (298.15K) or over a short temperature range. Furthermore, there is an absence of reliable liquid mixture heat capacity prediction techniques based on pure component heat capacities.²¹

Touloukian and Makita¹ made a compilation, and reviewed the heat capacities of 55 industrially-valuable pure substances. Zabransky, Domalski and co-workers² critically reviewed and compiled a two-volume set of collections of evaluated heat capacities of 1624 pure substances in their liquid state. However, many other important liquids do not feature in their collections, and some of the data may need to be reviewed and updated. Christensen et al.^{3, 4, 5} also compiled substantial collections of data based on the heat of mixing. Again, many industrially valuable systems are absent. In addition, the increase in reliability of vapour-liquid equilibria prediction procedures, from empirically determined H^E data, has led to the demand for high quality H^E data. These prediction procedures are based on the rigorous Gibbs-Helmholtz equation, and appear to be faster, more reliable, and particularly favourable in cases where direct measurement of the VLE of thermally unstable systems is unsuitable.²³

Based on the analysis made above, the Thermodynamics Research Unit in the School of Engineering at the University of KwaZulu-Natal, over the last few decades, has embarked on a number of projects to obtain accurate and reliable excess enthalpy and heat capacity data. These projects involved the identification and careful analysis of potential sources of data

discrepancies in equipment design, construction and operating procedures, and devising sound solutions for improved performance of designs and hence accuracy of data.

The main purpose, therefore, of the current project was to design, construct, and test a dual purpose flow calorimeter, in order to measure both excess enthalpy and the heat capacity of pure liquids and binary liquid mixtures, with a higher degree of precision, while keeping costs minimal. The new design incorporates a novel arrangement of heater-lead-in wires and a 2-module-in-series concept, to mitigate heat leaks to the environment, plus providing mechanisms for addressing the thermal effects of friction. Additional modifications, particularly on the electronic instrumentation side, have also been implemented, towards improving output data precision and ease of equipment operation.

The current design, like the previous models, will be limited to the measurement of heat of mixing of binary endothermic systems. However, since the scope of this project extends to measurement of heat capacities, the opportunity exists for thermodynamic consistency testing, as the two properties being measured are not independent from each other, but are related.

Chapter 2

2.0 Introduction to Excess Enthalpy and Heat Capacity

2.1 Excess Enthalpy (H^E)

Excess properties are essential in the description of extensive thermophysical properties of liquid solutions. They are a measure of the deviation of real properties of liquid solutions from ideal solution behaviour, at the same temperature, pressure and composition, that is,

$$M^E = \Delta M - \Delta M^{id} \quad (1)$$

ΔM in equation (1) can be defined as,

$$\Delta M = M - \sum_i x_i M_i \quad (2)$$

where M is the liquid solution molar real property,

M_i and x_i are the pure component molar property and its corresponding mole fraction in the mixture, respectively.

The molar property change of mixing of an ideal solution (ΔM^{id}) varies depending on the extensive property. Since, all excess properties exhibit zero values in an ideal solution (ΔM^{id}), each property can be deduced as follows:

$$\Delta H^{id} = 0 \quad (3)$$

$$\Delta V^{id} = 0 \quad (4)$$

$$S^{id} = -R \sum_i x_i \ln x_i \quad (6)$$

Using equation (1) above, excess enthalpy can be defined as

$$H^E = \Delta H^E - \Delta H^{id} \quad (7)$$

Using the definitions (2) and (3), and substituting for ΔH and ΔH^0 in equation (7) above, we get

$$\begin{aligned} H^E &= H - \sum_i x_i H_i - (0) \\ &= H - \sum_i x_i H_i \\ &= \Delta H \end{aligned} \quad (8)$$

From this result (8), it is evident that the excess enthalpy is equal to the enthalpy change of mixing, and thus excess enthalpy is often referred to as the enthalpy of mixing. The enthalpy change of mixing can either be positive (endothermic systems) or negative (exothermic systems). The sign convention, magnitude and axis of symmetry of excess enthalpy, are a

function of interactions between molecules which occur during the mixing process. For temperatures below T_c , H^E values of binary liquid mixture are a measure of the differences in strength of interactions between the two unlike fluid molecules and those of the like pure individual component molecules. Ott and Sipowska ⁶ further add that, in general, exothermic mixing results from relatively stronger unlike molecular interactions, compared to the pure components like molecular interactions, whereas an opposite scenario yields positive H^E . Typical H^E vs. composition curves are parabolic such that H^E tends to zero as either mixture component approaches purity. They can also have inflection points, that is, be both positive and negative over the x range.

The enthalpy of mixing pertinent to this project is a heat effect derived from mixing two pure liquid components. It is therefore important to distinguish this type of enthalpy from other heat effects which occur during mixing processes, such as the enthalpy of solution, and enthalpy of dilution. The former is a heat effect resulting from dispersal of a solute (gaseous or solid) in a liquid solvent, whereas the latter refers to the heat effect derived from mixing a solution with a corresponding pure liquid.⁷

The temperature and pressure coefficients of H^E can be illustrated by means of the following equation

$$dH^E = C_p^E dT + V^E (1 - T\sigma^E) dP \quad (9)$$

$$\text{hence } \left(\frac{\partial H^E}{\partial T} \right)_P = C_p^E = C_{p,mix} - \sum_i x_i C_{pi} \quad (10)$$

$$\text{and } \left(\frac{\partial H^E}{\partial P} \right)_T = V^E (1 - T\sigma^E) \quad (11)$$

The temperature dependence of H^E is represented by C_p^E as shown in equation (10) above. Temperature does have a considerable influence on excess enthalpy, and hence H^E values are always quoted at specific temperatures. Equation (11) shows the dependence of H^E on pressure. Except for pressures near critical, the values of the variables V^E and σ^E in liquid systems are small enough to be neglected. In such instances, therefore, the influence of pressure on excess enthalpy can safely be ignored.⁷

2.2 Heat Capacity (C_p)

Heat capacity refers to the amount of heat energy required to change the temperature of a substance by a single unit. Below $T_r = 0.7$ to 0.8 , heat capacities of liquids generally increase moderately with temperature while the effect of pressure is deemed negligible except at values of reduced pressure approximately equal to one. Prausnitz et al.⁸ further reveal that C_p^L is a strong temperature function at elevated temperatures and tends to infinity as T_r tends to 1. Frequently, the heat capacity is divided by the amount of substance, that is, molar and specific heat capacity, when expressed as per unit mole, and mass respectively. In thermodynamics, three types of heat capacity are described⁸⁴, that is,

- Isochoric
- Saturation
- Isobaric

2.2.1 Isochoric

This form of heat capacity is not easily determined experimentally for liquids, and is generally applicable in theoretical work.⁸⁴ It is heat capacity at constant volume and can be defined as,

$$C_v = \left(\frac{\partial E}{\partial T} \right)_v \quad (12)$$

2.2.2 Saturation

Saturation heat capacity is applicable to two-phase vapour-liquid systems. The subscript 'sat' describes the pressure variation with temperature along a vapour-liquid saturation curve. It is defined as,

$$C_{sat} = T \left(\frac{\partial S}{\partial T} \right)_{sat} \quad (13)$$

2.2.3 Isobaric

This is the most common and valuable type of heat capacity in most industrial calculations, and hence will be one of the main foci of this project. Isobaric heat capacity can be defined using the temperature dependence of enthalpy at constant pressure, i.e.

$$C_p = \left(\frac{\partial H}{\partial T} \right)_p \quad (14)$$

C_p can also be defined as an entropy derivative, that is,

$$\text{Since } \left(\frac{\partial H}{\partial T} \right)_T = T \left(\frac{\partial S}{\partial T} \right)_p$$

$$\text{therefore } C_p = T \left(\frac{\partial S}{\partial T} \right)_p \quad (15)$$

The two heat capacities, C_p and C_{sat} , can be related using the entropy dependence on temperature and pressure $[S = f(T, P)]^{84}$ i.e.

$$C_{sat} = C_p - T \left(\frac{\partial V}{\partial T} \right)_p \left(\frac{dP}{dT} \right)_{sat} \quad (16)$$

The relationship between C_p and C_v may also be described using the equation

$$C_p - C_v = \frac{TV\sigma^2}{\beta} \quad (17)$$

Data for C_p and C_{sat} are indispensable in many applications and therefore are widely published in literature.

Heat capacities and heats of mixing of liquids can be determined either by using various available experimental calorimetric techniques, or by using prediction methods.

2.3.0 Prediction procedures

The measurement of thermodynamic properties is often a cumbersome, time consuming, tedious, and costly process. This has motivated researchers to develop prediction procedures and correlations as alternatives or aids to empirical methods, whereby available experimentally-determined data are used. Although these prediction methods may seem more attractive, their main shortcoming has been the inferior degree of accuracy when compared to practical techniques. As a result, over the last few decades, tremendous effort has been dedicated to the refinement of existing techniques and the development of novel procedures for predicting H^E and C_p .

2.3.1 Prediction procedures and correlations for excess enthalpy

Estimation methods of molar H^E can generally be classified into two groups, that is,

- ✓ Empirical
- ✓ Theoretical (solution theory-based)

2.3.2 Empirical methods

These are mathematical models, in polynomial form, that are used to describe the quantitative behaviour of a thermodynamic property. They express the quantity of excess enthalpy at a particular temperature as a function of component mole fractions, and multiple experimental data-fitted parameters. The polynomial coefficients are determined using least squares methods while the number of parameters is determined by the degree of accuracy required. For binary systems, there are several empirical expressions available, including the universal Redlich-

Kister polynomial.

2.3.3 Solution theory-based methods

This approach describes the behaviour of a liquid mixture in terms of its molecular structure and the intermolecular forces that prevail. Solution theories have been developed over the years, such as the regular solution theory, two liquid theory and the Flory theory. One of the earliest solution theories, considered to be a regular solution theory was that of Van Laar.⁹ This model is based on the assumption that molecules mix randomly with insignificant directed interactions. However, in reality, intermolecular forces of considerable strength do exist in liquid solutions such that the mixing of molecules occurs in a non-random manner. Wilson¹² accounted for the non-random mixing behaviour of molecules, and this eventually led to the local composition theory. This new theory was based on differences in local composition, and the entire composition of the solution, which resulted in differences in sizes of molecules and intermolecular forces. These latter two results manifested in the short range order and the non-random orientation of molecules. This theory was accepted and eventually saw the advent of the famous Wilson equation, and other models based on the same theory, such as NRTL¹⁰ and the UNIQUAC.¹¹

These equations express G^E as a function of composition x and a number of adjustable parameters. Local composition model equations were devised for phase equilibrium calculations and evaluating activity coefficients but their application can be extended to relate thermodynamic properties.

Excess molar enthalpy can, in principle, be derived from other excess properties, such as the temperature coefficient of the molar G^E (Gibbs-Helmholtz equation), that is,

$$\left[\frac{\partial \left(\frac{G^E}{T} \right)}{\partial T} \right]_{P,x} = -\frac{H^E}{T^2} \quad (18)$$

The difficulties in obtaining sufficiently accurate temperature derivatives of molar G^E , leading to reliable H^E values, have rendered this method less popular than direct experimental calorimetric techniques.⁶

2.3.4 Prediction procedures and correlations for heat capacity

2.3.4.1 Prediction methods for pure liquid heat capacity

Prediction procedures for liquid heat capacity fall into two broad categories¹³, that is,

- ✓ QPPR (Quantitative-Property-Property-Relationship)
- ✓ QSPR (Quantitative -Structure-Property-Relationship)

2.3.4.1.1 QPPR methods

These methods rely on the physicochemical properties of substances in order to determine heat capacity. Corresponding states theorem (CST), thermodynamic and empirical methods are all affiliated to this group. Thermodynamic and CST methods focus on evaluating the heat capacity difference between liquid and ideal gas, i.e.

$$\Delta C_p = C_p^L - C_p^{g,id} \quad (19)$$

Coupling equation (17) with the two equations

$$C_p^{g,id} - C_v^{g,id} = \mathfrak{R} \quad (20)$$

$$C_v = C_v^{g,id} + \int_{\infty}^V T \left(\frac{\partial^2 P}{\partial T^2} \right)_V dV \quad (21)$$

a thermodynamic form of equation (19) can be represented as follows,

$$\Delta C_p = -\mathfrak{R} - T \int_V^{\infty} \left[\left(\frac{\partial^2 P}{\partial T^2} \right)_V \right]_T dV - T \frac{(\partial P / \partial T)_V^2}{(\partial P / \partial V)_T} \quad (22)$$

i.e. ΔC_p can be found from an EOS if the parameters are available/predictable.

Values of $C_p^{g,id}$ can be readily sourced from literature or else may be estimated from reliable techniques such as that of Benson.¹⁴

2.3.4.1.1.1 Corresponding state theorem (CST) methods

The CST states that, compared at equal T_r and P_r values, all fluids exhibit approximately equal values of the compressibility factor. Although this theorem is valid for simple fluids, a third parameter such as the acentric factor ω of Pitzer¹⁵ can be incorporated to extend the applicability of the former to much more complex fluids. Several researchers made modifications based on the work of van der Waals. Some of the conspicuous developments include those of Sakiadis and Coates¹⁶ who devised a technique to predict the heat capacity of liquid hydrocarbons with an impressive percentage uncertainty of 0.9 %. Bondi¹⁷ suggested a relatively simple criterion for determining ΔC_p as a function of only T_r and ω . This model and other similar ones were valid for relatively small reduced temperature ranges between 0.4 and 1 for non-polar systems and achieved a relatively poor 4 % prediction error.

Generally, the CST method has become unpopular, as researchers have tended to resort to more elegant methods.

2.3.4.1.1.2 Thermodynamic methods

These describe the thermodynamic relationship between the heat capacity difference ΔC_p along a saturation curve, and the change in pressure with temperature. Several attempts, by many researchers, to establish a sound and acceptable relationship, were unfruitful until Coniglio et al.¹⁸ They suggested the use of equation (22), in particular, of employing a modified version of the Peng-Robinson equation of state (EOS), in evaluating the isochoric pressure coefficient γ and $(\partial P/\partial V)_T$. The approach exhibited a percentage of uncertainty ranging from 1 to 10 % in predicting pure liquid heat capacities for 51 compounds. This unsatisfactory outcome was mainly attributed to sensitivity of $(\partial^2 P/\partial^2 T)_V$ to sample size. To overcome this, Coniglio et al.¹⁸ implemented modifications to their approach, which included an increase in sample size to 69. Coniglio's work was followed up by other researchers. One of the most prominent developments is the work of Diedrichs et al.¹⁹, who recently devised a prediction procedure (for polar and non-polar systems) based on a volume-translated Peng-Robinson (VTPR) equation of state. This method exhibited a remarkably low predicted mean deviation of 0.78 % from experimental C_p values over a wide temperature range.¹⁹

2.3.4.1.1.3 Empirical methods

Empirical methods are relatively simple to use but their limited range of applicability has prompted researchers to favour the semi-empirical.¹³ A typical technique was proposed by Pachaiyappan et al.²⁰ who devised a method of evaluating liquid heat capacity as a function of molar mass and two substance-specific parameters. The parameters for this model were obtained from a wide range of organic substances consisting of nine homologous series. This method however exhibits a relatively poor uncertainty of up to 5 %.

2.3.4.1.2 QSPR methods

The QSPR prediction methods rely solely on the assessment of the structural formula of a particular chemical compound. Distinct functional groups/fragments can be deduced from a homologous series. Heat capacities and other thermophysical properties can be predicted by summing up the values of fragments in accordance to a particular governing equation. These methods have therefore been referred to as group contribution methods.

Generally, the group contribution methods are faster and more reliable, particularly at low temperatures. However, these prediction methods tend to become unreliable at near-critical temperatures and may produce unsatisfactory results for certain substances.²³

2.3.4.2 Prediction procedures for liquid mixtures

There has been no major break-through, in terms of devising techniques for predicting, with good precision, mixture heat capacity as a function of pure component heat capacities by means of an equation (10). Lee and Kesler²⁵ proposed a thermodynamic model based on the refined CST of Pitzer¹⁵ for predicting C_p^L . A high precision multiple parameter modified version of the Benedict-Webb-Rubin (BWR) EOS, which extends into the supercritical pressures $\sim(2P_c)$, was used to evaluate the reduced volume coefficient of reduced pressure $(\partial P_r / \partial V_r)_{T_r}$ i.e.

$$\Delta C_p / \mathfrak{R} = \Delta C_v / \mathfrak{R} - 1 - [T_r (\partial P / \partial T)_{V_r}^2] / (\partial P_r / \partial V_r)_{T_r} \quad (23)$$

Equation (17) is versatile as it is applicable in evaluating C_p^L and C_v of both pure liquids and liquid mixtures, and other thermophysical properties. This method achieves considerable success in evaluating non-polar system properties up to critical temperatures and pressures.

Chapter 3

3.1 Calorimetry

The term refers to the measurement of thermophysical properties of materials using a calorimeter. A calorimeter is an instrument used to measure the thermal effect corresponding to a change in state of a material. This change in state of a material can be with respect to temperature, pressure, volume, phase, chemical composition and so on.

3.2 Classification of calorimeters

Calorimeters can be classified in various ways. Many researchers have suggested approaches to classification, but generally there has been no consensus on any single criterion to follow. Rouquerol et al.'s²⁷ review compared different classification methods against theirs, which is based on the exchange of heat between the system and surroundings. Two distinct, all-encompassing categories were derived: adiabatic and diathermal calorimeters. Within each broad category, two subdivisions were derived: passive and active. Rouquerol et al.²⁷ concluded their review by recommending the abovementioned classification method, as well as that of Hemminger and Sarge²⁸, for the description of modern calorimeters.

3.3 Description of Calorimeters

The classification procedure proposed by Rouquerol et al.²⁷ will be adopted in describing calorimeters. The description of calorimeters discussed by Hemminger and Sarge²⁸, as well as the Zielenkiewicz²⁶ methodical approach to classification, will also be considered. Emphasis will be laid on flow calorimetric techniques for H^E and C_p measurement as they are the main focus of this project.

3.4 Adiabatic calorimetry

This term refers to a perfectly insulated system where there is no exchange of heat between the system and its surroundings, but, in practice, this ideal situation is rare, if not non-existent. The imperfections in a calorimeter result in heat leakages through the walls of the vessel. However, in adiabatic calorimetry, certain design features can be implemented to make the calorimeter behave in a nearly adiabatic manner. These means, suggested by Rouquerol et al.²⁷, include:

Passive mechanisms

These involve increasing the thermal resistance between the system and the surroundings. Some of the passive means that can be employed include minimizing the leakage modulus (heat transfer coefficient), and reducing the time available for heat exchange.²⁹ Raal and Webley²⁴ used materials of low thermal conductivity (such as Teflon) and evacuated the vessel jacket. Due to the fact that an infinitely large thermal resistance is impractical, small leakages of heat are inevitable. Consequently, calorimeters cannot be rendered totally adiabatic using passive means, hence such kinds of calorimeters are referred to as semi-adiabatic or quasi-adiabatic. A correction for the unavoidable heat leak problem would therefore have to be made for accounting purposes.

Active mechanisms

Active mechanisms include the minimizing of temperature gradients across the system boundary. Automatic control systems, such as servomechanisms and PID controllers, are involved in manipulating the temperature of the thermostat so that it follows that of the system. The use of these sophisticated control devices in modern calorimetry efficiently minimizes the temperature gradients to such low levels that these calorimeters qualify to be considered as being truly adiabatic.²⁷

McGlashan³⁰, in 1961, reviewed the early mixing calorimeters (for H^E measurement) which all operated in an adiabatic mode. McGlashan's review³⁰ identified two important requirements, needed for accurate measurements, of mixing calorimeters. These, are:

- absence of vapour spaces and;
- provision for changes in volume which occur during mixing processes

Absence of vapour spaces serves the purpose of eliminating undesirable thermal effects that accompany phase change (evaporation or condensation) of volatile liquids in the presence of vapour spaces. If this requirement is not met, significant discrepancies in the measured property can result. Changes in the mixture volume during mixing must be accounted for lest the corresponding changes in system pressure influence the measured H^E . For significant increases in system pressure, the mixing vessel would have to be expandable or else mechanically strong

enough to withstand the high pressures. Most calorimeters reviewed by McGlashan³⁰ did not satisfy these two requirements. As a result, an improved adiabatic batch calorimeter to eliminate flaws in design with respect to the aforementioned requirements is described by Larkin and McGlashan.³¹

3.5 Diathermal calorimetry

Diathermal calorimetry is based on drawing thermal effects resulting from the source (system) to the sink (surroundings). Heat can be exchanged either passively or actively.

Passive

Passive means of heat exchange can be achieved through adequate thermal conduction, such that the magnitude of enthalpy generated, that remains stored within the system, is by far less than that which crosses the system boundary. The temperature of the system is passively controlled by a thermostat. Rouquerol et al.²⁷, Calvet and Prat³² and Evans³³ consider the Tian-Calvet calorimeter to be the most typical design based on this principle. Calorimeters which rely upon phase changes to effect isothermality are also part of this class.

Active

The thermal effect of the process is nullified by means of the so-called in-situ compensation mechanisms previously described. In-situ compensation is considered to be equivalent to heat conduction, as both methods are aimed at maintaining isothermality within the system. Power compensation is the most efficient method of neutralizing process thermal effects, and has become prominent in modern calorimetry.

Isothermal mode of operation

The term “isothermal” refers to the maintenance of a constant temperature with time at any point within the calorimeter vessel.²⁹ There are several ways that can be employed to effect temperature constancy. One method to maintain temperature constancy involves the addition of electrical energy using a heater to compensate for temperature drop in endothermic systems. Electrical cooling, using a Peltier cooler, is used to nullify the temperature rise in exothermic systems.

3.6 Construction principle

Single and Twin

Every calorimeter consists of at least one vessel where samples are located. The vessels of a twin calorimeters operate differentially to reduce heat leakages. Therefore, measurement performed using such designs is commonly referred to as differential calorimetry. In the twin system, the two cells are identical in construction, possess the same thermal properties and are subjected to the same surrounding conditions. With this kind of a set up, it is possible to use the reference cell to compensate for thermal effects incurred in the test vessel^{23, 24, 44, 57} or to run the main process in the test cell, while concurrently running a control in the reference cell.³⁴ Differential calorimetry is mainly applied in the determination of small heat quantities in which minute heat leaks may have significant impact on the accuracy of the measured property.²⁹ The latter is brought about by limiting the effect of temperatures changes in the environment.

A drawback, however, associated with twin calorimetry, results from the extra effort of constructing a reference cell, usually accompanied by the challenge of ensuring its similarity.

3.7 Description of calorimeters based on the nature of their vessels

3.7.1 Batch calorimeters

Batch calorimeters are closed systems in which heat effects are measured.²⁶ The intermittent operation associated with batch vessels constitutes a major disadvantage that sees lengthy time spans required to produce data points for the whole composition range. A thorough review of batch calorimeters for determining heats of mixing is given by Raal and Webley²⁴ who concluded by giving the strengths and shortcomings of this type of calorimetry.

3.7.2 Displacement (Titration) calorimeters

These calorimeters are open systems in which a second material (titrant) can be charged into the reaction vessel containing the first either at a predetermined constant rate or in small equal increments. Using such a charging procedure, a minimum of only two runs are sufficient to cover the whole composition range. A major advantage seen in displacement calorimeters is therefore related to the elimination of the cumbersome discarding, and reloading, of fresh components for each run, which is a prominent feature seen in batch vessels. The total time requirement is thereby significantly lowered, along with amounts of reagents consumed. Approximately 50 cm³ per component is required to cover the entire composition range.³⁰

The measurement of heats of mixing in endothermic systems, by means of the titration method, was first put forward by Van Ness and Mrazek³⁶ in 1961. Winterhalter and Van Ness³⁷ implemented modifications to the Van Ness and Mrazek³⁶ design that saw the incorporation

of a thermoelectric cooler, extending measurements to exothermic systems. Prominent and superior designs, among many other developments of the pioneering design of 1961, were those of Marsh et al.³⁹ and Ewing et al.³⁸. These involved filling the mixing vessel (of known volume) with mercury (also of known volume) and one liquid component. The second component (titrant) was introduced to the vessel using a motor from a motorized burette, and displaces mercury of equivalent volume so that the volume of the system is conserved on loading. The vessel is kept isothermal by addition of electrical energy. This procedure is often referred to as continuous titration. Modifications of this design such as that of French and Richards⁴⁰, Costigan and Hodges⁴¹, integrated the Peltier cooler. Remarkably precise and reliable heat of mixing data (within 0.1 to 0.2 % of highest H^E value) could be obtained using the Marsh and co-workers' designs.^{6, 30} In spite of this huge advantage, the latter and other types of displacement calorimeters exhibit a range of operation that is limited to ambient pressure, while temperatures could only be extended by a few Kelvins from that of the surroundings.⁶

3.7.3 Flow calorimetry

Flow calorimetry evolved from the former two calorimetric methods and essentially involves open systems. One of the motivations leading to the development of flow calorimeters was the need to rapidly³⁵ and precisely⁵⁷ determine thermophysical properties over wide temperature and pressure ranges, including the supercritical state. Marsh³⁰ reports that, to date, the most accurate excess enthalpy measurements determined using flow calorimetry were those made by McGlashan and Stoeckli.⁴² In the determination of liquid heat capacities, Wilhelm⁴³ states that most flow calorimeters used are developments of the Picker et al.³⁴ twin flow calorimeter. The need to provide for volume changes in the system accompanying mixing is eliminated while careful design of flow pathways eliminates vapour spaces. A major shortcoming, however, associated with flow calorimetry, is consumption of large amounts of samples of up to 300 cm³ per component, which limits the viability of measurement of scarce and expensive fluids.^{6, 30}

3.7.3.1 Flow Calorimetry for Excess Enthalpy

Naidoo and Raal²³ defined six important stages which can be used to describe a differential mixing flow calorimeter i.e.

- predetermination of liquid flow rates and percentage purity of the components
- temperature equilibration of the influent component streams
- mixing of the components inside the vessel
- accurate determination of the thermal effect produced in the mixing vessel
- accounting and correcting for frictional dissipation in the reference cell
- accurate determination of the calorimeter exit stream composition using a refractometer

3.7.3.1.1 Purity and flow rates of influent stream

Gas bubbles and vapour spaces

Gas bubbles constitute a serious source of systematic error in the calorimetric measurement of various properties, such as excess enthalpy, heat capacity, density and so on. Gases dissolved in the liquids may eventually lead to, among other problems, vapour spaces and uncertainties in material compositions. It seems common practice to purify feed by initially drying it, using an appropriate desiccant, then finally, by degassing it.^{42, 51, 57, 59} Although several different degassing methods have been reported in literature, distillation appears to be the most commonly used. The use of high purity feed eliminates the need to degas feed in the first place.

Feed flow rates

The fluid flowrates selected must not exceed limiting values beyond which temperature defects, and/or incomplete mixing in the fixed length equilibration coils, and mixing vessel, may be observed. A more serious challenge encountered in flow calorimetry is associated with pumping pulseless and reproducible flow rates. The former can be accomplished by employing pulse dampeners^{21, 24} or otherwise using non-pulsating pumps.

3.7.3.1.2 Temperature equilibration

Fluids are brought to the set calorimeter temperature by either passive or active heat exchange, prior to entering the calorimeter. In passive heat exchange, the influent liquids are passed through a thermostatted water bath in coiled tubes of predetermined length. A temperature controller is incorporated into the bath to monitor the bath temperature. The prevailing laminar flow heat transfer coefficients inside coils may be evaluated using correlations of the form

$$Nu = f\left(Pe, \frac{L}{D_{eq}}, \frac{\mu_b}{\mu_w}\right) \quad (24)$$

whereas, heat transfer rates between the tube wall and the bath can be obtained from

$$Nu = g\left(\text{Re}, \text{Pr}, \frac{\mu_b}{\mu_w}\right) \quad (25)$$

For straight tubes, typical examples of a correlations represented by equation (24) are those of Sieder and Tate ⁴⁵ for short lengths, and Mills ⁴⁶ (for both short and long tubes). Helical tubing correction, such as McAdams ⁴⁸, should be applied to the straight tube heat transfer correlations.

Chilton et al.⁴⁹ studied heat transfer coefficients in single phase agitated Newtonian liquid systems. The deductions from the study could be represented by the equation (25) above. The temperature defect ΔT represents the deviation of the exit temperature of the heat exchanger piped fluid from the set water bath temperature. A typical piping material used by Raal and Webley ²⁴ includes stainless steel such as the 316 L type. A prediction method was developed by Raal and Webley ²⁴ to estimate sufficient coil length corresponding to minimum ΔT , for both chlorinated and non-chlorinated organic compounds as well as for all liquid flowrates. The prediction procedure can be generally expressed by the equation

$$\ln\left(\frac{\Delta T}{\Delta T_0}\right) = f\left(\frac{\alpha L}{\dot{V}}\right) \quad (26)$$

where ΔT_0 is the constant temperature difference between the fluid and the water bath at the entrance region in °C.

Minor temperature gradients existing between heat exchanger exiting liquids can be cancelled by employing a concentric tubing system of Christensen et al.⁵⁰⁻⁵² Failure to equilibrate either fluid temperature will consequently result in erroneous H^E values according to equation (8).

3.7.3.1.3 Fluid mixing

The purpose of this section is to achieve homogeneity with respect to temperature, velocity, composition and fluid mixture physical properties, at every point at the vessel exit stream cross section. Flow calorimetry utilizes energy of fluids' motion coupled with mostly packed inserts (which can be heated electrically), or an ingenious injector design ⁴² to blend the passing fluids. A more systematic and efficient mixer-heater design by Raal and Naidoo ²³, similar to the open and twisted ribbon true Kenics design, was machined out of a nichrome ribbon. Chemineer ⁵³, a pioneering company in Kenics mixer design, reports that Kenics motionless mixers offer the lowest pressure drop of all the commercially available static mixers. The mechanism of mixing in Kenics static mixers is cleared described by Cybulski and Chemipan.⁵⁴ Joshi et al.⁵⁵ reports that the number of strata produced by a Kenics mixer S for a given number of elements N can

be predicted from the geometric progression,

$$S = 2^N \quad (27)$$

Construction materials for the mixing vessel are typically fluoropolymers such as Teflon (PFA and PTFE) or PVFD.

3.7.3.1.4 Determination of heat effect of mixing

From the first law of thermodynamics, a general steady state flow energy balance around a conduit yields,

$$\Delta H + \frac{\Delta u^2}{2} + g\Delta z = Q + W_s \quad (28)$$

where W_s represents shaft work

The properties H , Q and W_s in equation (28) are all specific. As the fluid flows through the conduit, changes in fluid velocity and elevation between the entrance and exit positions are negligible. Furthermore, no forms of shaft work are present so that equation (28) reduces to

$$\Delta H = Q \quad (29)$$

Q in the equation above represents the compensating heat energy generated by the resistance heater from a constant electrical current supply according to the Joule's first law.

From equation (8) it was shown that

$$\Delta H = H^E$$

hence $H^E = Q \quad (30)$

Unfortunately, the expected temperature fluctuations during the course of mixing are a result of other factors like fluid frictional heating, heat losses and thermistor dissipation, in addition to the actual heat of mixing. It is therefore vital that these accompanying thermal events be excluded from the primary measurement i^2R through a suitable correction. In exothermic mixing, a thermoelectric cooler, operating at a constant known rate higher than that of heat evolution, is incorporated in the design. The control heater is used in conjunction with the cooler in maintaining isothermality within the system.

3.7.3.1.5 Separation of heat of mixing from frictional heating

Frictional heating is deemed the most challenging problem in flow calorimetry for excess enthalpy.³¹ For single cell flow calorimeters, thermal effects of friction were accounted for by running a pure component, to be used in the experiment, through the vessel, and thus noting the associated frictional heat. The pure liquid employed is usually one of the feed components for the experiment under investigation. This calibration technique may be unreliable if the pure

fluid properties (density and viscosity) differ significantly from those of the mixture. As previously stated, Gustin and Renon⁴⁴ and later Raal and Webley²⁴ employed an additional (reference cell) vessel in compensating for thermal effects of viscous flow incurred in the test vessel. The latter procedure is valid if, and only if, the thermal effects due to friction and heat leaks in the reference module replicate those in the test module, a requirement that was overlooked by many workers. Lost work due to friction in the fluid stream in the mixing module manifests in fluid pressure drop, which is accompanied by an increase in system temperature (frictional dissipation). Identically constructed test and reference cells do not necessarily suffer equal pressure drops and hence thermal effects due to friction.⁵⁷ Furthermore, equal pressure drops in both modules will not automatically guarantee equal temperature increases in both modules as a result of friction. Therefore in order to account for frictional effects in heats of mixing, it is necessary to assess and establish an exact relationship between lw_f and the resulting temperature increases. One such relationship is described by Raal⁵⁸ who performed an analysis of entropy generation in flows with mixing.

3.7.3.1.6 Determination of downstream composition using the refractive index method

This step serves to verify the accuracy of initial feed mole fractions obtained from pump calibrations. After a suitable calibration procedure of the refractometer, using a typical standard system such as the inviscid hexane-cyclohexane, subsequent compositions of systems can be determined by passage of visible light through the sample. The relative composition of a system may be determined with an uncertainty of ± 0.00005 while the temperature is held within ± 0.03 K at normal atmospheric pressure.⁹⁴

3.7.3.1.7 Heinz and Lichtenthaler High Pressure Isothermal Flow calorimeter

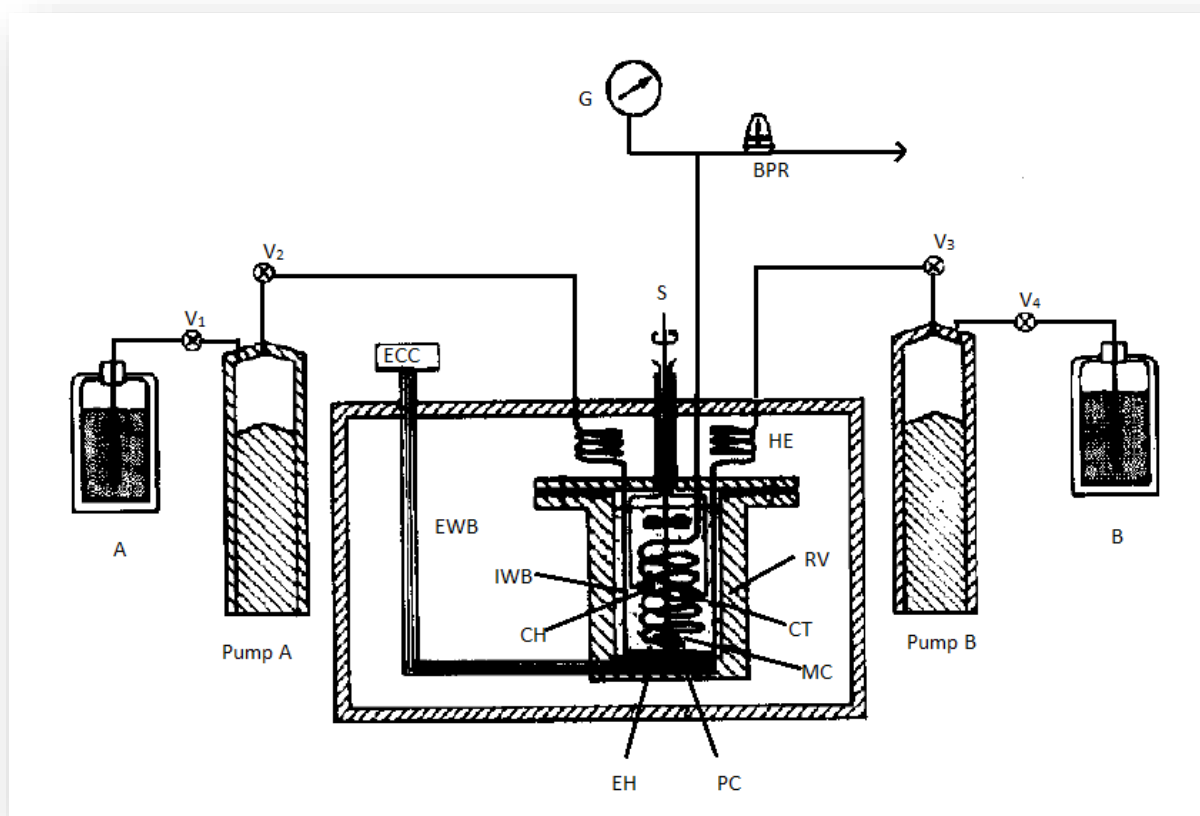


Figure 1: The Isothermal Flow Calorimeter of Heintz and Lichtenthaler (extracted from *Thermochimica Acta*, 1983, 69, 275)

This was among the first flow calorimeter models designed for liquid H^E measurement at elevated pressures. The 30 mL reaction vessel (RV) consists of an outer insulation, inside which lies an internal water bath (IWB). The IWB, whose temperature, T_i , is equal to that of the external water bath (EWB), buffers the reaction occurring inside the mixing coil (MC). T_i is held to within ± 0.001 K using a control thermistor (CT), while the agitator (S) maintains a uniform temperature across IWB. Pure liquids A and B, initially separated in their respective reservoirs, are pumped using their respective high pressure pumps associated with a back pressure regulating valve (BPR) to ensure measurement of processes over a wide pressure range of 1 to 600 atm. The system pressure is detected by a pressure gauge (G) shown in the diagram. The pure components are allowed to flow at variable rates to cover the whole composition range with stepwise adjustments. Limiting volumetric flowrate, corresponding to sufficient residence time for complete reaction for each run, is found by holding the ratio \dot{V}_A/\dot{V}_B constant while the individual flowrates are allowed to vary. The pumped liquids, A and B, flow in stainless steel tubing through the high pressure valves, V_1 to V_4 , into the external

water bath, in which equilibration inside heat exchangers (HE), takes place. After equilibration, the pressurized liquids are channelled the bottom of IWB where they enter into the 45 mm long mixing coil (MC). Using an analogous mechanism to the Ice calorimeter, the thermal effects of the mixing process are taken up by the immediate surrounding bath. For exothermic reactions, the Peltier cooler (PC), operating at a constant predetermined rate, withdraws heat from the IWB, and channels it to the sink (EWB). Likewise, the electric heater (EC) connected to an electronic control circuit (ECC), compensates for enthalpy deficit in the internal water bath, ensuring that isothermal conditions are maintained. Electrical calibration is carried out using the calibration heater (CH) shown.

Earlier, Christensen et al.⁵¹ and Siddiqi and Lucas⁵⁹ had reported designs similar to the abovementioned. In the former's design, the reaction vessel is instead immersed in an air bath in the low operation temperature range of 253-473 K, while the pressure regulating valve achieves a limiting pressure of 400 atmospheres. The brass reaction vessel contains a countercurrent heat exchanger, which equilibrates feed as well as products from the reaction capillary tube. The control heater is located between the Peltier cooler attached to the inner brass vessel wall, and the brass capillary tube. The capillary tube is a metallic equilibrium coil and is soldered between two brass plates (isothermal plates). For this design, the calibration heater is sandwiched between equilibrium coil turns. Prior to entering the capillary tube, the equilibrated reactants pass through concentric tubes for a distance equal to a single turn of the equilibrium coil. The latter design feature functions to equal the temperatures of the influent liquids. Mixing inside the 1800 m long, 1.59 mm (O.D) capillary tube is facilitated by an insert of crimped wire (shown in Figure 2 below). The long mixing pathway provides sufficient residence times for high fluid flow rates therefore allows greater thermal effects to be determined with same degree of accuracy as low flow rates. Furthermore, use of air as bath fluid widens the operation temperature range of the apparatus. Heintz and Lichtenthaler⁵⁶ report that despite these modifications, H^E data published from this high pressure calorimeter were limited to maximum operation pressure of 50 atmospheres.

Subsequent modifications were implemented in the Christensen et al.^{51, 52} reaction vessel by Christensen et al.⁵⁰ that saw the brass isothermal plate being substituted for a copper cylinder. This modification serves minimizing thermal resistance between the isothermal cylinder and the fluid sample. In this design, the coiled capillary mixing tube is wound on the lower bottom half section of the vertical cylinder while the Peltier cooler is attached to the top of the cylinder. An electric heater is wound on the upper section of the cylinder compensates for heat removed from the system while a back pressure regulator along the fluid exit tubing controls operation

pressures to a maximum value of 200 atmospheres. The operating temperatures of this calorimeter still remained at low ranges of about 253-475 K.

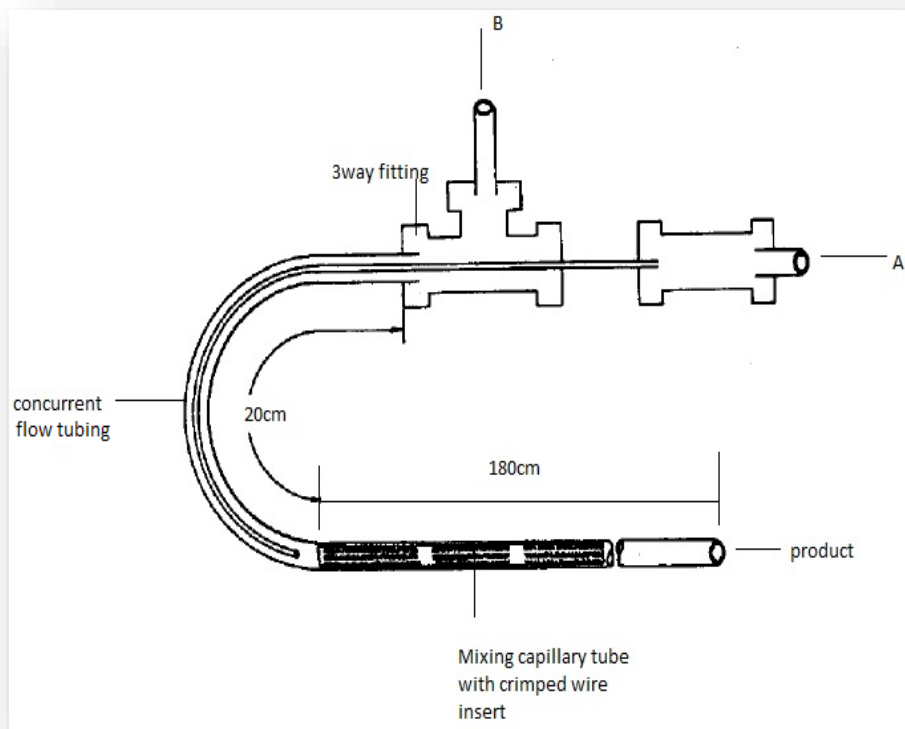


Figure 2: The Christensen et al.⁵² mixing pathway (extracted from *Thermochimica Acta*, 1983, 69, 279)

Christensen and Izatt⁵⁰ further modified the latter design to widen the operating temperatures of the calorimeter. Since the upper operating temperature of a calorimeter is restricted by the Peltier cooler, Christensen and Izatt⁵⁰ substituted the cooler for a controlled thermal leak channel. This modification saw an increase in the upper operating temperature limit to 673 K.

3.7.3.2 Flow calorimetry for heat capacity

In an ideal flow calorimeter for heat capacity measurement, electrical power (Q) is applied to a flowing fluid and the resulting temperature change (ΔT) is noted. However, as previously highlighted, every calorimeter design displays a measure of imperfection that facilitates heat leaks to the surroundings. Heat capacity measurements by Hei and Raal²¹, reveal some of the most critical steps involved in either elimination or accounting for heat leaks i.e.

- Accounting for the inevitable conductive heat losses via lead-in-wires
- Accounting for convective heat transfer losses through vessel walls
- Design of features to counter heat losses

3.7.3.2.1 Heat losses through conduction

Conductive heat losses are undoubtedly the chief source of data discrepancy in flow calorimetry for heat capacity.²¹ The material of construction for the heater ribbon is the same as that previously described, while the ideal lead-in-wire material properties necessarily include high electrical conductivity (low electrical resistance), as well as low thermal conductivity. However, for most metals, there exists a positive correlation between electrical resistance and thermal conductivity according to Wiedemann-Franz's Law.⁴⁷ Therefore the excellent electrical conductivities of typical lead-in-wire materials, such as copper and platinum, are associated with equally high thermal conductivities, which facilitate heat leakages through conduction to the environment. Because of the inevitable nature of these losses, Hei and Raal²¹ developed a means of quantifying them so as to make necessary corrections. A rigorous mathematical model was developed to predict the axial wire and fluid temperature distributions in a five zone calorimeter model shown in Figure (3) below. The incoming fluid temperature T_e is detected by sensor 1 in zone 1, after which the fluid experiences a marked increase in enthalpy in zone 3, as a result of high heat transfer coefficients from the heat generation zone. At the exit (zone 5), the fluid's exit temperature is detected by sensor 2. This model assumes that heat generation occurs only in the central nichrome element and that temperature was uniform in the radial wire direction such that heat is propagated only in the axial direction.

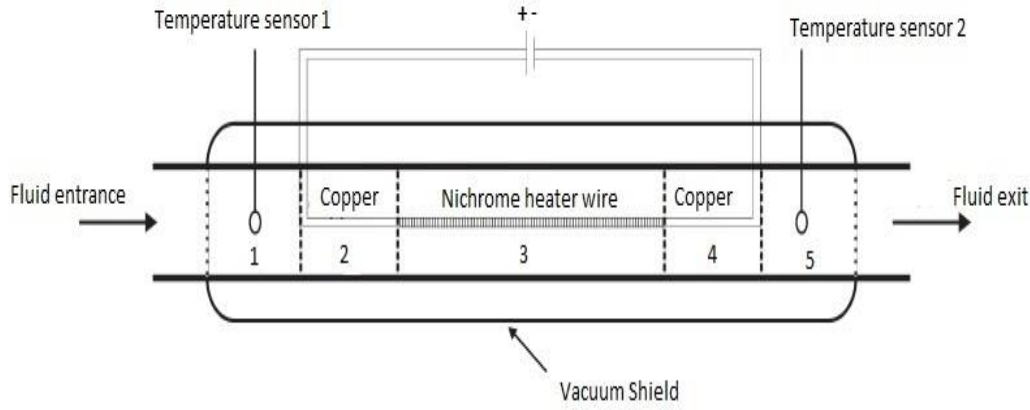


Figure 3: A five zone model of a flow calorimeter vessel (extracted from *AIChEJ*, 2009, 55, 207)

A wire temperature profile differential equation was derived from an energy balance on a differential portion located along the central heat generation zone i.e.

$$Q_{gen} + Q_{cond,in} = Q_{cond,out} + Q_{conv,out} \quad (31)$$

$$\frac{d^2\theta}{dX^2} + \frac{QBf^2}{ka} - \frac{hBf^2}{ka(\theta - T)} = 0 \quad (32)$$

A heat balance carried out on the flowing fluid system yields,

$$Q_{gained} = Q_{conv,in} - Q_{conv,out} \quad (33)$$

Similarly, a differential equation can be formulated to represent the fluid temperature profile along the horizontal differential portion dX , that is,

$$\left(\frac{C_p^L}{hBf} \right) \frac{dT}{dX} = \left(\frac{U}{hBf} \right) (T - T_e) \frac{dA}{dX} - (\theta - T) \quad (34)$$

By double differentiating equation (34) and combining the derivative with equations (32) and (34), a third order differential equation was derived to represent the variation of fluid temperature with the horizontal length i.e.

$$\frac{d^3T}{dX^3} + \left[\frac{hBf}{C_p^L} + \left(\frac{U}{C_p^L} \right) \frac{dA}{dX} \right] \frac{d^2T}{dX^2} - \left(\frac{hBf^2}{ka} \right) \frac{dT}{dX} + \left(\frac{Q''hB^2f^3}{kaC_p^L} \right) - \left(\frac{UhBf^2}{kaC_p^L} \right) (T - T_e) \frac{dA}{dX} = 0 \quad (35)$$

Assuming that perfect insulation from convective losses, through the vessel wall, is provided by the vacuum jacket, the terms containing the overall heat transfer coefficient U can reasonably be neglected, thus simplifying the complex equation. Laminar heat flow rates from the wire to the fluid can be estimated using the aforementioned Mills⁴⁶ correlation.

The solutions to equation (35) therefore express T as a function of distance X , and through

equation (34), the axial wire temperature profile may also be obtained.

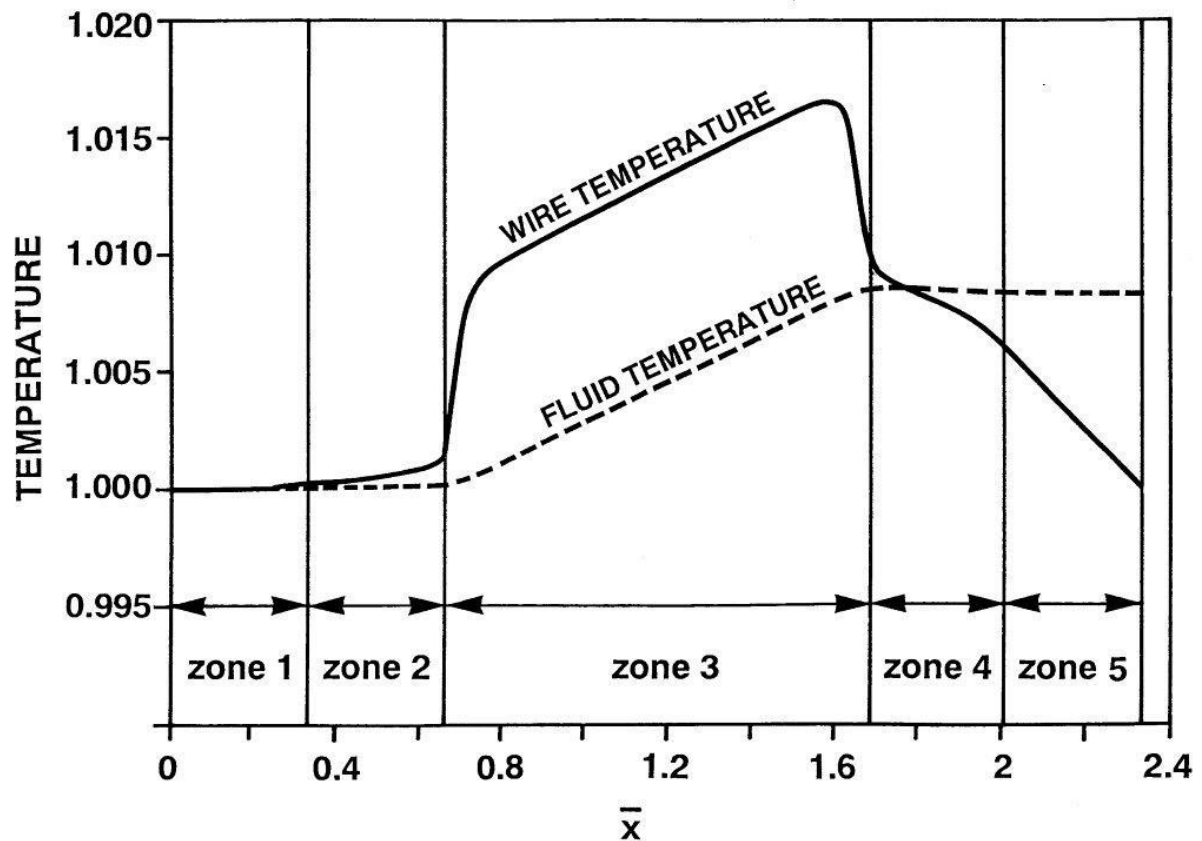


Figure 4 shows dimensionless fluid and wire temperatures as a function of dimensionless length for n-hexane (extracted from *AIChEJ*, 2009, 55, 208)

For purposes of versatility, equation (35) and its solutions may be normalized by expressing them in terms of dimensionless variables \bar{X} , \bar{T} and $\bar{\theta}$ i.e.

$$\bar{T} = \frac{(T - T_e)}{T_{ref}}, \quad \bar{\theta} = \frac{(\theta - T_e)}{T_{ref}} \quad \text{and} \quad \bar{X} = \frac{X}{\Delta X_3}$$

where T_{ref} is the reference temperature of a perfectly insulated system i.e. $(T - T_e)_{ideal}$

and ΔX_3 is the length of the heat generation zone

The dimensionless temperature \bar{T} depends on not only the dimensionless length \bar{X} but on fluid physical properties, flowrate and calorimeter characteristics contained in the dimensionless groups, as well. An example of this relationship is given in Figure 4 above for n-hexane.

Conductive heat losses via the lead-in-wires at both extremes q_{HL} can be computed from Fourier's Law i.e.

$$q_{HL} = -k_c a \frac{d\bar{\theta}}{d\bar{X}} \quad (36)$$

at values $X = 0$ and $X = X_5$ representing the wire extremes.

The subscript c here refers to the lead-in-wire construction material such as a copper.

Hei and Raal ²¹ and Raal ²² observed that the value of q_{HL} was significantly greater at the exit as evidenced by the steep negative slope of the $\bar{\theta}$ vs. \bar{X} graph, which falls below that of the fluid in zones 4 and 5 (Figure 4). An attractive fractional heat loss correlation was developed by Raal and Hei ²¹ that shows the dependence of the quotient (q_{HL}/Q) separately on λ , \dot{V} as well as the fluid physical properties. This correlation was capable of providing reliable estimates of conductive heat leaks for selected liquids (organics) except for water.²² Hei and Raal ²¹ and Raal ²² further suggested an alternative to the abovementioned correlation that involves the three dimensionless groups that were obtained from equation (35) i.e.

$$\pi_1 = \frac{hBf(\Delta x_3)}{\dot{m}C_P^L}$$

$$\pi_2 = \frac{hBf^2(\Delta x_3)^2}{k_m a}$$

and $\pi_3 = \frac{Q'' hB^2 f^3(\Delta x_3)^3}{\dot{m}C_P^L k_m a T}$

Raal ²² reports that values of conductive heat losses range up to 20 % of the power input and vary inversely with both \dot{V} and C_P^L .

3.7.3.2.2 Heat losses through convection

Although not as significant as conductive losses via the lead-in-wires, convective heat leaks pose a considerable problem as far as accuracy of heat capacity measurements is concerned. A relatively simple experimental procedure such as the one described by Raal ²² and Hei and Raal ²¹ can be used to account for losses through the walls. This procedure involves bringing the fluid temperature slightly above or below that of the external bathing fluid, using a set up similar to the previously described equilibration apparatus. After the fluid's temperature has been controlled to a desired base temperature, it is allowed to flow through the calorimeter so that the changes in fluid enthalpy, in the absence of an electrical power input, can be determined. An energy balance on the incompressible flowing system through the vessel can be expressed as

$$q_{CV} = \Delta H = C_P^L \Delta T + \frac{\Delta P}{\rho} = UA(\Delta T)_{LM} \quad (37)$$

At each experimental temperature, changes in the value of C_P^L and ρ are assumed to be negligible so that the pressure drop term in equation (37) is a measure of lost work due to friction lw_f . Equation (37) permits evaluation of $U_i A_i$ from either

➤ Direct pressure drop measurements i.e.

$$U_i A_i = \frac{\dot{n} C_{P_i}^L \Delta T + \dot{m} \Delta P_i / \rho_i}{(\Delta T)_{LMi}} \quad (38)$$

or

➤ Estimates of frictional lost work ²¹ i.e.

$$U_i A_i = \frac{\dot{V} / M_r (\rho_{1i} C_{P1i}^L \Delta T_{1i} - \rho_{2i} C_{P2i}^L \Delta T_{2i})}{(\Delta T)_{LM1i} - (\Delta T)_{LM2i}} \quad (39)$$

where (1) and (2) are two different but close temperatures either above or below water bath temperature.

Once $U_i A_i$ has been found for a particular fluid and flowrate, $(\Delta T)_{LM}$ and hence q_{CV} can be determined simply from the terminal temperatures of a module. The frictional lost work term can, likewise, be determined directly from pressure drop measurements or else from the equation

$$\dot{m} l w_f = \dot{n} C_P^L \Delta T + U_i A_i \Delta T_{LM} \quad (40)$$

Hei and Raal ²¹ found the magnitude of $l w_f$ insignificant compared to that of q_{CV} for all liquids they used. Furthermore, convective heat losses were found to increase with fluid flowrate.

3.7.3.2.3 Evaluation of C_p

The unknown molar heat capacity of a fluid can be determined from the experimental equation

$$Q - q_{HL} - q_{CV} = \dot{n} C_P^L \Delta T + \dot{m} \Delta P / \rho \quad (41)$$

where q_{HL} and q_{CV} are functions of unknown C_p^L

Despite C_p^L being the only unknown variable in equation (41), no algebraic method exists for solving this type of equation. This is due to fact that the exponential nature of the abovementioned q_{HL} correlation ²¹ results in C_p^L being implicitly defined in equation (41). Hei and Raal ²¹ successfully employed numerical methods (numerical iteration) in solving equation (41) for C_p^L .

3.7.3.2.4 Design features to reduce conductive heat losses

As stated previously, conductive heat losses can be as high as 20 % of the total energy input and are considerable greater at the calorimeter exit as described above. To counter conductive heat losses at the exit, Hei and Raal ²¹ proposed looping of the heater ribbon so that the copper

wires enter and exit the vessel on the fluid inlet flow side. This feature should ensure that most of the heat that would have otherwise escaped into the external surrounding is absorbed by the cooler influent liquid stream.

3.7.3.2.5 Prominent heat capacity flow calorimeter designs

Picker et al.³⁴ pioneered the technique of non-static calorimetry for determining thermophysical properties of liquids. The latter's design was based on the principle of thermal balance i.e. for equal power input and fluid flow rates in both modules, the observed difference in temperature ΔT is solely a function of the difference in fluid heat capacities. The reported overall uncertainty in solution heat capacity measurement using this instrument is 0.5 %.³⁴ For a single experimental run, approximately 4 cm³ of solution are consumed.³⁴ Similar to the Picker et al.³⁵ heat of mixing calorimeter, steady state conditions could be attained in less than 1 minute. Even though the Picker et al.³⁴ calorimeter exhibits satisfactory accuracy and measurement rapidity, Hakin and Bhuiyan⁶¹ report that measurements made using this instrument are limited to ambient pressures and temperatures in the neighbourhood of $278 \leq T \leq 343$ K. Immediate improvements to the Picker et al.³⁴ design were made by Smith-Magowan and Wood⁶² and Rodgers and Pitzer.⁶³ The latter were the pioneers of high temperature and pressure aqueous solution heat capacity measurement using flow calorimetry. Valyashko and Gruszkiewicz⁶⁵ state that modifications such as the Smith-Magowan and Wood⁶² design enable measurements in the range $320 \leq T \leq 603$ K and pressures in excess of 175 atm to be made. The former also reported that, using the high temperature and pressure modifications of the Picker et al.³⁴ calorimeter, the ratio $C_P^L/C_{p,o}^L$ can be determined with an uncertainty of 0.01 %. Rodgers and Pitzer⁶³ reported a high temperature and pressure completely automated twin module flow calorimeter for C_P^L measurement of concentrated aqueous electrolyte solutions. Using this design, measurements at 700 K and 400 atmospheres can be performed with an uncertainty of 0.03 % in the determination of $C_P^L/C_{p,o}^L$.

Chapter 4

4.0 Equipment Design and Operation Procedure

The present flow calorimeter design is based on the original design by Raal and Webley.²⁴ Design features of a heat of mixing calorimeter and heat capacity calorimeter described in the previous chapter were merged in the development of this design. To this end, the following design features have been incorporated:

Differential mode of operation

The differential mode of operation serves to simultaneously account for viscous flow heating and heat leaks incurred during fluid mixing. Thus, excess enthalpy measurements can be made accurately. It further allows the reference module to be used for heat capacity measurements.

Robustness

Robust modules consisting of reinforced Teflon bodies, coupled together using stainless steel screws. The fragile glass vacuum housing^{21, 24} has been replaced by a much stronger PVC tube.

Looped static mixer/heater

A highly efficient motionless mixer/heater, in a novel looped configuration, blends the liquids with resultant low pressure drop, and addresses the persistent conductive heat leak problem in flow calorimetry for heat capacity measurements.

RTD sensors

Thermistor detectors^{23, 24} have been replaced by more stable and accurate resistance temperature detectors in the form of Pt-100 sensors.

Pt-100 sensor holders

Thin-walled leak-proof, tailor-made Pt-100 sensor holders were machined to anchor the glass bulb sensors firmly into the flow path. The metal mass was kept to a minimum to improve temperature response times.

Wider flow path

Narrow 1.588 mm (O.D) flow tubing^{23, 24} has been replaced with thin walled 3.175 mm (O.D) tubing. This feature serves to minimize fluid pressure losses while maintaining reasonably low reagent consumption and time constants (rapid instrument response).

Absolute pressure transmitters

The differential pressure transducers used in previous models^{23, 24} have been replaced by absolute pressure transmitters. The latter, connected through crossover valves, enable measurement of not only pressure differential across each module but absolute pressure at designated points in the apparatus as well.

Two water bath systems

A two water bath system enables fluid systems to be circulated through two different

temperature environments. These are required for measuring convective heat losses by controlling the fluid temperature from the second bath to a value different from that of the main bath. The additional bath also functions as a temperature re-equilibration option.

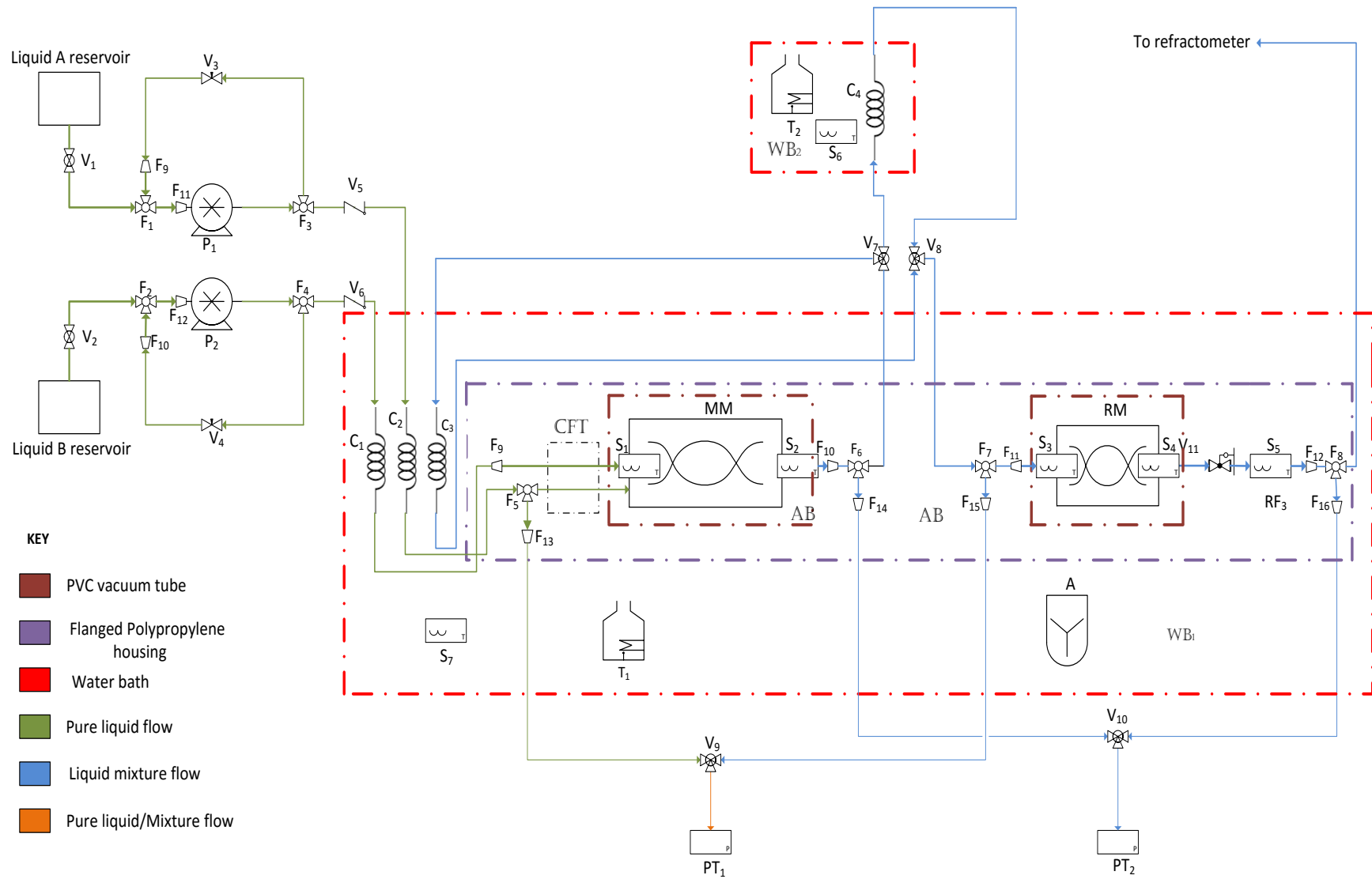
Gear pumps

Reciprocating pumps ^{21, 23, 24} have been replaced by gear pumps which provide pulseless discharge suitable for sensitive electronic circuitry.

Data acquisition system

System temperatures and pressures in the current design are monitored using a modern state-of-the-art programmable input/output data acquisition unit, replacing the analog detector circuits based on Wheatstone's bridges ^{23, 24} and digital multimeter readouts ²¹, employed in previous calorimeter models.

Figure 5: Piping and Instrumentation Diagram of the calorimeter



KEY:

MM - Mixing module

RM - Reference module

WB - Water bath

AB - Air bath

CFT - Coaxial flow tubing

P1, P2 - Ismatec microgear high pressure pumps for liquids **A** and **B** respectively

C1-C4 - 3.175 mm (O.D) stainless steel passive heat exchanger equilibration coils

T1, T2 - PolyScience temperature controllers

A - Overhead mechanical agitator

S1-S7 - Wika platinum resistance thermometers

PT1, PT2 - Wika pressure transmitters

V1, V2 - Swagelok stainless steel ball valves (1/4 inch tube ends)

V3, V4 - Swagelok stainless steel metering valves (1/8 inch tube ends)

V5, V6 - Swagelok stainless steel Poppet check valves (1/4 inch tube ends)

V7, V8 - Swagelok stainless steel 4-way ball valves (1/8 inch tube ends)

V9, V10 - Swagelok stainless steel 4-way ball valves (1/16 inch tube ends)

V11 - Swagelok PFA 40 series ball valve (throttling valve) (1/4 inch tube ends)

F1 - F2 - Swagelok PFA compression "Tee" union fittings (1/4 inch tube ends)

F3 - F8 - Swagelok stainless steel compression "Tee" union fittings (1/8 inch tube ends)

F9 - F12 - Swagelok stainless steel reducing union fittings (1/4 inch * 1/8 inch tube ends)

F13 - F16 - Swagelok stainless steel reducer fittings (1/8 inch * 1/16 inch tube ends)



Figure 6: Layout of various components of calorimeter apparatus

4.1.1 The liquid flow path

The description given below makes reference to the piping and instrumentation diagram shown in Figure 5. Liquids are initially stored at room temperature in their respective reservoirs. When valves V_1 and V_2 are opened, the liquids are drawn into 6.35 mm (O.D) stainless steel tubing and into their respective pumps P_1 and P_2 . The latter discharge a low pressure flow through 3.175 mm (O.D) stainless steel tubing into the calorimeter apparatus. Fluid by-pass channels around both pumps serve as overpressure protection and feed flowrate control. Check valves, V_5 and V_6 , are positioned immediately downstream of the pumps to prevent backflow of either pure liquid onto the other during circulation of one liquid. Prior to entering the calorimeter, the influent liquids **A** and **B** pass through 3.5 m of heat exchanger coils C_1 and C_2 immersed in thermostatted water bath WB_1 . The liquids then enter the calorimeter apparatus as shown in Figure 5. The calorimeter apparatus consists of all equipment components contained in the flanged polypropylene housing. Upon entering the polypropylene housing, pressure tappings through fittings F_5 , F_6 , F_{13} , F_{14} and crossover valves V_9 and V_{10} facilitated measurement of liquid pressure drop across MM. A 30 mm long concurrent heat exchanger (CFT), fabricated from concentric 9.525 mm (O.D) stainless steel and 6.35 mm (O.D) stainless steel tubing, is interposed between branches of feed stream lines (Figure 9). The heat exchanger serves to eliminate minor liquid temperature differences which may be present after equilibration in coils C_1 and C_2 (important in binary system measurements). After passing through CFT, liquid **B** splits into two streams with 3.175 mm (O.D) PFA electrical break fittings interposed along each stream, and is injected into mixing cells in MM. Fluid **A** enters MM through 6.35 mm stainless steel tubing, flows into the Teflon body of MM then finally mixes with **B** in the PFA mixing tubing. Liquid **A** inlet temperature (equal to **B**) is sensed by S_1 . The mixed product exits MM through a 6.35 mm (O.D) flow channel where its temperature is sensed by S_2 , after which the size of the flow path is reduced back to 1.588 mm [or 3.175mm (O.D) size tubing] in order to keep the equipment reagent consumption low. The mixture product then flows into V_7 where it is directed either to C_3 in WB_1 or C_4 in WB_2 for temperature re-equilibration. Re-equilibrated liquid product flows into V_8 where it is directed to RM where it flows in similar channels as **A** in MM. Liquid inlet and exit temperatures to RM are detected by S_3 and S_4 respectively, while pressure tappings through fittings F_7 , F_8 , F_{15} , F_{16} and valves V_9 and V_{10} provide means for measuring pressure drop across RM. The exiting mixture is throttled by V_{11} , after which its temperature is sensed finally by S_5 before the flow path diameter is reduced again to 1.588 mm. Samples may be withdrawn at the end of the flowpath for density and refractive index analyses

otherwise a pure liquid is recirculated by directing the calorimeter exit stream back to the reservoir.

4.2 Details of construction

4.2.1 Ismatec microgear pumps

Ismatec microgear pumps (P_1 and P_2 in Figures 5 and 6) were selected for pumping liquids from their respective reservoirs. The selected type of Ismatec microgear pump consists of two components i.e. an analog REGLO-Z model pump drive (control unit) and a REGLO-Z pump head. The pump utilizes a magnetic coupling between a hollow cylindrical driving magnet on its front side and a pump drive screwed onto it to create a mechanical force which drives microgears inside the pump head. A REGLO-Z pump head (model Z-181) was selected for use with the REGLO-Z controller. This pump head is a suction shoe type of pump head driven by graphite microgears capable of delivering a continuous, reproducible and pulseless discharge.⁷⁰ The gears deliver a constant 0.042 ml/min per revolution, adjustable in steps of 1 rpm (2.1 ml/min) regardless of system pressure. This translates to a minimum and maximum volumetric flowrate of 2.1 ml/min and 210 ml/min respectively.⁷⁰

Bypass channels around pumps P_1 and P_2 were incorporated using fittings F_1 - F_4 , F_9 , F_{10} as well as valves V_3 and V_4 .

The bypasses served the following purposes:

- i. Providing auxiliary flow paths with lesser resistance to flow. Since the selected REGLO Z-181 model does not possess an internal bypass mechanism, an external one was designed to guard against exceeding permissible pressures. The metering valves V_3 and V_4 were used to provide fine control of flowrates hence pressure on the discharge lines
- ii. Allowing splitting of large pump head discharge increments of 2.1 ml/min to smaller values so as to increase the number of different mixture compositions that can be produced during measurements of binary systems. Metering valves (V_3 and V_4), with repeatable flow adjustment Vernier handles, were used to retain a portion of pumps discharge with $1/25^{\text{th}}$ of a turn accuracy

It was found necessary to provide sufficient available pressure to overcome head losses in tubing and fittings and possibly cavitation. This was achieved through

- Elevating the 1 litre stainless steel liquid reservoirs a few centimeters above the pump level. This provided adequate head to drive liquid into the pump and ensured that a Net Positive Suction Head was maintained for all types of liquids
- Making the suction lines twice as wide (6.35 mm O.D) as the discharge lines. This guarantees decrease in suction line pressure drop

4.2.2 Temperature equilibration

4.2.2.1 Design and performance of coils

Influent liquids were pumped into equilibration coils C_1 and C_2 immersed in WB_1 . C_1 and C_2 were constructed by coiling 3.5 m lengths of 3.175 mm (O.D), 316 stainless steel tubing into two helices having nominal radii of 100 mm. The coil lengths, estimated from guidelines given by Raal and Webley²⁴, were adequate in ensuring close temperature approach of liquids of widely varying properties and flowrates to the bath temperature. Temperature defects on the tube side fluid were observed to decrease with:

- Increase in coil length
- Increase in fluid volumetric flowrate
- Increase in fluid thermal diffusivity

Although heat exchanger coil length could be further elongated to optimize temperature equilibration, the consequent rise in pressure drop limited coil length to practically viable values of approximately 3.5 m. Similarly, extremely high flowrates (≥ 30 ml/min) created pressure build-up within the modules beyond permissible equipment working pressures leading to mechanical wear and fluid leakage particularly around Teflon sections of the apparatus.

4.2.3 Design and performance of water baths

The design and construction/selection of water baths was influenced mainly by the following factors;

- The need to fully submerge the entire calorimeter apparatus and/or the heat exchanger coil(s)
- The need to have uniform temperature distribution throughout the water bath at any set thermostat value
- The need to have high heat transfer rates to the immersed heat exchanger coil(s)
- The need to minimize heat losses to the surroundings thus enabling higher operating temperatures to be attained

4.2.3.1 Water bath 1

A 600 mm deep insulated water bath was specially constructed by Laboratory Equipment and Supplies, as baths of such great depths were not readily commercially available. This depth was found sufficient to totally submerge the polypropylene cylinder housing the calorimeter apparatus. The 400 mm long and wide robust bath, constructed from stainless steel metal sheets, had a massive internal capacity of 96 litres. A PolyScience immersion heater/circulator (Model 7306), clamped centrally along the bath wall (Figure 6) was used to control/thermostat the water bath temperature to within ± 0.05 °C. The large capacity of this bath however restricted the maximum attainable temperature using a PolyScience 7306 model on an uncovered water bath to a value less than 50 °C.⁶⁶ Polystyrene chips were used to effectively cover the bath top surface resulting in approximately 10 °C rise in highest bath attainable temperature. An IKA RW 14 basic overhead stirrer with two 90 mm long paddles (spaced 100 mm apart) was mounted on the top edge of the bath. The stirrer, set at constant rotational speed of 500 revs/min, maintained turbulent conditions in the bath for optimizing heat transfer to the equilibration coils and temperature uniformity. Water bath tests, with the overhead stirrer, revealed that both horizontal and vertical bath temperature gradients became negligibly small (< 0.01 °C) while the time taken for the water to reach heater temperature was shortened. The temperature of the bath was monitored by sensor S₇ which was supported by 12.7 mm (O.D) stainless steel tube holder. Silicon oil was used to fill the air gap between the holder wall and the temperature probe.

4.2.3.2 Water bath 2

This 27 litre bath was fabricated in the workshop using stainless steel metal sheets. The bath was made by inserting a smaller metal box (300 mm*300 mm*300 mm) into a larger one (400 mm*400 mm* 400mm). The resulting 100 mm gap between the walls of the sheets was filled with thick insulation that effectively minimized heat transfer through the walls. A PolyScience immersion heater/circulator (Model 7306), similar to the above-mentioned, was used to control the bath temperature. Due to the smaller bath capacity, there were no observable temperature gradients. The bath temperature was monitored by sensor S_6 which was supported likewise by a similar sized stainless steel holder.

4.2.4 Polypropylene housing



Figure 7: Flanged polypropylene tube that housed calorimeter modules

The figure shown above is a picture of a calorimeter housing fabricated from a polypropylene tube of 5 mm wall thickness. The base of the tube was sealed while its top terminated with a flange which was glued to the tube. A polypropylene lid sealed the flanged end of the tube through stainless steel bolts and nuts. A Viton O-ring, positioned between the lid and the flange, provided a water-tight seal. Leak-free Swagelok compression male fittings, screwed on top of

the lead, provided inlet and exit for pressure tubing, module feed and discharge stream tubing and electrical wiring tubing respectively (Figure 8). PDT pipe clips, each supported by a stainless steel arm bolted to the supporting stainless steel bath frame, held the polypropylene tube firmly at its top and bottom within the bath.

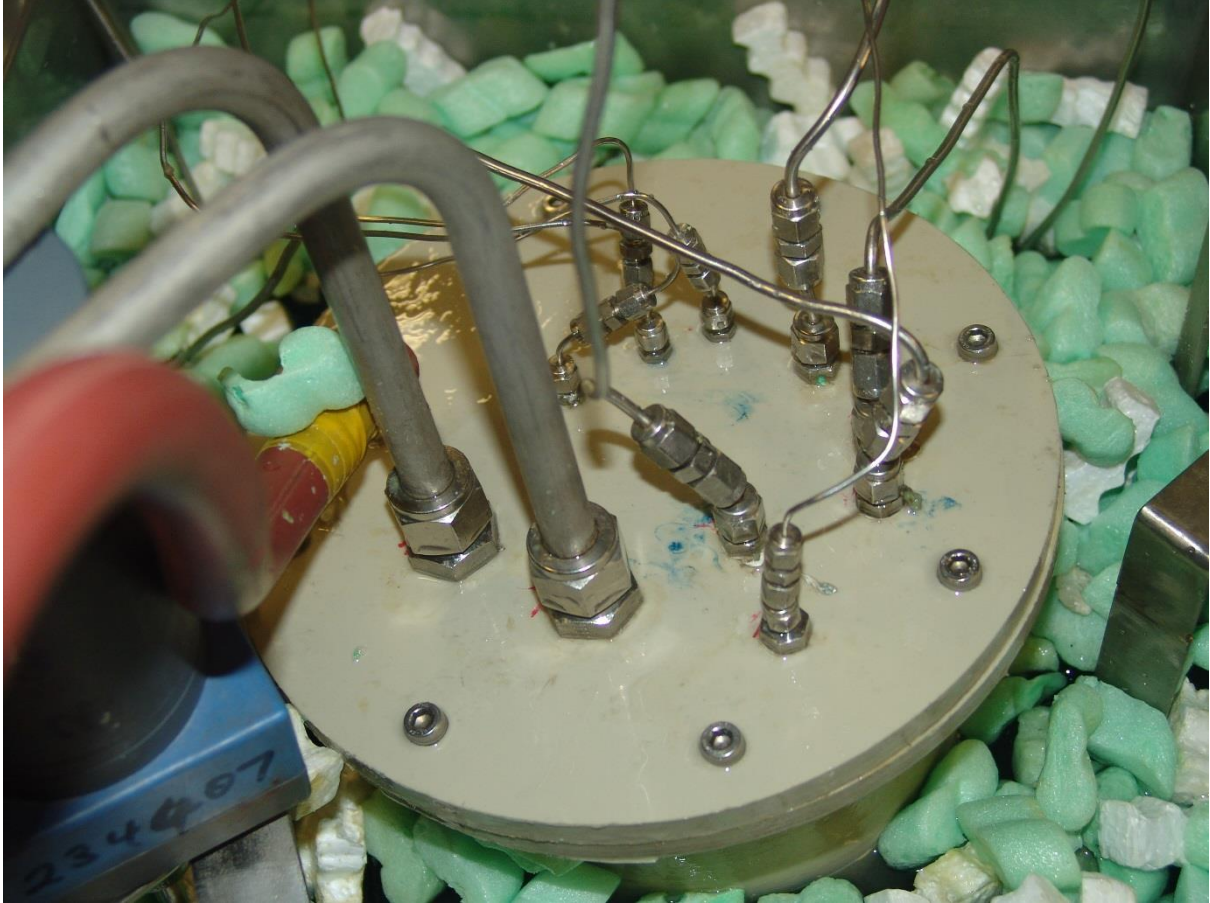


Figure 8: Closed propylene housing partly immersed in water bath

4.2.5 Calorimeter modules

A number of calorimeter module designs were tried before a final one was reached. Only construction details of the latter will be described.

4.2.5.1 Mixing module

Figure 9 below shows a longitudinal section through the mixing and associated tubing.

FIGURE 9

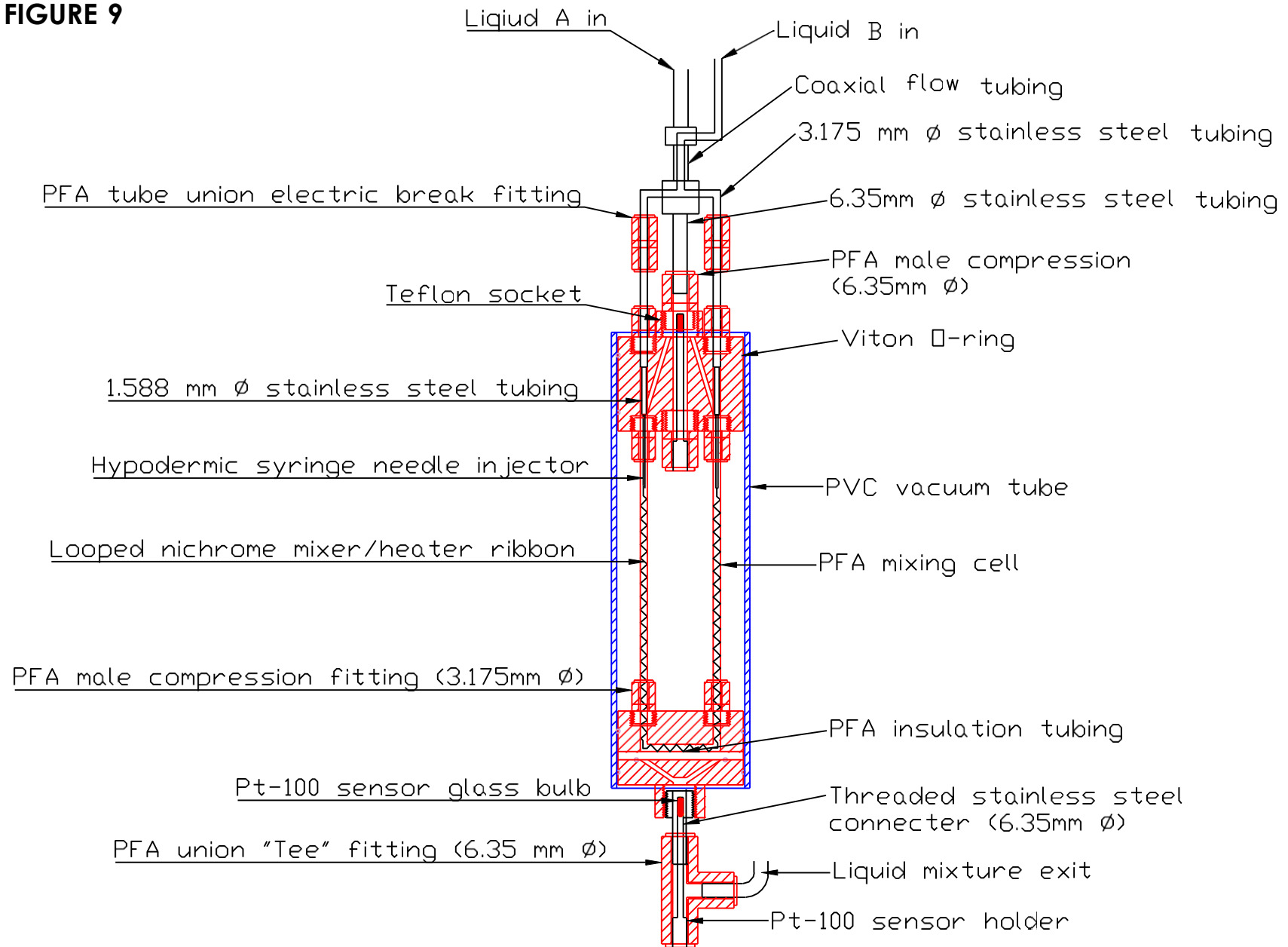




Figure 10 shows Mixing module (Left) and Reference module (Right) assembled together (without Pt-100 sensors)

The mixing module (MM) is the main unit of the calorimeter and hence a detailed description will be given. The features of MM shown in Figure 10 above can be divided into six main sections i.e.

The top piece

This section includes a PTFE Teflon body on the fluid entrance side and the fittings attached to it. The top piece was fabricated from a single 67 mm diameter, 51 mm thick glass-reinforced PTFE Teflon cylindrical block. The latter construction material is strong and rigid and thus, unlike pure Teflon, does not deform under calorimeter working pressure (<500 kPa) to create fluid leakage pathways. The Teflon block diameter was trimmed down along its length from the top to create an elevated socket on the Teflon surface. Thermal isolation of the module at

the top was facilitated by O-rings around the circumference of the cylindrical block which provided an air-tight seal between the Teflon block and vacuum tube. A 6.35 mm wide flow channel, spanning from the base of the socket through to the bottom of the cylindrical block, accommodated the Pt-100 stainless steel holder (housing an inlet temperature sensing Pt-100) as shown in Figure 9. Two vertical channels on either side of the socket provided pathways for injectors through which liquid **B** entered the mixing cells. Two oblique channels on either side of the holder channel, facilitated liquid **A** feed via the socket to flow into annuli of injector channels leading to the mixing cells (Figure 9). A third vertical channel through the cylinder block allowed exit of the Pt-100 sensor leads.

Mixing cells

These were fabricated from a 1000 mm long, 3.175 mm (O.D) PFA tubing. The long mixing path, susceptible to significant heat generation from larger pressure drop, was split into two 500 mm long streams as shown in Figure 9. A static heater/mixer element was fabricated from a flat nichrome ribbon. The mixer was constructed by twisting the ribbon at 3 mm intervals in an alternating clockwise and anticlockwise manner to form numerous mixing elements. One end of the mixer/heater was flush-fitted through one narrow PFA tubing length, passed through the bottom piece Teflon body path and finally flush-fitted through the second PFA tubing length forming a novel looped configuration shown in Figure 9. The pair of mixing cells were brought together, coiled and tied to form compact modules (Figure 10). The ends of the mixer/heater were silver-soldered to the protruding syringe needle ends of the injectors to form electrical connections, which also inevitably facilitated some heat conduction to the surroundings. Looping of the mixer/heater therefore enabled countercurrent absorption of conductive heat leaks via injector electrical contact by the influent liquid streams. Although modules in this design were not evacuated by drawing a vacuum, convective heat losses were nevertheless minimized by thermally isolating the modules using PVC vacuum tubes.

The bottom piece

This refers to the exit section of the module and consisted of a PTFE body, stainless steel connector as well as associated PFA fittings. A 67 mm diameter, 35 mm thick glass-reinforced PTFE cylindrical block was reduced likewise to form an equally sized socket at its base. The block was divided along its diameter to produce two asymmetrical sections in order to create a path for looping the nichrome ribbon. Mixed product from the mixing cells exited through two Teflon channels on the upper section. These channels were connected, on the lower side of the upper section, by a groove through which the continuous mixer/heater ribbon passed. A piece of PFA tubing insert, positioned in the groove, functioned to insulate the heater ribbon from

the PTFE body. Two oblique channels on the lower section facilitated discharge of the mixed product from the bottom piece via the socket at its base as shown in Figure 9. The two asymmetrical sections were coupled together using four stainless steel screws and nuts while a Viton O-ring was employed in fluid-tight sealing of the two surfaces. A Swagelok PFA “Tee” fitting was used in supporting a stainless steel Pt-100 sensor holder (housing exit fluid sensing Pt-100). A thin walled stainless steel connector, screwed to the bottom socket, facilitated coupling of the “Tee” fitting to the bottom piece (Figure 9). The bottom piece was then coupled to the top piece using stainless steel screws and nuts to form a robust and compact module that could easily be slid as a unit into the PVC vacuum tube. Plastic wrappings around the threaded stainless steel screws protected the PFA mixing cells from the abrasive screw surfaces.



Figure 11: Stainless steel holder used for anchoring Pt-100 sensor in flowpaths

Pt-100 sensor holder

Five stainless steel Pt-100 sensor holders were tailored to fit into the 6.35 mm diameter PFA fitting flow channels. The holders were fabricated from 6.35 mm diameter stainless steel rods. Each rod was bored longitudinally from one end to approximately 2 mm away from the opposite end to create a 3 mm (I.D) hollow path. The outer wall of the rod was then reduced along its diameter to 4.5 mm from the sealed end for approximately three quarters of the rod's length. The resulting 1.5 mm wall thickness offered minimal resistance to heat transfer and

ensured rapid sensor response. Attempts to further reduce the rods' wall thickness resulted in perforation of the thin walls and damage to the holders. The 6.35 mm (O.D) holder end was gripped by the ferrules of the PFA fitting to anchor it firmly in the flow path. Dead spaces which could accommodate stagnant liquid pockets between the fitting and holder were filled with Teflon tape. All the Pt-100 holders were installed with the only metal-to-Teflon contact being through the small ferrules to reduce/eliminate temperature gradients from conductive effects. Pt-100 glass bulb sensors were fitted into the holders through the open ends until the bulbs rested on the sealed end while its leads exited through the open ends. A heat transfer paste provided good thermal contact between sensor bulb and holder wall.

Injectors

These were constructed by joining in series short lengths of stainless steel tubing of 3.175 mm (O.D) and 1.588 mm (O.D) to 0.8 mm (O.D) hypodermic syringe needles. The three lengths were arranged in decreasing diameter order and brazed together to form strong leak-proof joints. The 3.175 mm (O.D) injector ends were connected to the feed tubing through Swagelok PFA union straight fittings. The interposed 1.588 mm (O.D) tubing provided clearance of the injectors from 3.175 mm diameter vertical Teflon channels thus facilitating liquid **B** to flow through the annular paths. The injectors terminated with hypodermic syringe needles of approximately 0.13 mm² internal cross sectional area which extended a few millimetres into the PFA mixing cells leaving sufficient clearance for liquid **A** flow as well. The extremely narrow injector terminals, discharged thin, high velocity jets of liquid **B** into mixing cells thereby enhancing dispersion of liquid **B** into liquid **A**.

PVC vacuum housing

The PVC tubes shown in the Figure 12 below were used in thermal isolation of the calorimeter modules. The semi-transparent tubes of 4 mm wall thickness served minimizing heat transfer through conduction and convection via the two PTFE bodies of the modules. The modules were fitted tightly into the vacuum housing by sliding one end through with the aid of a silicon lubricant.



Figure 12: The two PVC vacuum tubes used for housing calorimeter modules

4.2.5.2 Reference module

The reference module (RM) was identical in construction to the mixing module. The mixing cells were however deliberately constructed 10 mm shorter in length resulting in fluid streams experiencing slightly lesser pressure drop than in MM. The latter would then be compensated for using the downstream throttling valve. Furthermore, stainless steel injectors in RM functioned merely as heater leads since the feed to RM entered solely via Teflon body paths (similar to those of liquid A in MM).

4.2.6 The heating circuit

The fairly simple heating circuit for each module comprised a resistor (nichrome heater) and an ammeter connected in series to the same DC power source. The MM circuit featured, in addition, electric break fittings.

DC power supply

A GW (model GPS 3030) DC power supply employed in this calorimeter design satisfied all power requirements for all experimental work carried out. The latter features variable voltage and current output with 30 V and 3 A being the respective maximum ratings. Current supply to the heater was adjusted by varying the voltage output.⁶⁸ This stable power supply to the heater was crucial in the establishment of thermal equilibrium during heating experiments.

Ammeter

A UNI-T (model UT60B) digital multimeter was employed in the measurement of current in the series heating circuit. This model is capable of measuring DC current within 0.4 mA to 10 A range. The same digital multimeter model was used to measure resistance of the two nichrome mixer/heater ribbons.

Resistance heater

15.1 Ω and 12.9 Ω nichrome 80 ribbons functioned as heat generation zones in modules MM and RM respectively. The small nominal temperature coefficient of resistance for nichrome 80 saw the heater resistance values remain practically constant over the working temperatures of the calorimeter. This implied that power input could simply be determined with sufficient degree of accuracy from Joule's first law.

Electrical break fittings

These Swagelok PFA union straight fittings, installed immediately downstream of the cocurrent heat exchanger on liquid B feed lines, electrically isolated the heating circuit from the entire apparatus as shown in Figures 9 and 10. The fittings were incorporated only in the first module circuit as injectors functioned as charge carriers in addition to being fluid pathways.

Heater leads

Stainless steel injectors of negligible electrical resistance were silver-soldered to the nichrome resistance heater to make electrical contacts. Electrical crimps were then silver-soldered along the 3.175 mm (O.D) sections of the injectors onto which insulated copper electrical extensions were soldered to make electrical contacts. The copper extensions, connected to the DC power source, exited the polypropylene housing via 12.7 mm (O.D) stainless steel tubing.

4.2.7 Detection system

This involves the electronic hardware and software that are involved in sensing, acquisition, transmission, processing and display of temperature and pressure variables.

4.2.7.1 Temperature sensors

Resistance temperature detectors (RTDs)

RTDs are the most accurate, stable and exhibit the most linear change in output signal with respect to temperature among available temperature sensing devices.⁷² Platinum Resistance Thermometers (PRTs) display the above mentioned desirable properties to a superior degree and have a wider operating temperature span than other RTDs.⁷² Class A Pt-100 sensors were found to be the most suitable devices for calorimeter fluid temperature sensing. RTDs are however subject to self-heating errors but these are minimal in modern electronic detection circuits. Two types of Class A Pt-100 sensors were therefore selected to suit two different measurement requirements i.e.

- WIKA glass resistors (for detecting temperature along fluid flow path)

These consist of a bifilar platinum wire that is fused inside a glass body measuring 2.7 mm (O.D) * 13 mm. By virtue of their relatively small size, they can easily be fitted into narrow fluid flow paths using suitably designed holders (Figure 11). Three wire connection leads were chosen for current supply and transmission of 4-20 mA analogue output.

- WIKA temperature probes (for water bath temperature detection)

These have the platinum element and leads enclosed in a stainless steel protective sheath. Their big sizes enable them to be used as stand-alone sensors and facilitate multiple lead wire connections to be made. Four wire Sheath type class A Pt-100 sensors were selected for measurement of bath temperatures T_6 and T_7 .

The relationship between electrical resistance and temperature for a Pt-100 sensor is described using the Callender-Van Dusen equation^{72,73} i.e.

$$R(T) = R_o[1 + AT + BT^2 + CT^3(T - 100)] \quad (42)$$

where $R(T)$ is the resistance at temperature T °C,

R_o is the nominal resistance (resistance at 0 °C)

and A , B and C are the RTD scaling constants

For temperatures greater than 0 °C, the constant C takes a value of zero so that equation (42) reduces to

$$R(T) = R_o[1 + AT + BT^2] \quad (43)$$

4.2.7.2 Pressure sensors

WIKA Absolute pressure transmitters

Two general purpose pressure sensors were selected for detecting system dynamic pressure at four points along the flow path. WIKA S-10 models of 0-16 bar (PT₁) and 0-10 bar (PT₂) spans were selected for pressure measurements.

4.2.7.3 Data acquisition unit

An advanced electronic unit capable of not only data acquisition and logging of calorimeter temperature and pressure variables but embedded control as well was selected. The embedded control feature was however not utilized in this project.

4.2.7.3.1 Compact RIO (cRIO) system

This is a high precision and sophisticated National Instruments (NI) reconfigurable embedded control and data acquisition system. The complete hardware of the selected data acquisition system included:

- a compact RIO 9073 chassis housing an FPGA chip and a real time controller
- C series I/O modules
- Constant voltage power supply

4.2.7.3.2 Reconfigurable NI cRIO 9073 chassis

This unit features up to eight slots for C series I/O module connection and an industrial processor integrated with a programmable FPGA chip. High level synthesis design software such as NI LabView offers simplified programming of FPGAs. Using NI LabView, simple logical block diagrams can be transformed into digital hardware circuitry. Graphical high level synthesis approach, in the form of the installed LabView (2013 version), allowed development of graphical codes to perform tasks equivalent to the early hardware-based approaches^{23, 24} involving Wheatstone's bridge, comparator (null detector) and so on. The on-board processor provides real time responses for control functions, data logging and analysis.⁷⁴ The NI 9073 chassis also is also equipped with a DRAM for embedded operation and non-volatile memory for data logging operations.⁷⁵ For connection and interaction with peripherals (including a host PC), the cRIO 9073 chassis is equipped with a single Ethernet and an RS232 serial port.⁷⁴

4.2.7.3.3 NI C series analog input modules

These hardware receive the input signals from the outside world and then perform conditioning and digitization processes. In cRIO systems, these hardware units are plugged directly into FPGA chassis. These modules feature built-in signal conditioning and isolation mechanisms that precede digitization.

NI 9217 analog input module

This is a four channel analog input module that supports only 3 and 4 wire, 100 Ω RTDs. Two NI 9217 modules were therefore selected for connecting the seven calorimeter PRTs. NI 9217 modules feature a remarkable resolution⁷⁷ which is crucial in resolving minute temperature differences hence current input differences associated with microcalorimetry. To counter the previously-mentioned problem of RTD self-heating, NI 9217 dissipates an excitation (sense) current of only 1 mA per channel.⁷⁷ The incorporated safety and isolation voltages ensured highly accurate temperature measurements.

NI 9203 analog input module

This is an eight channel analog input module compatible with current input in the range ± 20 mA.⁷⁹ A current loop enabled a sensor to source voltage directly from the DC power supply and transmit analog current signal to the NI 9203 module. Similarly, the high resolution of this module, together with built-in safety and isolation voltages, facilitated optimal acquisition of pressure sensors' output signal.

PR electronics transmitter isolator

Although National Instruments C series modules feature built-in signal conditioning and isolation mechanisms, pressure readings obtained from the S-10 sensors were highly unstable due to noise. A 2-channel PR 2-wire transmitter isolator (model 3186AI) was therefore connected in series between each pressure transmitter and the NI 9203 module to filter out noise contribution effects by eliminating ground loops.⁸⁰

4.2.7.3.4 DC power supply

A 24 V National Instruments (NI PS-15 model) DC power supply was selected to supply steady power to the NI 9073 chassis. This model was adequate in meeting the power needs of the chassis and well as powering the two pressure transmitters.

4.2.7.3.5 Host PC

A dedicated Proline Pentium 4 computer was selected for displaying digital output data from NI 9073 chassis. The system ran on a Microsoft Windows 8 operating system on which

important supporting softwares such as NI LabView and Microsoft Office 2013 packages were installed.

Chapter 5

5.0 Experimental procedure

5.1 Calibrations

5.1.1 Pump calibration

The current calorimeter, like the previous designs, did not incorporate a flow measuring device such as flow meter or hydrometer. The calibration procedure therefore involved weighing collected volumes of liquid over accurately measured time periods. Initial pump 1 calibration and testing of the equipment were performed using de-ionized water which entered the mixing module via stainless steel injectors. Water volumes were collected at the reference module exit while its temperature, and hence its density, were determined from sensor readings. Weights were measured to a very high degree of accuracy using the KERN (model ABT 100-5 M) analytical balance, while an Anton Paar (model DMA 5000) analog laboratory density meter was employed in measuring liquid densities. Subsequent pump 1 calibrations were performed using n-butanol and with flow entering the mixing module via the Teflon body path (section 4.2.5.1). Experimental measurements of pump 1 calibration are given in appendix E.

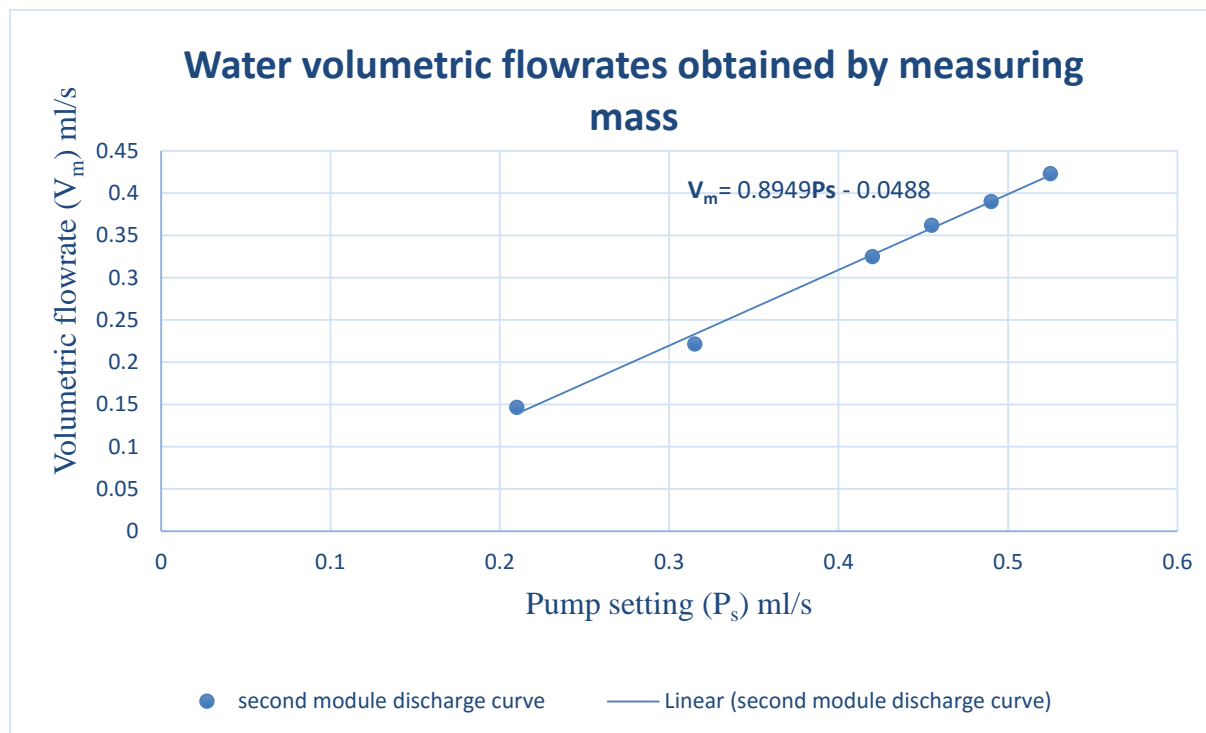


Figure 13 (a): Pump 1 calibration graph with De-ionized water as reference liquid

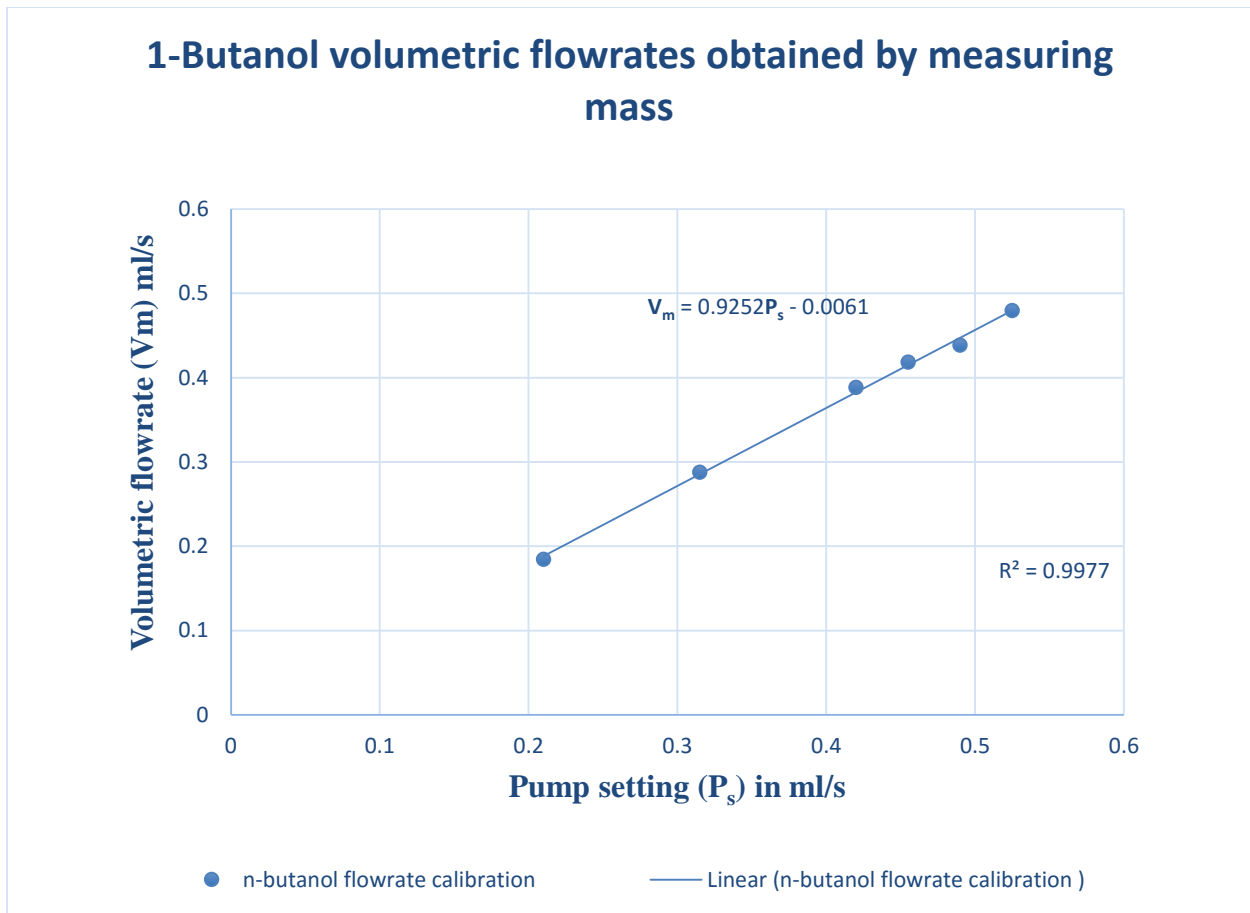


Figure 13 (b): Pump 1 calibration graph with 1-Butanol as reference liquid

5.1.2 RTD calibration

Calibration of PRTs can be performed using two methods i.e. characterization and tolerance testing.⁸³

5.1.2.1 Characterization calibration

This method involves empirically establishing a resistance-temperature relationship for each probe under test (PUT) by obtaining unique scaling/calibration coefficients. The following steps were followed in Pt-100 sensors' calibration;

- a) Tying the seven PUTs to the reference/standard probe (WIKA temperature calibrator) and ensuring close contact of the sensor heads
- b) Placing the probes in the WIKA standard bath. The bath cavity was flooded with silicon oil to ensure sufficient immersion of the probes
- c) Setting the NI 9217 modules using the installed NI LabView to display "Raw resistance" values for each probe on Labview project

- d) Noting “actual” standard probe real time temperature values on the connected WIKA readout
- e) Calculating average resistance values for each PUT corresponding to a stable (constant) standard probe temperature
- f) Fitting “actual” temperature-average resistance pairs of values to the Callender-Van Dusen equation (Equation 42) to obtain scaling coefficients and a nominal resistance (R_o) value unique to each PUT and calibration
- g) Entering and saving the unique calibration parameters for each PUT into LabView and finally setting the NI 9217 modules to display temperatures values

For reasons of accuracy, the calibration process was conducted beginning from the upper selected calibration temperature and working downwards. The variables described in (f) above were obtained for the test and subsequent calibration from Microsoft Excel quadratic plots of Resistance vs. Temperature. Actual experimental measurements of temperature calibrations as well as values of calibration parameters are given in appendix F. Sensor 5 was omitted after test calibration as its function is related to measurement of heats of mixing.

5.1.2.2 Tolerance testing

This type of calibration simply compares resistance output from a PUT with values defined by some standard (e.g. IEC 60751 or ITS-90) at the same temperature. In this project real time temperatures, instead, from the seven PUTs were compared with reference probe (still tied together in the standard bath) values after characterization and the results are displayed in appendix F. This procedure allowed evaluation of differences between the WIKA reference probe and the PUTs readings (uncertainty) and also differences between matched PUTs. The latter differences are crucial in the determination of actual temperature changes that take place during heat capacity and excess enthalpy measurements. Results of Pt-100 sensor tolerance testing are given in appendix G.

5.1.3 Pressure transmitter calibration

Pressure transmitters were calibrated in a similar manner to the Pt-100 sensors. A Swagelok stainless steel union “Tee” fitting was used in connecting the two WIKA S-10 absolute pressure transmitters to the reference transmitter [WIKA Mensor pressure controller (model CPC 8000)]. Since pressure varies linearly with transmitter output current, the calibration procedure was aimed at obtaining gain and uncertainty parameters for each transmitter. This involved, likewise,

- a) Setting the NI 9203 module to display “Raw current” values on the block diagram of LabVIEW project
- b) Noting “actual” real time absolute pressure values on the Mensor pressure controller
- c) Calculating average output current values for each transmitter corresponding to a stable calibrator pressure
- d) Fitting calibrator pressure (P)-average current (i) pairs of values for each transmitter to the function $P = gi + k$ to obtain unique gain (g) and offset (k) values for the calibration
- e) Entering and saving the calibration coefficients to the $P = f(i)$ function for each transmitter on the NI LabVIEW project block diagram

Actual experimental values and calibration results are given in appendix H.

5.1.3.1 Tolerance testing

After the transmitters had been calibrated using the above procedure, they underwent tolerance testing to determine, similarly, uncertainty and calibration correction factors. The tolerance testing procedure is parallel to that of the RTDs described above and the values of experimental measurements are given in appendix I.

5.2 Procedure for measuring pure liquid Heat Capacity

While convective heat losses and fluid friction could be determined relatively easier, a rigorous procedure for measuring/estimating heat losses through conduction had to be developed. Measurement of pure liquid molar heat capacity (C_p^L) proceeded via the following steps;

- a) Developing a correlation for conductive heat leaks as a function of volumetric flowrate, power input, fluid properties as well as calorimeter characteristics
- b) Designing and carrying out experiments to evaluate unknown constants for the correlation in (a) above
- c) Testing predicting capabilities of the developed heat leak correlation on each pure liquid
- d) Developing a universal conductive heat leak correlation that applies to fluids of widely varying thermophysical properties
- e) Applying the developed universal conductive heat loss correlation to measure molar heat capacities of each pure liquid using experimental equation (41)

5.2.1 Development of conductive heat leak correlation

A correlation for conductive heat leaks was developed from the dimensionless groups described in section 3.7.3.2.1 as follows;

- i. Developing a fourth dimensionless group by dividing group π_3 by group π_1 i.e.

$$\frac{\pi_3}{\pi_1} = \frac{\left[\frac{Q'' h B^2 f^3 (\Delta x_3)^2}{\dot{m} C_p^L k_m a T} \right]}{\left[\frac{h B f (\Delta x_3)}{\dot{m} C_p^L} \right]} = \left[\frac{Q'' B f^2 (\Delta x_3)^2}{k_m a T} \right] = \pi_4 \quad (44)$$

This step reduced the number of π groups sufficient to correlate q_{HL} to only two, that is, π_1 and π_4 . At this stage, the conductive heat loss correlation could be represented as

$$q_{HL} = \psi [\pi_1]^{n_1} [\pi_4]^{n_4} \quad (45)$$

where n_1 and n_4 are exponents associated with the π groups and ψ represents equipment properties (characteristic length, diameter etc.)

- ii. Factoring equipment constant f from group π_1 and constants $[B, f^2, (\Delta x_3)^2, a]$ from group π_4 into a single equipment term ψ reduced the correlation to

$$q_{HL} = \psi' \left[\frac{hB(\Delta x_3)}{\dot{m}C_p^L} \right]^{n_1} \left[\frac{Q}{k_m LT} \right]^{n_4} \quad (46)$$

where L is a length dimension on the heater ribbon

For convenience, all equipment terms were collected into ψ' i.e.

$$q_{HL} = \psi'' \left[\frac{h}{\dot{m}C_p} \right]^{n_1} \left[\frac{Q}{T} \right]^{n_4} \quad (47)$$

- iii. Selection of an appropriate heat transfer coefficient h correlation from literature. No correlation for h for the complicated flow path or heater arrangement could be found. However, a correlation used successfully by Hei and Raal ²¹, for characterising heat transfer from the heater to the tube wall, is that of Mills ⁴⁶ and was therefore adopted in this work i.e.

$$Nu = \frac{hD_{eq}}{k_L} = 3.66 + \frac{0.065 \left(\frac{D_{eq} \cdot Pe}{L_t} \right)}{1 + 0.04 \left(\frac{D_{eq} \cdot Pe}{L_t} \right)^{\frac{2}{3}}} \quad (48)$$

where $Pe = (\rho u D_{eq} C_p^L / k_L)$ and L_t is the length of the mixing tube

Substituting $(4\dot{V} / \pi D_{eq}^2)$ for u , α for the fluid property ratio $(k_L / \rho C_p^L)$ in equation (48) and simplifying yielded

$$h = \frac{k_L}{D_{eq}} \left[3.66 + \frac{0.065 \left(\frac{4}{\pi} \right) \left(\frac{\dot{V}}{\alpha L_t} \right)}{1 + 0.04 \left(\frac{4}{\pi} \right)^{\frac{2}{3}} \left(\frac{\dot{V}}{\alpha L_t} \right)^{\frac{2}{3}}} \right] \quad (49)$$

- iv. Substituting h in equation (47) with the expression in equation (49), factoring out unknown equipment constant D_{eq} , introducing equipment constant L_t and simplifying the expression yielded

$$q_{HL} = \psi''' \left[\frac{3.66 + \frac{0.065 \left(\frac{4}{\pi} \right) \left(\dot{V} / \alpha L_t \right)}{1 + 0.04 \left(\frac{4}{\pi} \right)^2 \left(\dot{V} / \alpha L_t \right)^{2/3}}{\left(\dot{V} / \alpha L_t \right)} \right]^{n_1} \left[\frac{Q}{T} \right]^{n_4}$$

$$= \lambda [\pi'_1]^{n_1} [\pi'_4]^{n_4} \quad (50)$$

Equation (50) represents the final form of the conductive heat leak correlation which can also be represented in a linear form using logarithms i.e.

$$\ln q_{HL} = \ln \lambda + n_1 \ln[\pi'_1] + n_4 \ln[\pi'_4] \quad (51)$$

5.2.2 Determination of exponents n_1 , n_4 and calorimeter properties λ

Three fluids of widely differing and well known properties (including heat capacity) were selected in the experimental work associated with evaluation of these three parameters i.e. de-ionized water, n-butanol and toluene. The following experimental procedure was designed for the measurement of the unknown correlation parameters i.e.

Determination of the overall heat transfer coefficient $U_i A_i$ (no heating of element)

Overall heat transfer coefficients across the reference module walls for each pure liquid were obtained as functions of volumetric flowrate by

- i. Setting crossover valve V_7 to direct flow towards C_4 (Figure 5) i.e. to divert flow to the 2nd water bath
- ii. Setting the temperature controller in water bath 2 a few degrees above water bath 1 temperature
- iii. Using pump 1 to circulate pure liquid along the flow path as described section 4.1.1

Each pure liquid was circulated around the apparatus until thermal equilibrium had been achieved, a process which took a minimum time of one hour depending on type of fluid and flowrate used. Initial measurements were made using de-ionized water with $U_i A_i$ estimated using equation (39), as proposed by Hei and Raal.²¹ In subsequent measurements using n-butanol and toluene, $U_i A_i$ was evaluated from measured pressure drop.

Measurement of conductive heat losses q_{HL}

“Heating experiments” were conducted which involved varying power input to the reference module at each pump setting. Power input Q was generally kept low enough to induce a temperature rise of not more than 2°C in the passing liquid. Knowledge of $U_i A_i$ values from preceding experiments allowed convective heat losses q_{CV} through module walls to be evaluated from equation (37). The latter, together with lost work due to friction lw_f values, were deducted from the total heat loss q_{total} in the computation of q_{HL} . Experimental values of q_{HL} from “heating experiments”, fluid properties and flowrate as well as power input were then fitted into linearized correlating equation (51) to evaluate the unknown exponents n_1 , n_4 and λ for each pure liquid. Values of exponents n_1 and n_4 for each liquid were obtained from the gradients of graphical plots while λ was evaluated from equation (51) (Chapter 6). The predictive capabilities of the conductive heat leak correlation, derived from each liquid, were then tested on all three liquids. The liquid whose parameters provided the best q_{HL} predictions was selected as the reference liquid.

5.2.3 Development of universal heat leak correlation

The selected heat transfer correlation above contains the Peclet number (a product of Reynolds and Prandtl numbers raised to equal exponents). This results in fluid viscosity variables cancelling out each other out and deprivation of the developed q_{HL} correlation of variation in fluid viscosity effects. To overcome this problem, the heat leak correlation was modified by incorporating an additional dimensionless group involving the viscosity ratio (μ_x/μ_R) i.e.

$$q_{HL} = \lambda \left[\frac{3.66 + \frac{0.065 \left(\frac{4}{\pi} \right) \left(\frac{\dot{V}}{\alpha L_t} \right)}{1 + 0.04 \left(\frac{4}{\pi} \right)^{2/3} \left(\frac{\dot{V}}{\alpha L_t} \right)^{2/3}}}{\left(\frac{\dot{V}}{\alpha L_t} \right)} \right]^{n_1} \left[\frac{Q}{T} \right]^{n_4} \left[\frac{\mu_x}{\mu_R} \right]^{n_5} = \lambda [\pi_1']^{n_1} [\pi_4']^{n_4} [\pi_5']^{n_5} \quad (52)$$

where μ_x and μ_R are the respective liquid under test and reference liquid average viscosities evaluated from literature polynomial temperature functions

With λ , n_1 and n_4 known (derived from reference liquid), fluid properties for each liquid were fitted into the universal conductive heat leak correlation (Equation 52). Several values of

exponent n_5 were then inspected to find a common one that provided best predictions of q_{HL} for all three liquids.

5.2.2.1 Measurement of heats of mixing

The procedure for measuring heats of mixing for the current differential flow calorimeter is the same as that previously described by Hei and Raal.²¹ Due to the extensive scope of the project, only details of work related to heat capacity measurements could be undertaken.

Chapter 6

6.0 Results and discussions

Experimental measurements were carried out as described in section 5.2.2 to determine the unknown conductive heat leak correlation parameters. The results of the experiments for each pure liquid are given below (sections 6.1 to 6.3). Results of the predicting abilities of the derived conductive heat leak correlation and its extended version (universal correlation) at various flowrates are shown in section 6.4. Molar heat capacities of the three liquids were calculated at various flowrates and temperatures (in the neighbourhood of 30 °C) from the same experiments used in the evaluation of conductive heat loss correlation parameters. Numerical iteration was applied in solving equation (41) for C_p^L , accurate to two decimal places (section 6.5). Due to the large volume of data and calculations involved in “heating experiments”, only sample results conducted at pump setting 15 are given in this chapter. Conductive heat leak experiment results for the three liquids at lower flowrates are given in appendices A, B and C.

Chemicals of the highest commercial grade as well as highly pure de-ionized water from the unit laboratory were used in this study. The purity of these reagents was determined by measurement of refractive indices and densities, and then comparing with literature values (Appendices A, B and C). The observed excellent agreement with literature values implied that the chemicals were of sufficient purity and hence were used without further purification.

6.1 Experimental fluid: De-ionized water

Table 1.2.0: Measurement of De-ionized water $U_i A_i$ values at various flowrates for lower temperature feed

Pump setting	\dot{V} (ml/s)	T_7 (°C)	T_6 (°C)	T_4 (°C)	T_3 (°C)	Corrected $T_4 - T_3$ (°C)	T_{mean} (°C)	$(\Delta T)_{LM}$ (°C)
6	0.1466	29.96	39.83	33.24	33.24	0.03	33.24	-3.2650
9	0.2218	29.96	39.84	34.57	33.62	-0.02	34.60	-4.6200
12	0.3249	29.95	39.83	35.32	35.48	-0.13	35.40	-5.4347
13	0.3623	29.96	39.84	35.81	36.04	-0.20	35.93	-5.9494
14	0.3901	29.96	39.83	36.07	36.32	-0.22	36.20	-6.2194
15	0.4230	29.96	39.84	36.25	36.50	-0.22	36.38	-6.3994

ρ (g/ml)	\dot{n} (mol/s)	C_p' (J/mol°C)	$U_i A_i$ (W/°C)
0.9946	0.0081	75.2340	0.0116
0.9942	0.0123	75.2340	0.0277
0.9939	0.0179	75.2340	0.0642
0.9937	0.0200	75.2340	0.0774
0.9936	0.0215	75.2340	0.0829
0.9928	0.0233	75.2340	0.0882

Table 1.2.1: Measurement of De-ionized water $U_i A_i$ values at various flowrates for higher temperature feed

Pump setting	\dot{V} (ml/s)	T_7 (°C)	T_6 (°C)	T_4 (°C)	T_3 (°C)	Corrected $T_4 - T_3$ (°C)	T_{mean} (°C)	$(\Delta T)_{LM}$ (°C)
6	0.1466	29.96	42.83	34.28	34.30	0.01	34.29	-4.3150
9	0.2218	29.96	42.84	36.21	36.31	-0.07	36.26	-6.2849
12	0.3249	29.96	42.82	36.97	37.21	-0.21	37.09	-7.1145
13	0.3623	29.96	42.83	37.70	38.03	-0.30	37.87	-7.8890
14	0.3901	29.96	42.83	37.97	38.32	-0.32	38.15	-8.1690
15	0.4230	29.95	42.83	38.18	38.53	-0.32	38.36	-8.3890

ρ (g/ml)	\dot{n} (mol/s)	C_p' (J/mol°C)	$U_i A_i$ (W/°C)
0.9943	0.0081	75.2340	0.0116
0.9946	0.0123	75.2340	0.0277
0.9933	0.0179	75.2340	0.0642
0.9930	0.0200	75.2340	0.0774
0.9929	0.0215	75.2340	0.0829
0.9928	0.023	75.2340	0.0882

C_p' is the literature molar heat capacity of water evaluated from the NIST ThermoML polynomial equation.⁹⁰

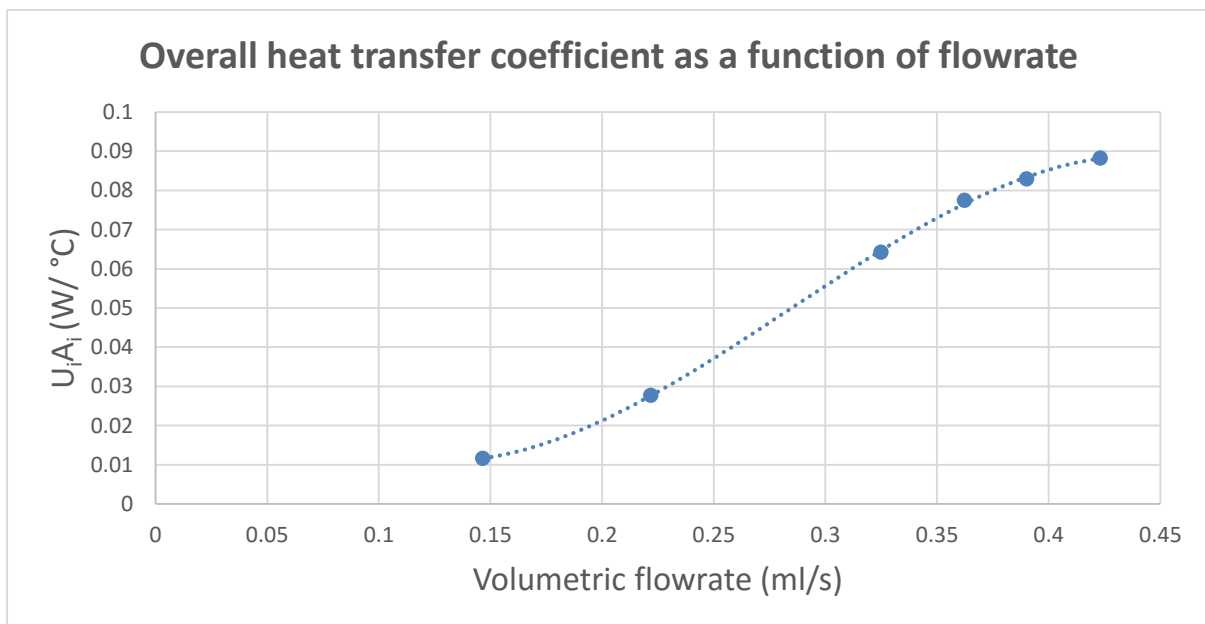


Figure 14 (e): Variation of De-ionized water overall heat transfer coefficient with flowrate

Table 1.3.4: Measurement of De-ionized water conductive heat losses at pump setting 15

\dot{V} (ml/s)	T_7 (°C)	T_6 (°C)	T_4 (°C)	T_3 (°C)	Corrected $T_4 - T_3$ (°C)	T_{mean} (°C)	$(\Delta T)_{LM}$ (°C)	μ_{wat}^* (mPa.s)	μ_{tol}^* (mPa.s)
0.4230	29.96	30.53	30.50	29.95	0.53	30.23	-0.1329	0.7946	0.5206
0.4230	29.96	30.42	30.59	29.95	0.62	30.27	-0.1496	0.7939	0.5203
0.4230	29.96	30.53	30.67	29.96	0.69	30.32	-0.1933	0.7931	0.5201
0.4230	29.96	30.42	30.87	29.97	0.88	30.42	-0.2579	0.7913	0.5194
0.4230	29.96	30.53	31.06	29.96	1.08	30.51	-0.2695	0.7898	0.5189

ρ (g/ml)	\dot{n} (mol/s)	C_p' (J/mol°C)	$U_i A_i$ (W/°C)
0.9956	0.0234	75.2340	0.0882
0.9956	0.0234	75.2340	0.0882
0.9957	0.0234	75.2340	0.0882
0.9956	0.0234	75.2340	0.0882
0.9957	0.0234	75.2340	0.0882

k^{**} (W/m K)	q_{cv} (W)	$\frac{\dot{V}}{\alpha L_f}$	Q_{ideal} (W)	Q (W)	q_{total} (W)	q_{HL} (W)	$\frac{q_{HL}\%}{Q}$
0.6151	-0.0117	7.1556	0.9330	1.0114	0.0783	0.0666	6.5842
0.6151	-0.0132	7.1548	1.0915	1.1610	0.0695	0.0563	4.8499
0.6152	-0.0171	7.1541	1.2148	1.3210	0.1062	0.0891	6.7486
0.6154	-0.0228	7.1520	1.5492	1.6718	0.1226	0.0999	5.9740
0.6155	-0.0238	7.1505	1.9014	2.0640	0.1626	0.1389	6.7277

$\ln q_{HL}$	π'_1	$\ln \pi'_1$	π'_4	$\ln \pi'_4$	$\ln \lambda$	Average $\ln \lambda$
-2.7092	0.5820	-0.5414	0.0335	-3.3974	1.5997	1.5160
-2.8769	0.5820	-0.5413	0.0384	-3.2609	1.2885	
-2.4175	0.5821	-0.5412	0.0436	-3.1333	1.6139	
-2.3038	0.5822	-0.5409	0.0550	-2.9012	1.4835	
-1.9743	0.5823	-0.5407	0.0676	-2.6934	1.5946	

* μ_{wat} and μ_{tol} are literature water and toluene viscosities evaluated from the NIST Thermodata Engine (TDE)⁹¹ and Santos et al.⁸⁶ equations respectively

** k is the literature water thermal conductivity evaluated from Ramires et al.⁹² equation.

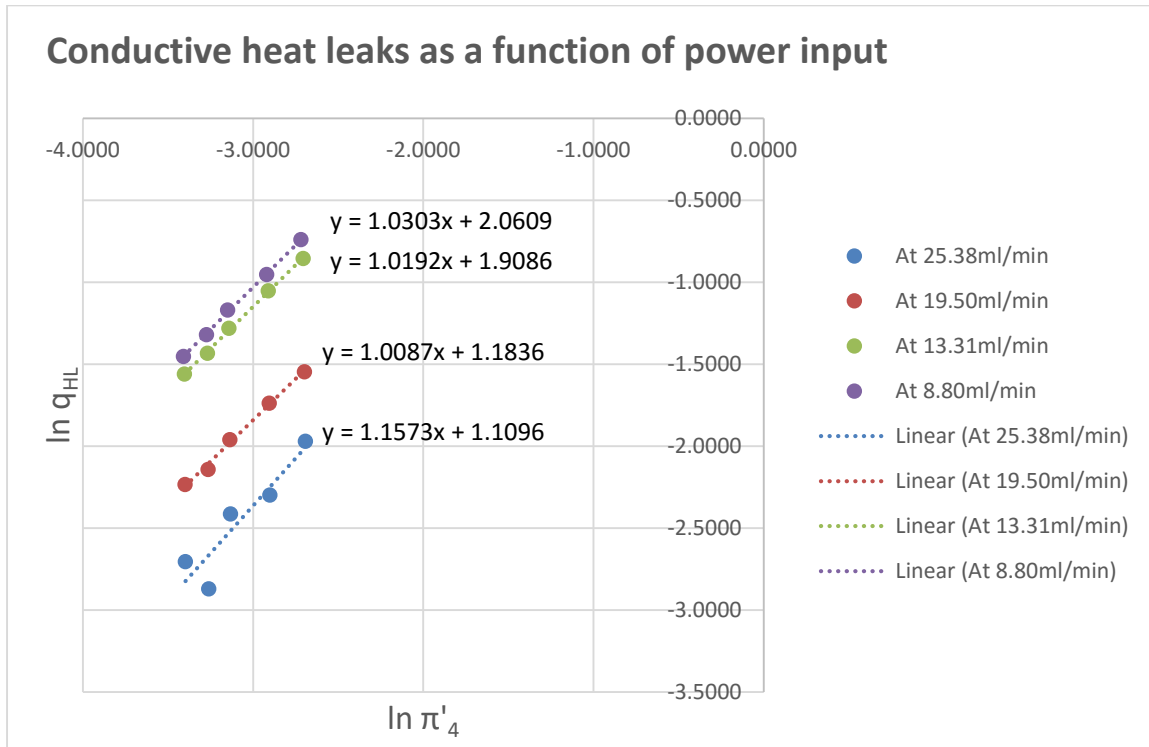


Figure 14 (f): Dependence of De-ionized water conductive heat leaks on power input (from equation 51)

Table 1.4: Evaluation of exponent n_4 for De-ionized water

Line 1 gradient	1.0303
Line 2 gradient	1.0192
Line 3 gradient	1.0087
Line 4 gradient	1.1573
Average gradient	1.0535

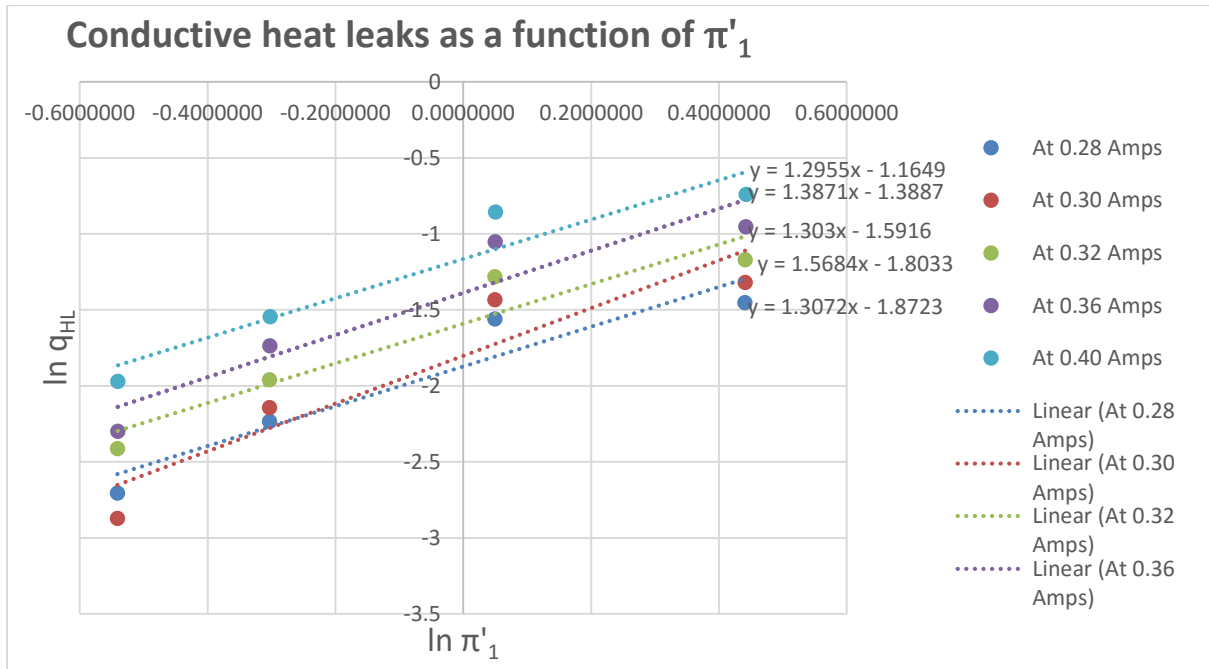


Figure 14 (g): Dependence of De-ionized water conductive heat leaks on flowrate (from equation 51)

Table 1.5: Evaluation of exponent n_1 for De-ionized water

Line 1 gradient	1.2955
Line 2 gradient	1.3871
Line 3 gradient	1.3030
Line 4 gradient	1.5684
Line 5 gradient	1.3072
Average gradient	1.3722

Table 1.6: Evaluation of calorimeter properties using De-ionized water

Pump setting	6	9	12	15
Average $\ln \lambda$ per pump setting	1.5169	1.9355	1.7258	1.5203
Average $\ln \lambda$ for all flowrates	1.6746			
λ	5.3366			

6.2 Experimental Liquid: 1-Butanol

Table 2.2: Determination of 1-Butanol $U_i A_i$ values at various flowrates

Pump setting	\dot{V} (ml/s)	T_7 (°C)	T_6 (°C)	T_4 (°C)	T_3 (°C)	Corrected $T_4 - T_3$ (°C)	T_{mean} (°C)	$(\Delta T)_{LM}$ (°C)
6	0.1846	29.97	39.84	32.33	32.63	-0.31	32.48	-2.5118
9	0.2880	29.97	39.84	33.67	33.87	-0.21	33.77	-3.8040
12	0.3885	29.97	39.84	34.58	34.88	-0.31	34.73	-4.7633
13	0.4184	29.97	39.84	34.78	35.13	-0.36	34.96	-4.9878
14	0.4388	29.97	39.84	35.04	35.41	-0.38	35.23	-5.2577
15	0.4796	29.97	39.84	35.23	35.59	-0.37	35.41	-5.4429

ρ (g/ml)	\dot{n} (mol/s)	ΔP (kPa)	ΔP correction factor (kPa)	Corrected $\Delta P / \rho$		C'_p (J/mol°C)	$U_i A_i$ (W/°C)
				(J/kg)	(J/mol)		
0.8033	0.0020	3.1224	3.5000	8.2436	0.6110	182.6871	0.0456
0.8023	0.0031	7.9176	3.5000	14.2305	1.0548	183.6742	0.0325
0.8016	0.0042	13.9348	3.5000	21.7502	1.6121	184.4148	0.0518
0.8014	0.0045	15.8696	4.0000	24.7933	1.8377	184.5891	0.0619
0.8012	0.0047	18.1173	4.0000	27.6052	2.0461	184.7986	0.0652
0.8011	0.0052	20.3471	4.0000	30.3930	2.2527	184.9424	0.0673

C'_p is the literature molar heat capacity of n-butanol evaluated from the cubic spline polynomial function.⁸⁴

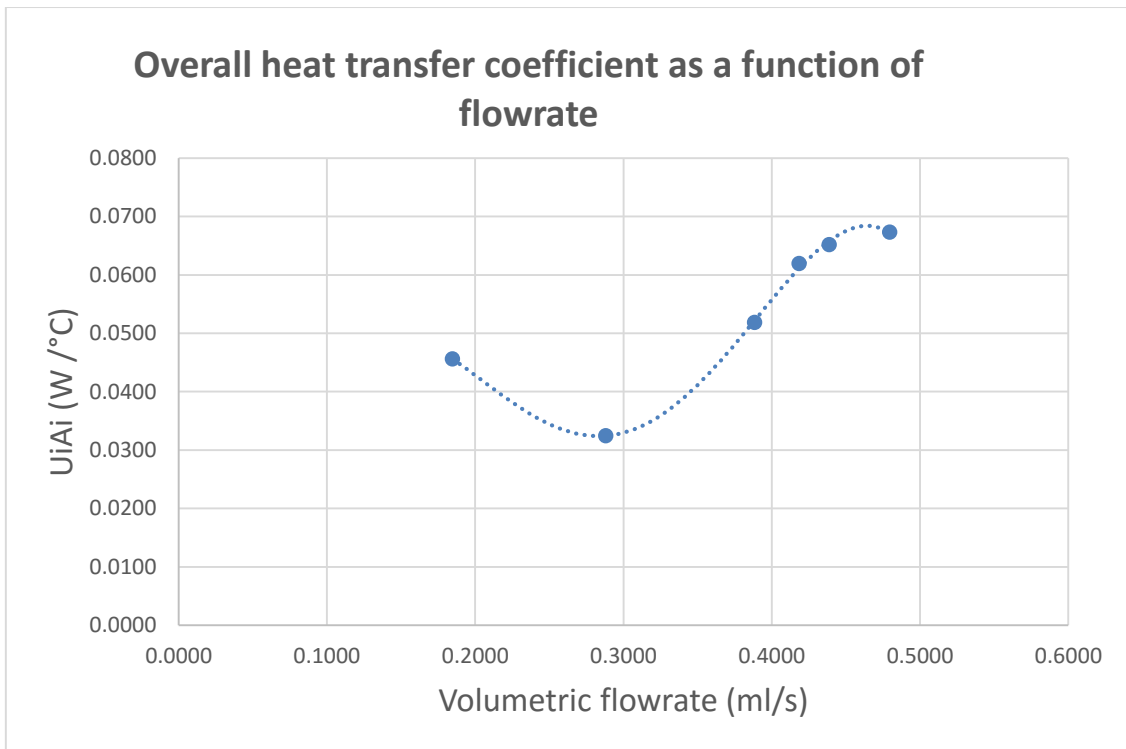


Figure 15 (d): 1-Butanol overall heat transfer coefficient variation with flowrate

Table 2.3.4: Measurement of 1-Butanol conductive heat leaks at pump setting 15

\dot{V} (ml/s)	T_7 (°C)	T_6 (°C)	T_4 (°C)	T_3 (°C)	Corrected $T_4 - T_3$ (°C)	T_{mean} (°C)	$(\Delta T)_{LM}$ (°C)	μ_{but}^* (mPa.s)	μ_{tol}^* (mPa.s)
0.4796	26.96	30.84	30.35	30.02	0.32	30.19	-0.1863	2.3406	0.5208
0.4796	29.97	30.84	30.43	30.02	0.4	30.23	-0.1964	2.3382	0.5206
0.4796	29.96	30.84	30.55	30.05	0.49	30.30	-0.2761	2.3336	0.5201
0.4796	29.96	30.84	30.77	30.05	0.71	30.41	-0.3394	2.3269	0.5195
0.4796	29.96	30.84	31.05	30.07	0.97	30.56	-0.4396	2.3178	0.5186

ρ (g/ml)	\dot{n} (mol/s)	ΔP (kPa)	ΔP correction factor (kPa)	Corrected $\Delta P / \rho$		C'_p (J/mol°C)	$U_i A_i$ (W/°C)
				(J/kg)	(J/mol)		
0.8051	0.0052	21.9649	4.000	32.2507	2.3904	180.9553	0.0673
0.8051	0.0052	21.9379	4.000	32.2183	2.3880	180.9852	0.0673
0.8050	0.0052	21.8901	4.000	32.1611	2.3838	181.0413	0.0673
0.8049	0.0052	21.7828	4.000	32.0305	2.3741	181.1237	0.0673
0.8048	0.0052	21.8253	4.000	32.0889	2.3784	181.2361	0.0673

k^{**} (W/m K)	q_{cv} (W)	$\frac{\dot{V}}{\alpha L_t}$	Q_{ideal} (W)	Q (W)	q_{total} (W)	q_{HL} (W)	$\frac{q_{HL}}{Q}\%$
0.1480	-0.0125	15.9269	0.3017	0.3302	0.0286	0.0285	8.6233
0.1480	-0.0132	15.9301	0.3771	0.4180	0.0408	0.0400	9.5796
0.1479	-0.0186	15.9362	0.4621	0.5160	0.0539	0.0477	9.2486
0.1479	-0.0228	15.9452	0.6698	0.7430	0.0732	0.0627	8.4413
0.1479	-0.0296	15.9567	0.9155	1.0114	0.0958	0.0786	7.7732

$\ln q_{HL}$	π'_1	$\ln \pi'_1$	π'_4	$\ln \pi'_4$	$\ln \lambda$	Average $\ln \lambda$
-3.5586	0.2936	-1.2256	0.0109	-4.5153	1.7481	1.7895
-3.2179	0.2935	-1.2257	0.0138	-4.2810	1.8665	
-3.0423	0.2934	-1.2261	0.0170	-4.0728	1.8444	
-2.7690	0.2933	-1.2265	0.0244	-3.7118	1.7752	
-2.5432	0.2931	-1.2271	0.0331	-3.4084	1.7133	

* μ_{but} and μ_{tol} are literature n-butanol and toluene viscosities evaluated from BASF⁸⁵ and Santos et al.⁸⁶ equations respectively

** k is the literature n-butanol thermal conductivity evaluated from BASF polynomial equation.⁸⁷

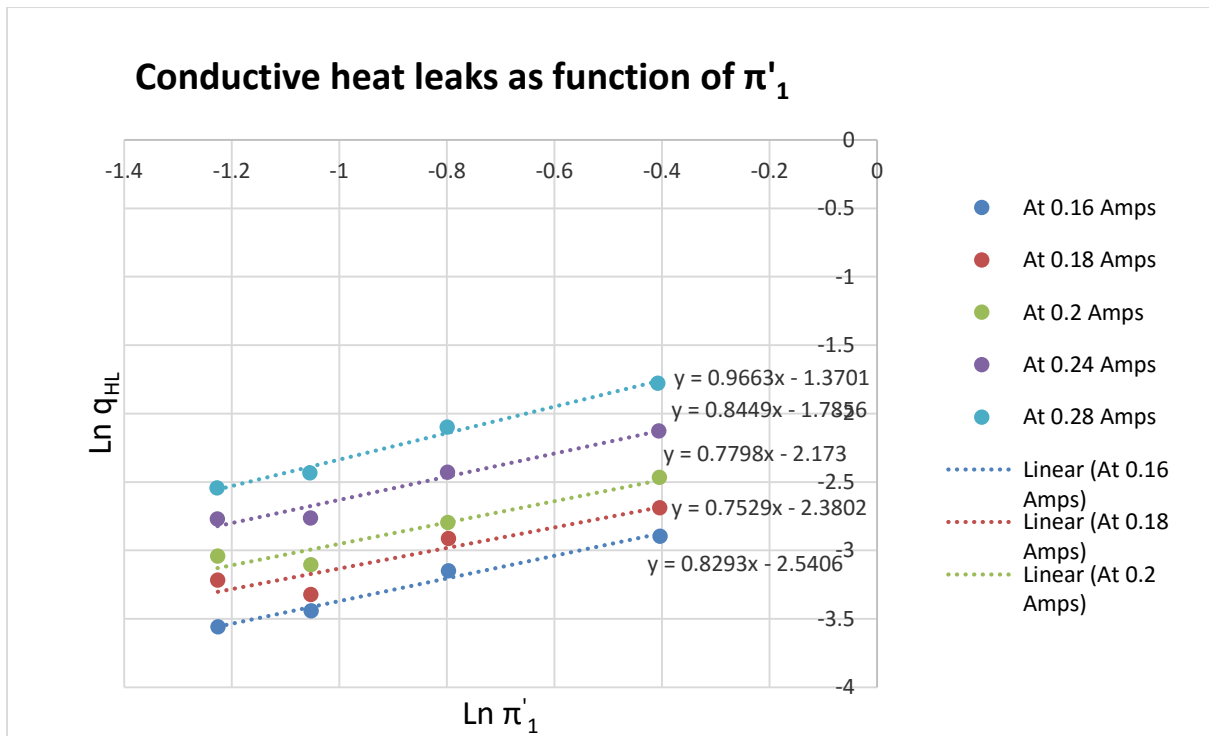


Figure 15 (e): Dependence of 1-Butanol conductive heat leaks on flowrate (from equation 51)

Table 2.4: Evaluation of exponent n_1 for 1-Butanol

Line 1 gradient	0.9663
Line 2 gradient	0.8449
Line 3 gradient	0.7798
Line 4 gradient	0.7529
Line 5 gradient	0.8293
Average gradient	0.8346

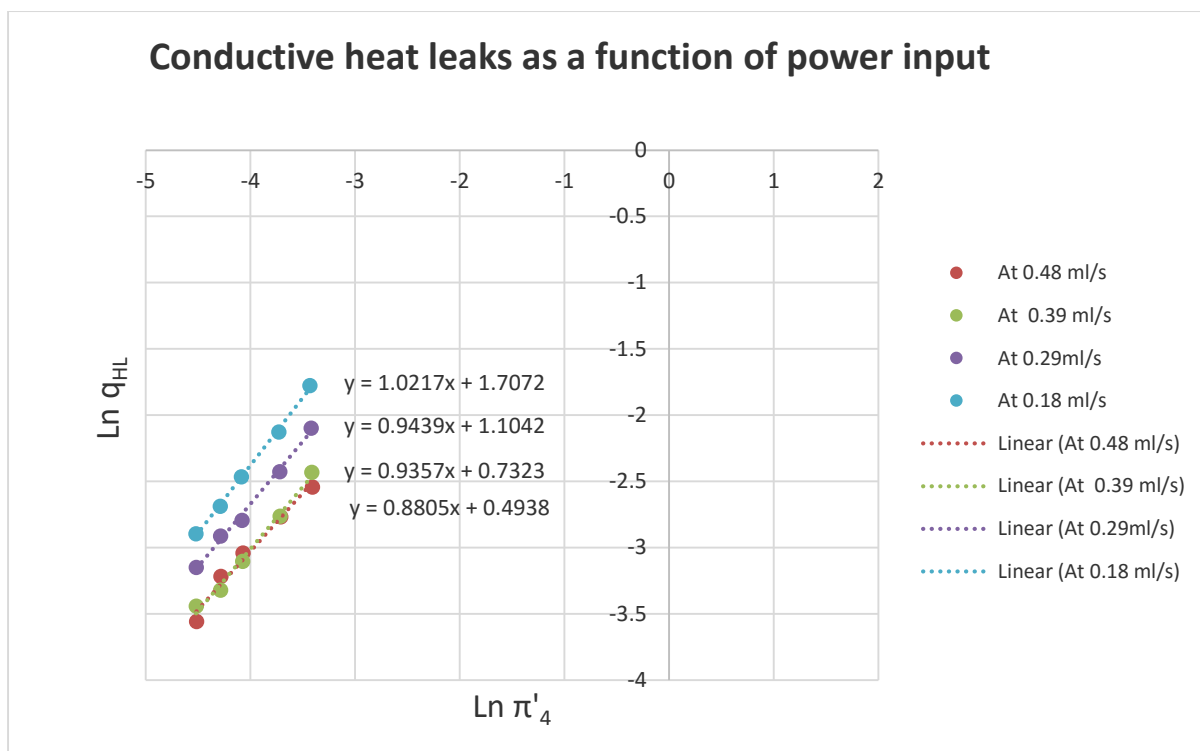


Figure 15 (f): Dependence of 1-Butanol conductive heat leaks on power input (from equation 51)

Table 2.5: Evaluation of exponent n_4 for 1-Butanol

Line 1 gradient	1.0217
Line 2 gradient	0.9439
Line 3 gradient	0.9357
Line 4 gradient	0.8805
Average gradient	0.9455

Table 2.6: Evaluation of calorimeter properties using 1-Butanol

Pump setting	6	9	12	15
Average $\ln \lambda$ per pump setting	1.7561	1.7909	1.6638	1.7895
Average $\ln \lambda$ for all flowrates	1.75001			
λ	5.7549			

6.3 Experimental fluid: Toluene

Table 3.2: Determination of Toluene $U_i A_i$ values at various flowrates

Pump setting	\dot{V} (ml/s)	T_7 (°C)	T_6 (°C)	T_4 (°C)	T_3 (°C)	Corrected $T_4 - T_3$ (°C)	T_{mean} (°C)	$(\Delta T)_{LM}$ (°C)
6	0.1849	29.96	39.85	31.23	31.54	-0.32	31.38	-1.4198
9	0.2805	29.96	39.84	32.50	32.89	-0.41	32.70	-2.7312
12	0.3743	29.96	39.85	33.13	33.55	-0.43	33.34	-3.3805
13	0.4132	29.96	39.84	33.45	33.90	-0.46	33.68	-3.7181
14	0.4461	29.96	39.84	33.80	34.21	-0.42	34.01	-4.0460
15	0.4785	29.96	39.85	33.85	34.24	-0.40	34.04	-4.0827

ρ (g/ml)	\dot{n} (mol/s)	ΔP (kPa)	ΔP correction factor (kPa)	Corrected $\Delta P / \rho$		C'_p (J/mol°C)	$U_i A_i$ (W/°C)
				(J/kg)	(J/mol)		
0.8565	0.0017	-0.5897	3.5000	3.3978	0.3131	159.1368	0.0620
0.8553	0.0026	2.0778	3.5000	6.5213	0.6009	159.5186	0.0628
0.8547	0.0035	5.0909	3.5000	10.0511	0.9261	159.7078	0.0718
0.8541	0.0038	5.6255	3.5000	10.6841	0.9844	159.8062	0.0768
0.8542	0.0041	7.1808	3.5000	12.5044	1.1522	159.9019	0.0696
0.8541	0.0044	8.2281	3.5000	13.7311	1.2652	159.9130	0.0711

C'_p is the literature molar heat capacity of toluene evaluated from the NIST ThermoData Engine (TDE) equation.⁸⁸

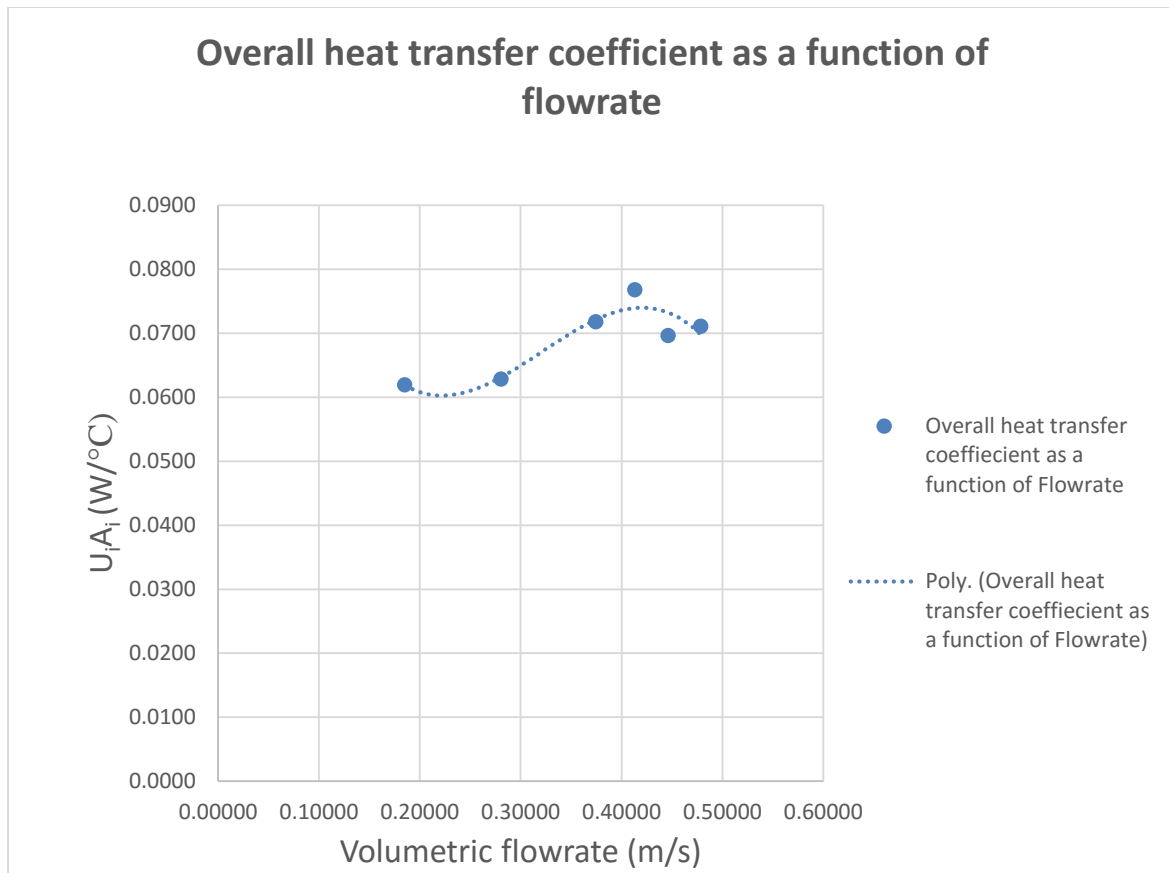


Figure 16 (d): Toluene overall heat transfer coefficient variation with flowrate

Table 3.3.4: Measurement of Toluene conductive heat leaks at pump setting 15

\dot{V} (ml/s)	T_7 (°C)	T_6 (°C)	T_4 (°C)	T_3 (°C)	Corrected $T_4 - T_3$ (°C)	T_{mean} (°C)	$(\Delta T)_{LM}$ (°C)	μ_{tol}^* (mPa.s)
0.4785	29.96	31.04	30.36	30.02	0.33	30.19	-0.1813	0.5208
0.4785	29.96	31.04	30.51	30.06	0.44	30.28	-0.2642	0.5203
0.4785	29.96	31.04	30.61	30.05	0.55	30.33	-0.2901	0.5200
0.4785	29.96	31.04	30.73	30.03	0.69	30.38	-0.3006	0.5197
0.4785	29.96	31.04	31.00	30.00	0.99	30.50	-0.3158	0.5189

ρ (g/ml)	\dot{n} (mol/s)	ΔP (kPa)	ΔP correction factor (kPa)	Corrected $\Delta P / \rho$		C_p' (J/mol°C)	$U_i A_i$ (W/°C)
				(J/kg)	(J/mol)		
0.8569	0.0044	9.3581	3.5000	15.0062	1.3827	158.7913	0.0711
0.8568	0.0044	9.2948	3.5000	14.9336	1.3760	158.8182	0.0711
0.8567	0.0044	9.2130	3.5000	14.8389	1.3673	158.8328	0.0711
0.8567	0.0044	9.1332	3.5000	14.7467	1.3588	158.8471	0.0711
0.8566	0.0044	9.1962	3.5000	14.8222	1.3657	158.8816	0.0711

k^{**} (W/m K)	q_{cv} (W)	$\frac{\dot{V}}{\alpha L_r}$	Q_{ideal} (W)	Q (W)	q_{total} (W)	q_{HL} (W)	$\frac{q_{HL}\%}{Q}$
0.1292	-0.0129	13.6728	0.2341	0.2528	0.0188	0.0120	4.7552
0.1292	-0.0188	13.6767	0.3091	0.3302	0.0211	0.0085	2.5609
0.1292	-0.0206	13.6787	0.3899	0.4180	0.0280	0.0135	3.2230
0.1291	-0.0214	13.6805	0.4860	0.5160	0.0300	0.0146	2.8358
0.1291	-0.0225	13.6851	0.7007	0.7430	0.0423	0.0260	3.4939

$\ln q_{HL}$	π'_1	$\ln \pi'_1$	π'_4	$\ln \pi'_4$	$\ln \lambda$	Average $\ln \lambda$
-4.4209	0.3029	-1.1942	0.0084	-4.7825	2.0335	1.6673
-4.7728	0.3029	-1.1945	0.0109	-4.5185	1.4154	
-4.3072	0.3028	-1.1946	0.0138	-4.2846	1.6449	
-4.2245	0.3028	-1.1948	0.0170	-4.0755	1.5166	
-3.6512	0.3027	-1.1951	0.0244	-3.7148	1.7261	

* μ_{tol} is the literature toluene viscosity evaluated from Santos et al. equation.⁸⁶

** k is the literature toluene thermal conductivity evaluated from Ramirez et al. equation.⁸⁹

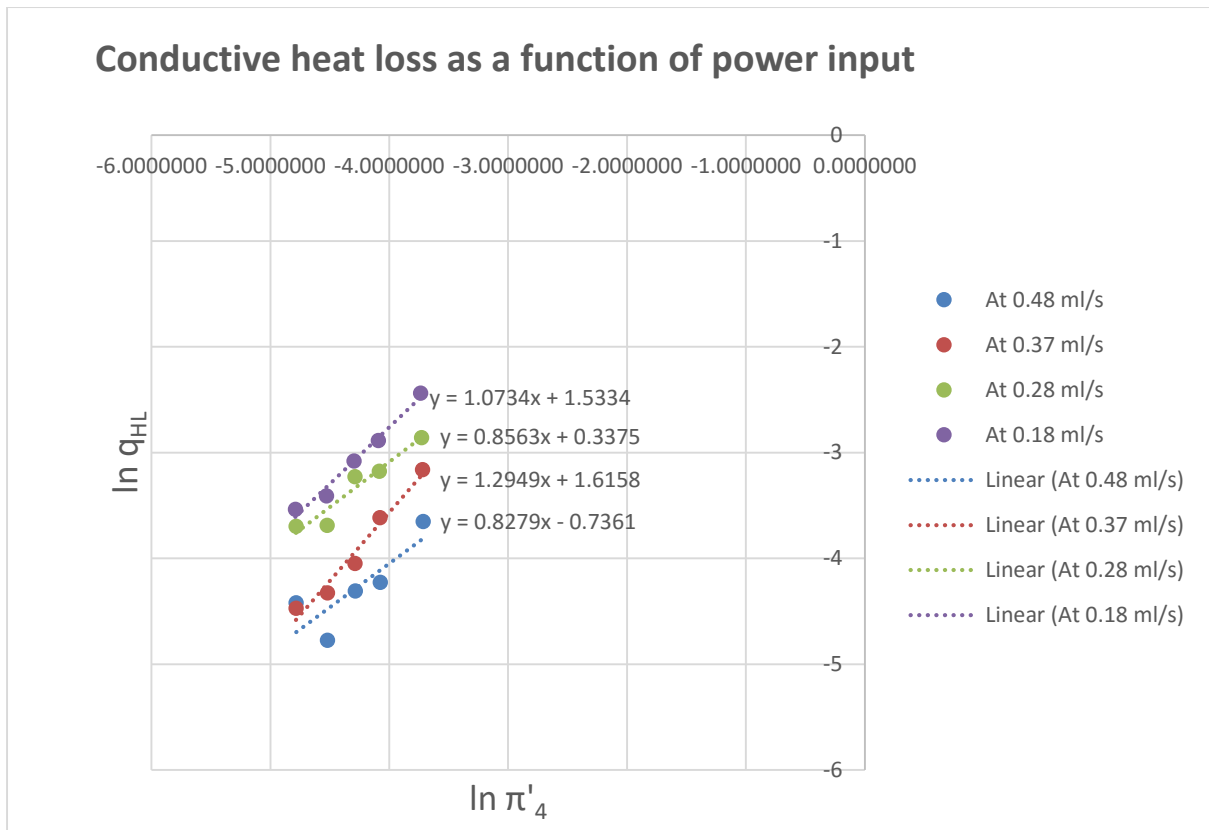


Figure 16 (e): Dependence of Toluene conductive heat leaks on power input (from equation 51)

Table 3.4: Evaluation of exponent n_4 for Toluene

Line 1 gradient	1.0734
Line 2 gradient	0.8563
Line 3 gradient	1.2949
Line 4 gradient	0.8279
Average gradient	1.0131

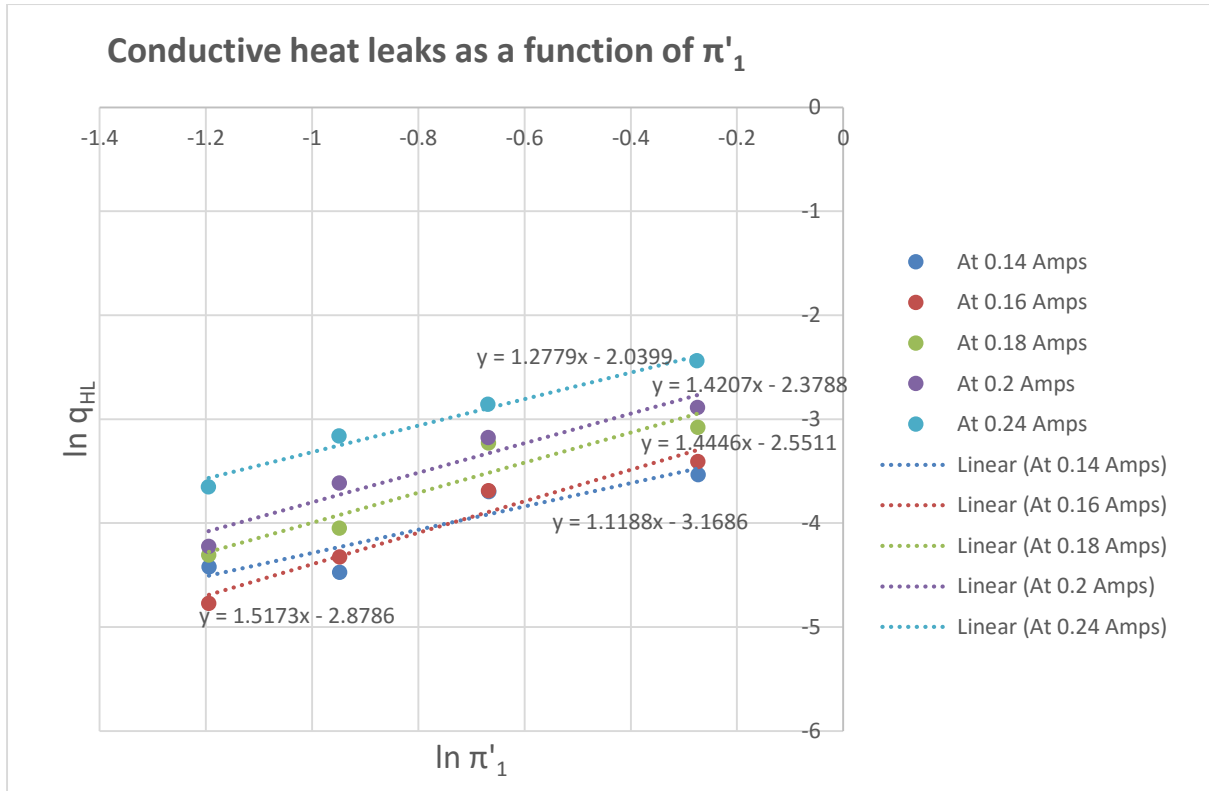


Figure 16 (f): Dependence of Toluene conductive heat leaks on flowrate (from equation 51)

Table 3.5: Evaluation of exponent n_1 for Toluene

Line 1 gradient	1.2779
Line 2 gradient	1.4207
Line 3 gradient	1.4446
Line 4 gradient	1.5173
Line 5 gradient	1.1188
Average gradient	1.35586

Table 3.6: Evaluation of calorimeter properties using Toluene

Pump setting	6	9	12	15
Average $\ln \lambda$ per pump setting	1.6343	1.9044	1.6872	1.6673
Average $\ln \lambda$ for all flowrates	1.7233			
λ	5.6030			

6.4 Predicting capabilities of the conductive heat leak correlation

Reference liquid: Toluene

Experimental liquid: De-ionized water

Table 4.1.1: Conductive heat loss predictions at 0.15 ml/s

Experimental $\frac{q_{HL}}{Q}$ %	*Predicted $\frac{q_{HL}}{Q}$ %	**Predicted $\frac{q_{HL}}{Q}$ %
23.09	32.23	37.32
22.99	32.18	37.25
23.47	32.12	37.17
23.03	31.98	36.98
23.08	31.80	36.74

Table 4.1.2: Conductive heat loss predictions at 0.22 ml/s

Experimental $\frac{q_{HL}}{Q}$ %	*Predicted $\frac{q_{HL}}{Q}$ %	**Predicted $\frac{q_{HL}}{Q}$ %
20.75	19.03	22.05
20.51	19.02	22.03
20.99	19.00	22.01
20.87	18.96	21.95
20.57	18.90	21.86

Table 4.1.3: Conductive heat loss predictions at 0.32 ml/s

Experimental $\frac{q_{HL}}{Q}$ %	*Predicted $\frac{q_{HL}}{Q}$ %	**Predicted $\frac{q_{HL}}{Q}$ %
10.57	11.83	13.71
10.08	11.82	13.70
10.63	11.82	13.69
10.50	11.80	13.67
10.30	11.78	13.64

Table 4.1.4: Conductive heat loss predictions at 0.42 ml/s

Experimental $\frac{q_{HL}}{Q}$ %	*Predicted $\frac{q_{HL}}{Q}$ %	**Predicted $\frac{q_{HL}}{Q}$ %
6.58	8.58	9.95
4.85	8.58	9.95
6.75	8.58	9.95
5.97	8.57	9.93
6.73	8.57	9.93

Reference liquid: Toluene

Experimental liquid: n-butanol

Table 4.2.1: Conductive heat loss predictions at 0.18 ml/s

Experimental $\frac{q_{HL}}{Q}$ %	*Predicted $\frac{q_{HL}}{Q}$ %	**Predicted $\frac{q_{HL}}{Q}$ %
16.73	10.19	17.22
16.27	10.17	17.18
16.47	10.10	17.05
16.03	10.03	16.91
16.71	9.95	16.75

Table 4.2.2: Conductive heat loss predictions at 0.29 ml/s

Experimental $\frac{q_{HL}}{Q}$ %	*Predicted $\frac{q_{HL}}{Q}$ %	** Predicted $\frac{q_{HL}}{Q}$ %
12.98	5.98	10.12
12.99	5.98	10.10
11.84	5.95	10.04
11.88	5.94	10.02
12.13	5.90	9.94

Table 4.2.3 Conductive heat loss predictions at 0.39 ml/s

Experimental $\frac{q_{HL}}{Q}$ %	*Predicted $\frac{q_{HL}}{Q}$ %	** Predicted $\frac{q_{HL}}{Q}$ %
9.68	4.23	7.15
8.64	4.22	7.14
8.70	4.23	7.15
8.50	4.22	7.12
8.69	4.19	7.08

Table 4.2.4: Conductive heat loss predictions at 0.48 ml/s

Experimental $\frac{q_{HL}}{Q}$ %	*Predicted $\frac{q_{HL}}{Q}$ %	** Predicted $\frac{q_{HL}}{Q}$ %
8.62	3.35	5.67
9.58	3.35	5.67
9.25	3.35	5.67
8.44	3.35	5.66
7.77	3.34	5.64

Reference liquid: Toluene

Experimental liquid: Toluene

Table 4.3.1: Conductive heat loss predictions at 0.18 ml/s

Experimental $\frac{q_{HL}}{Q}$ %	*Predicted $\frac{q_{HL}}{Q}$ %	** Predicted $\frac{q_{HL}}{Q}$ %
11.53	12.12	12.12
10.02	12.09	12.09
11.02	12.06	12.06
10.81	12.00	12.00
11.75	11.89	11.89

Table 4.3.2: Conductive heat loss predictions at 0.28 ml/s

Experimental $\frac{q_{HL}}{Q}$ %	*Predicted $\frac{q_{HL}}{Q}$ %	** Predicted $\frac{q_{HL}}{Q}$ %
9.82	7.12	7.12
7.59	7.11	7.11
9.48	7.10	7.10
8.09	7.07	7.07
7.73	7.02	7.02

Table 4.3.3: Conductive heat loss predictions at 0.37 ml/s

Experimental $\frac{q_{HL}}{Q}$ %	*Predicted $\frac{q_{HL}}{Q}$ %	** Predicted $\frac{q_{HL}}{Q}$ %
4.52	4.86	4.86
4.00	4.86	4.86
4.18	4.86	4.86
5.22	4.86	4.86
5.70	4.84	4.84

Table 4.3.4: Conductive heat loss predictions at 0.48 ml/s

Experimental $\frac{q_{HL}}{Q}$ %	*Predicted $\frac{q_{HL}}{Q}$ %	** Predicted $\frac{q_{HL}}{Q}$ %
4.76	3.49	3.49
2.56	3.48	3.48
3.22	3.49	3.49
2.84	3.49	3.49
3.49	3.48	3.48

* Percentage fractional conductive heat loss predicted from $q_{HL} = 5.6[\pi_1]^{1.36} [\pi_4]^{1.01}$

** Percentage fractional conductive heat loss predicted from $q_{HL} = 5.6[\pi_1]^{1.36} [\pi_4]^{1.01} [\pi_5]^{0.35}$

6.5 Measured Molar Heat Capacities

Experimental liquid: De-ionized water

Table 5.1.1: Measured molar heat capacities at 0.15 ml/s

Temperature of measurement (°C)	Literature C_p (J/mol K)	Converging value for C_p (J/mol K)	% Error in measured C_p
30.60	75.23	none	-
30.69	75.23	none	-
30.80	75.23	none	-
31.03	75.23	none	-
31.30	75.23	none	-

Table 5.1.2: Measured molar heat capacities at 0.22 ml/s

Temperature of measurement (°C)	Literature C_p (J/mol K)	Converging value for C_p (J/mol K)	% Error in measured C_p
30.42	75.23	73.29	2.58
30.50	75.23	72.97	3.00
30.56	75.23	73.72	2.02
30.72	75.23	73.63	2.14
30.90	75.23	73.32	2.55

Table 5.1.3: Measured molar heat capacities at 0.32 ml/s

Temperature of measurement (°C)	Literature C_p (J/mol K)	Converging value for C_p (J/mol K)	% Error in measured C_p
30.30	75.23	71.93	4.40
30.37	75.23	71.45	5.03
30.42	75.23	72.01	4.29
30.55	75.23	71.91	4.42
30.68	75.23	71.73	4.65

Table 5.1.4: Measured molar heat capacities at 0.42 ml/s

Temperature of measurement (°C)	Literature C_p (J/mol K)	Converging value for C_p (J/mol K)	% Error in measured C_p
30.23	75.23	72.10	4.17
30.27	75.23	70.57	6.21
30.32	75.23	72.25	3.97
30.42	75.23	71.57	4.87
30.51	75.23	72.25	3.96

Experimental Liquid: n-butanol

Table 5.2.1: Measured molar heat capacities at 0.18 ml/s

Temperature of measurement (°C)	Literature C_p (J/mol K)	Converging value for C_p (J/mol K)	% Error in measured C_p
30.37	181.09	179.75	0.74
30.47	181.17	178.61	1.41
30.70	181.34	179.75	0.87
30.96	181.54	179.08	1.35
31.25	181.76	181.69	0.04

Table 5.2.2: Measured molar heat capacities at 0.29 ml/s

Temperature of measurement (°C)	Literature C_p (J/mol K)	Converging value for C_p (J/mol K)	% Error in measured C_p
30.29	181.03	187.87	3.78
30.38	181.10	188.04	3.83
30.57	181.24	185.56	2.83
30.69	181.33	185.77	2.45
30.95	181.53	186.77	2.89

Table 5.2.3: Measured molar heat capacities at 0.38 ml/s

Temperature of measurement (°C)	Literature C_p (J/mol K)	Converging value for C_p (J/mol K)	% Error in measured C_p
30.29	181.03	186.64	3.10
30.35	181.08	184.43	1.85
30.38	181.10	184.54	1.90
30.56	181.23	184.31	1.70
30.77	181.39	184.98	1.98

Table 5.2.4 Measured molar heat capacities at 0.48 ml/s

Temperature of measurement (°C)	Literature C_p (J/mol K)	Converging value for C_p (J/mol K)	% Error in measured C_p
30.19	180.96	187.13	3.41
30.23	180.99	189.23	4.55
30.30	181.04	188.65	4.20
30.41	181.12	187.04	3.27
30.56	181.24	185.79	2.51

Experimental liquid: Toluene

Table 5.3.1: Measured molar heat capacities at 0.18 ml/s

Temperature of measurement (°C)	Literature C_p (J/mol K)	Converging value for C_p (J/mol K)	% Error in measured C_p
30.39	158.85	157.41	0.91
30.53	158.89	154.06	3.04
30.66	158.93	156.51	1.51
30.85	158.98	156.24	1.72
31.20	159.08	158.58	0.32

Table 5.3.2: Measured molar heat capacities at 0.28 ml/s

Temperature of measurement (°C)	Literature C_p (J/mol K)	Converging value for C_p (J/mol K)	% Error in measured C_p
30.39	158.81	163.57	3.00
30.53	158.84	159.31	0.29
30.66	158.87	163.02	2.61
30.85	158.93	160.46	0.96
31.20	159.00	159.92	0.57

Table 5.3.3: Measured molar heat capacities at 0.38 ml/s

Temperature of measurement (°C)	Literature C_p (J/mol K)	Converging value for C_p (J/mol K)	% Error in measured C_p
30.36	158.81	157.62	0.72
30.33	158.83	156.73	1.33
30.42	158.86	157.05	1.14
30.48	158.87	158.90	0.02
30.65	158.92	159.82	0.57

Table 5.3.4: Measured molar heat capacities at 0.48 ml/s

Temperature of measurement (°C)	Literature C_p (J/mol K)	Converging value for C_p (J/mol K)	% Error in measured C_p
30.19	158.79	160.20	0.89
30.28	158.82	156.53	1.44
30.33	158.83	157.63	0.76
30.38	158.85	156.98	1.18
30.50	158.88	158.11	0.48

6.6 Discussions

Pump calibrations

Differences observed in pump calibrations using de-ionized water were a result of the liquid injection via the narrow syringe needle flow paths [Figure 13 (a)]. Large flow resistances inside syringe needles were believed to have caused non-linearity of pump calibration i.e. pressures at the pump discharge may have exceeded maximum values for reproducibility. Subsequent calibrations performed via the Teflon body paths using butanol and toluene yielded linear plots [Figure 13 (b) and Table 7.3].

Inlet temperature

At constant bath temperatures T_6 and T_7 , inlet temperatures to the reference module T_3 increased with volumetric flowrate for all the liquids during $U_i A_i$ measurements [Figures 14 (a), 14 (c), 15 (a) and 16 (a)]. This was directly a result of increase in heat transfer rates with flowrate as the liquids passed through water bath 2 inside the heat exchanger coil. Temperature defects (fluid failure to reach bath 2 temperature) were however observed in all liquids at all flowrates and decreased with increase in liquid thermal conductivity. This was attributed mainly to improper equilibration in water bath 2 as well as heat losses incurred along the tubing between the two baths. Although efforts to counter the latter were implemented by submerging valve V_8 in water bath 2 (Figure 5) and insulating the reference module feed tubing with rubber (Figure 8), liquids continued to experience defects. These defects presented a challenge controlling and setting temperature for measuring molar heat capacities during “heating experiments.”

Temperature change variation with flowrate

The amount of heat given up by each liquid passing through the reference module is a function of its inlet temperature, flowrate as well as fluid properties. The temperature difference ($T_4 - T_3$) was observed to generally increase with volumetric flowrate for all the three liquids [Figures 14 (b), 14 (d), 15 (c) and 16 (c) in appendices A, B and C]. This was a result of increases in inlet temperature T_3 with flowrate (as stated above) thereby leading to larger temperature difference driving forces for convective heat losses through module walls as the liquids passed through. The magnitude of this temperature difference was suspected to increase with fluid thermal diffusivity α as well, in which case water and toluene were deemed to lose the most and least amounts of heat respectively. Frictional heating, which increases with fluid

viscosity and flowrate, was implicated in anomalies observed in temperature change profiles at certain flowrates in n-butanol and toluene experiments [Figures 15 (c) and 16 (c) in appendices B and C].

Overall heat transfer coefficient variation with flowrate

The two methods used in estimating $U_i A_i$ provided reliable estimates of the overall heat transfer coefficient. Behaviour of $U_i A_i$ vs. \dot{V} functions [Figures 14 (e), 15 (d) and 16 (d)] appeared to be more or less a reflection of the temperature changes which were observed during experiments. In general, $U_i A_i$ increases continuously with volumetric flowrate. In de-ionized water experiments, heat diffusion through the module walls dominated viscous flow heating resulting in a monotonic $U_i A_i$ vs. \dot{V} function. However, the effect of frictional heating on n-butanol and toluene net temperature changes was evidenced by the fluctuations in $U_i A_i$ vs. flowrate curves. The relatively slow movement of heat (smaller α values) through these organics (particularly toluene) along a temperature gradient saw heat transfer rates changing inappreciably with volumetric flowrate as shown in Figure 16 (d).

Lost work due to friction

The measured pressure drops of each liquid increased almost linearly with flowrate (Figures 15 (b) and 16 (b) in appendices B and C) while viscosity also played a big part in determining the magnitude of pressure drop. Viscous n-butanol, as expected, exhibited pressure drop values that were more than twice those of mobile toluene at the same flowrate. The extent to which frictional dissipation impacted net enthalpy changes varied from liquid to liquid depending on the measured pressure drop and density of the liquid. The lost work due to friction of a relatively dense and mobile liquid like water could be reasonably neglected while that of butanol and toluene could not be ignored particularly at flowrates in excess of 0.45 ml/s (Tables 2.3.4 and 3.3.4).

Convective heat losses

Although the modules were housed in PVC tubing to minimize heat losses to the surroundings, significant heat losses through the Teflon walls were still observed. These losses were much greater in magnitude than frictional heating in all the liquids used (Tables 2.3.4 and 3.3.4). Values of q_{CV} were found to increase rapidly with flow rate and temperature gradient. Furthermore, convective heat losses were also found to be fluid-property dependent as described above.

Conductive heat losses

Conductive heat leaks via heater lead-in-wires could not to be completely eliminated despite looping of the nichrome mixer/heater ribbon. Similar to the findings of Hei and Raal ²¹, q_{HL} was found to decrease with increasing flowrate. Although a clearly defined trend could not be established, conductive heat leaks were perceived to also be sensitive to fluid properties contained in fluid thermal diffusivity α . For a reasonably low current input, q_{HL} appeared insensitive to power input Q as evidenced by nearly constant fractional conductive heat leak values at constant flowrates (q_{HL} measurements tables in appendices A, B and C). In developing the q_{HL} correlation, toluene was chosen as the reference liquid values as correlation parameters derived from it provided better predictions for the two low viscosity liquids. The developed universal heat leak correlation adequately accounted for substantial deviations of liquid viscosity from that of the reference liquid to provide reliable q_{HL} predictions for all three experimental liquids (Tables in section 6.4). In determination of exponent n_5 , values less than 0.35 improved the quality of water heat loss predictions while those greater than this value favoured n-butanol thus a compromise value of 0.35 was selected. Substantial prediction errors by both correlations were however observed for de-ionized water at 0.15 ml/s (Table 4.1.1). This was most likely due to the deviation from linearity of the calibration point (0.15 ml/s). Comparisons of Hei and Raal ²¹ and current n-butanol (q_{HL}/Q) experimental measurements reveal an approximately 4 % improvement in performance of the current design. This observed decrease in conductive heat leaks was attributed to looping of the heater ribbon. Better current design performance was expected at higher flowrates as absorption of conductive heat losses by the incoming liquid stream increases with heat transfer coefficient h . Design comparisons, again, at similar flowrates using water however showed no improvement in current work q_{HL} reduction (probably due to water calibration anomalies in this work).

Heat capacities

Heat capacities measured using the universal conductive heat leak correlation were compared with values from literature. Generally good to excellent agreements were noted with errors ranging between 0.02 % and 6.21% (section 7.5). Accuracy of measurements appeared to be strongly influenced by the quality of q_{HL} predictions. Best q_{HL} predictions and hence C_P^L measurements were obtained for all liquids at lower flowrates (particularly at pump setting 9). The extensive flow rates used in the experiments proved to be invaluable in finding values optimum for C_P^L measurement. The choice of the function f , made of up of the functions $q_{HL}(C_P^L)$ and $q_{CV}(C_P^L)$, in the experimental equation $C_{Pn+1}^L = f(C_{Pn}^L)$ (Equation 41), appears to

have been fitting for convergence of fixed point iterations for all the three liquids used in this work. However, the lack of converging C_p^L values using the iterative procedure on de-ionized water at pump setting 6 (Table 5.1.1) was a result of abovementioned large q_{HL} predictions errors.

Chapter 7

Conclusions

By merging design features of heat of mixing calorimeters^{23,24} and heat capacity calorimeters²¹, an instrument has been developed capable of measuring endothermic heats of mixing as well as heat capacities of liquids of widely differing thermophysical properties. Using the current design, molar heat capacities of liquids of widely differing thermophysical properties could be measured with a low uncertainty of not more than 2 % of recommended literature values (at optimal flowrate setting). The quality of the measured molar heat capacities appears to be strongly sensitive to the quality of the predicted conductive heat losses, a principal source of error in flow calorimetry for heat capacity. It is therefore vital that conductive heat losses be accounted for precisely in order to obtain high quality C_p^L data. Fixed point iteration proved to be a reliable method for solving equation (41) for C_p^L and convergence (to 2 d.p) was achieved in a few successive iterations, with the starting point in the neighbourhood of literature values. The methods used in the measurement of conductive and convective heat losses, during development of the q_{HL} correlation, yielded reasonable and reproducible results. Heat losses via convection, through the module walls, were considerably large and generally increased with overall heat transfer coefficients and temperature difference driving forces. The two methods used to estimate $U_i A_i$, although reliable, remain burdensome and time consuming and hence development of a reliable correlation for $U_i A_i$ as a function of flowrate and fluid properties will certainly ease measurement of q_{CV} . Additionally, drawing sufficient vacuum around the modules will perhaps provide the most effective management and potential elimination of convective heat losses. The new q_{HL} correlation, derived from dimensionless groups suggested by Hei and Raal²¹, provided satisfactory to excellent heat loss predictions only for liquids of similar viscosities. This correlation adequately accounted for water's somewhat unique properties such as very high thermal conductivity and heat capacity, a feat not achieved by the correlation developed previously by Hei and Raal²¹. The additional π group involving the viscosity ratio incorporated the dependence of q_{HL} on viscosity, thereby extending applicability of the correlation to liquids of widely differing viscosities. The versatility of the universal correlation however remains to be tested on other types of liquids such as organic acids, halogenated hydrocarbons and so on. However, with the dependence of q_{HL} on the major thermophysical fluid properties (ρ, μ, k, C_p) having been successfully established and tested in this work, the reliability potential of the universal correlation on any other type of liquid is very high. Looping of the heater ribbon enhanced the design's performance by reducing heat losses through

conduction to the surroundings. Despite this innovation, conductive heat leaks remained significantly large but decreased rapidly with increase in flowrate for all the liquids, and thus gave guidance on the choice of volumetric flowrates optimal for C_p^L measurement. Furthermore, conductive heat losses were shown to be sensitive to fluid properties as well. Water was observed to be more susceptible to conductive heat leaks at lower flowrates than organics as evidenced by larger (q_{HL}/Q %) values. While the use of high flowrates minimizes heat leaks through conduction and hence measurement errors, better q_{HL} predictions and hence molar heat capacity measurements generally appear to require lower flowrates. However, a looped heater, coupled with very high flowrates in a robust design, has the potential to significantly lower and possibly eliminate conductive heat losses. This may be the ultimate solution to the conductive heat leak problem and could thus render flow calorimetry a more favourable option for modern C_p measurement compared to techniques such as scanning calorimetry, from both economic and ease of usage perspectives. On the other hand, the inevitable frictional energy losses, whose significance increases with flowrate, were shown to be a considerable factor in accurately determining C_p^L , particularly for lighter and viscous fluids. As far as the measurement of H^E is concerned, the ability of this design to compensate for effects of frictional heating incurred during fluid mixing, like the Raal and Webley design²⁴, is expected to yield high quality results.

References

1. Y.S. Touloukian, T. Makita, *Thermophysical Properties of Matter, Specific Heats of Nonmetallic Liquids and Gases, IFI/ Plenum, New York, 1970, 6.*
2. M. Za'bransky', V. Ru'z'ic'ka, Jr., and E. S. Domalski, *Heat Capacity of Liquids: Critical Review and Recommended Values, J. Phys. Chem. Ref. Data, 2001, 30, 1199.*
3. J.J. Christensen, R.W. Hanks and R.M. Izatt, *Handbook of heats of mixing, John Wiley and Sons, New York, 1982.*
4. C. Christensen, J. Gmehling, P. Ramsussen, U. Wiedlich and T. Holderbaum, *Heats of mixing data collection, DECHEMA Chemistry Data Series, 1984, 3.*
5. J.J. Christensen, R.L. Rowley and R.M. Izatt, *Handbook of heats of mixing, Supplementary Volume, John Wiley and Sons, New York, 1988.*
6. B.J. Ott and J.T. Sipowska, *J. Chem. Eng. Data 1996, 41, 987.*
7. J.M. Smith, H. C. Van Ness and M. M. Abbott, *Introduction to Chemical Engineering Thermodynamics, McGraw-Hill International edition, 2005.*
8. B. E. Poling, J.M. Prausnitz and J.P. O'Connell, *Properties of Gases and Liquids, McGraw-Hill Professional Company, 2004.*
9. J.J. Van Laar, *Sechs Vortrage uber das Thermodynamische potential, Vieweg, Braunschwieg, 1906, cited by W. E. Acree, Thermodynamic Properties of Non Electrolyte Solutions, 1984, 74.*
10. H. Renon and J.M. Praunitz, *AICHEJ, 1968, 14, 135.*
11. D.S. Abrams and J.M. Praunitz, *AICHEJ, 1975, 21, 116, cited by J.M. Smith, H. C. Van Ness and M. M. Abbott, Introduction to Chemical Engineering Thermodynamics, McGraw-Hill International edition, 2005.*
12. G.M. Wilson, *J. Am. Chem. Soc., 1964, 86, 127, J.M. Smith, H. C. Van Ness and M. M. Abbott, Introduction to Chemical Engineering Thermodynamics, McGraw-Hill International edition, 2005, 448.*
13. M. Za'bransky', M.Kolska', V. Ru'z'ic'ka and A. Malijevesky in E. Wilhelm and T. Letcher (editors), *Heat Capacities: Liquids, Solutions and Vapours, RSC Publishing, 2010, 421.*
14. S.W. Benson and D. M. Golden in by H. Eyring, D. Henderson and W. Jost (editors), *Physical Chemistry Treatise, 1975.*
15. K.S. Pitzer, *Thermodynamics, 3rd Ed., App. 3, McGraw-Hill, New York, 1955.*

16. B.C. Sakiadis, J. Coates, *AIChE J*, 1956, 2, 88.
17. A. Bondi, *Ind. Eng. Chem, Fundamentals*, 1966, 5, 442.
18. L. Coniglio, E. Rauzy, C. Berro, *Fluid Phase Equilibria*, 1993, 87, 53.
19. A. Diedrichs, J. Rarey, J. Gmehling, *Fluid Phase Equilibria*, 2006, 248, 56.
20. V. Pachaiyappan, S.H. Ibrahim, N.R. Kuloor, *Chem Eng. Chem Metal. Eng.*, 1967, 74, 241.
21. T.K. Hei, J.D. Raal, *AIChEJ*, 2009, 55, 206.
22. J.D. Raal in E. Wilhelm and T.M. Letcher (editors), *An Analysis of Conductive Heat Losses in a Flow Capacity for Heat Capacity Measurement, Heat Capacities: Liquids, Solutions and Vapours*, RSC Publishing, 2010, 41.
23. J.D. Raal, P. Naidoo, *Fluid Phase Equilibria*, 1990, 27, 147.
24. J.D. Raal, P. A. Webley, *AIChEJ*, 1987, 33, 604.
25. B.I. Lee, M.G. Kesler, *AIChEJ*, 1975, 21, 510.
26. W. Zielenkiewicz, *Journal of Thermal Analysis and Calorimetry*, 2008, 91, 663.
27. J. Rouquerol, I. Wadsö, T.J. Lever, P.J. Haines in M.E. Brown, P.K. Gallagher, (editors), *Handbook of Thermal Analysis and Calorimetry*, Elsevier B.V., 2008, 5, 13.
28. W. Hemminger, S. Sarge in M.E. Brown, P.K. Gallagher (editors), *Handbook of Thermal Analysis and Calorimetry*, Elsevier, Amsterdam, 1999, 1, 1.
29. J.P. McCullough and D.W. Scott in D.C. Gennings (editor), *Precision Measurement and Calibration*, NBS Publishing, 1968, 6, 1.
30. K.N. Marsh in M.L. McGlashan (editor), *Chemical Thermodynamics*, 2007, 1, 1.
31. M.L. McGlashan and J.L. Larkin, *J.Chem. Soc.* 1961, 3425.
32. E. Calvet and H. Prat, *Microcalorimetrie; applications physico-chimiques et biologiques*, Masson, Paris, 1956, 7-10 cited by J. Rouquerol, I. Wadsö, T.J. Lever, P.J. Haines in M.E. Brown, P.K. Gallagher (editors), *Handbook of Thermal Analysis and Calorimetry*, Elsevier B.V., 2008, 5, 37.
33. W. J. Evans in H.D. Brown (editor), *Biochemical Microcalorimetry*, ACADEMIC PRESS, 1969, 257-273 cited by J. Rouquerol, I. Wadsö, T.J. Lever, P.J. Haines in M.E. Brown, P.K. Gallagher, (editors), *Handbook of Thermal Analysis and Calorimetry*, Elsevier B.V., 2008, 5, 39.
34. P. Picker, P.A. Leduc, P.R. Phillip, J.E. Desnoyers, *J. Chem. Thermodynamics*, 1971, 3, 631.

35. P.Picker, J. Jolicourr, J.E. Desnoyers, *J. Chem. Thermodynamics*, 1969, 1, 469.
36. R.V. Mrazek, H.C. Van Ness, *AIChEJ*, 1961, 7, 190.
37. D.R. Winterhalt and H.C. Van Ness, *J. Chem. Eng. Data*, 1966, 11, 189.
38. M. B. Ewing, K. N. Marsh, R. H. Stokes and C.W. Tuxford, *J. Chemical Thermodynamics*, 1970, 2, 751.
39. R. H. Stokes, K. N. Marsh, and R. P. Tomlins, *J. Chem. Thermodynamics*, 1969, 1, 211.
40. H.T. French and A. Richards, *J. Chem. Thermodynamics*, 1979, 11, 671, cited by B.J. Ott and J.T. Sipowska, *J. Chem. Eng. Data* 1996, 41, 989.
41. M.J. Costigan and L.J. Hodges, K.N. Marsh, R.H. Stokes, C.W. Tuxford. *Aust. J. Chem.*, 1980, 33, 2103, cited by B.J. Ott and J.T. Sipowska, *J. Chem. Eng. Data* 1996, 41, 989.
42. M.L. McGlashan and H.F. Stoeckli, *J. Chem. Thermodynamics*, 1969, 1, 589.
43. E. Wilhelm, *Heat Capacities: Liquids, Vapours and Solutions*, RSC Publishing, 2010, 1.
44. J.L. Gustin and H. Renon (1973), *J. Chem. Eng. Data*, 1973, 18, 164.
45. E.N. Sieder and G.E. Tate, *Ind. Eng. Chem.*, 1936, 28, 1429.
46. F. Mills, *Heat Transfer*, Irwin, Boston, 1992, cited by J.D. Raal in E. Wilhelm, T.M. Letcher (editors), *Heat Capacities: Liquids, Solution and Vapours*, RSC Publishing, 2010, 41.
47. G. Wiedemann, R. Franz, *Ann. Phy. Lpz.*, 1853, 89, 497, cited by G. V. Chester, A. Thellung, *Pro. Phys. Soc.*, 1961, 77, 1005.
48. W.H. McAdams, *Heat Transmission*, 2nd ed., McGraw-Hill, New York ,1942, cited by J.D. Raal, P. A. Webley, *AIChEJ*, 1987, 33, 605.
49. T.H. Chilton, T.B. Drew, R.H. Jebens, *Ind. Eng. Chem*, 1944, 510, 36.
50. J.J. Christensen, B.J. Ott, C.E. Stouffer, G.V. Cornett, B.F., R.C, Whirlin, U.K. Deiters, *J. Chem. Thermodynamics*, 1986, 18, 1, cited by B.J. Ott and J.T. Sipowska, *J. Chem. Eng. Data* 1996, 41, 987.
51. J.J. Christensen, L. D. Hansen, D. J. Eatough, R. M. Izatt, R. M. Hart, *J. Chem. Thermodynamics*, 1978, 10, 25 cited by A. Heintz, R.N. Lichtenthaler, *Thermomica Acta*, 1983, 69, 280.
52. J.J. Christensen, L. D. Hansen, D. J. Eatough, R. M. Izatt, D.J. Eatough, R.M. Hart, *Rev. Sci. Instrum.*, 1981, 52, 1226. Cited by A. Heintz, R.N. Lichtenthaler, *Thermomica Acta*, 1983, 69, 280.
53. www.chemineer.com

54. A. Cybulski and ZD Chemipan, *Institute of Physical Chemistry, polish Academy of Sciences, Warsaw, Poland*, Technical Code 1.1.4.
55. P. Joshi, K.D.P Nigam, E.B. Nauman, *The Chemical Engineering Journal and The Biochemical Engineering Journal*, 1995, 59, 265.
56. A. Heintz, R.N.Lichtenthaler, *Thermomica Acta*, 1983, 69, 273.
57. Elliot and Wormald, *Journal of Chemical Thermodynamics*, 1976, 8, 881
58. J.D. Raal, *AIChEJ*, 1993, 39, 715.
59. M.A. Siddiqi and K. Lucas, *J. Chem. Thermodynamics*, 1982, 14, 1183.
60. J.J. Christensen and R.M. Izatt, *Thermomica Acta*, 1984, 71, 117, cited by W. Zielenkiewicz, *Journal of Thermal Analysis and Calorimetry*, 2008, 91, 666.
61. A.W. Hakin, M.M. Bhuiyan (2010) in E. Wilhelm, T.M. Letcher (editors) *Heat Capacities: Liquids, Solution and Vapours*, RSC Publishing, 2010, 132.
62. D. Smith-Magowan, R.H. Wood, *J. Chem. Thermodynamics*, 1981, 13, 1047.
63. P.S.Z. Rodgers and K.S. Pitzer, *J. Phys. ChemI*, 1981, 85, 2886.
64. P.S.Z. Rogers, J. Sandarusi, *Rev.Sci. Instruments*, 1990, 61, 3440.
65. V.M. Valyashko, M.S. Gruszkiewicz in V.M. Valyashko (editor), *Hydrothermal Properties of Materials*, John Wiley and Sons, 2008, 271.
66. PolyScience Operators Manual.
67. www.omega.com/temperature/pdf.ni80.pdf.
68. GW instek DC Power Supply User Manual (GPS-S Series).
69. UNI-T model UT60B/C/E: Operation Manual.
70. Ismatec Reglo-Z Analog Pump Operating Manual.
71. www.swagelok.com/downloads/WebCatalogs/EN/MS-01-176.pdf.
72. <http://www.ni.com/tutorial/7115/en/>.
73. http://de-de.wika.de/upload/DS_IN0017_GB_20804.pdf.
74. www.sine.ni.com/nips/cds/view/p/lang/en/nid/205621.
75. www.ni.com/datasheet/pdf/en/ds-204.
76. www.ni.com/white-paper/6983/en/.
77. www.ni.com/pdf/manuals/374187c.pdf.
78. www.ni.com/datasheet/pdf/en/ds-193.
79. www.ni.com/pdf/manuals/374070.pdf.
80. www.prelectronics.com/media/193219/3100_folder_US.pdf.
81. KERN & Sohn GmbH Operating Instructions for Analytical Balance.

82. Anton Paar maintenance and calibration record.
83. Fluke: How to calibrate an RTD/PRT application note.
84. M. Za'bransky', V. Ru'z'ic'ka, Jr. and V. Majer, *J. Phys. Chem. Ref. Data*, 1991, 20, 2.
85. BASF polynomial equation for n-butanol viscosity.
86. F. J. V. Santos, C. A. Nieto de Castro, J.H. Dymond, N.K. Dalaouti, M.J. Assael and A. Nagashima, *J. Phys. Chem. Ref. Data*, 2006, 35, 1.
87. BASF polynomial equation for n-butanol thermal conductivity.
88. Aspen Physical Property System/General Pure Component Liquid Heat Capacity (THRSWT 6)/submodel 506.
89. M.L.V. Ramires, C. A. Nieto de Castro, R. A. Perkins, Y. Nagasaki, A. Nagashima, M. J. Assael, W. A. Wakeham, *J. Phys.Chem. Ref. Data*, 2000, 29, 2.
90. Aspen Physical Property System/General Pure Component Liquid Heat Capacity (THRSWT 6)/submodel 503.
91. Aspen Physical Property System/General Pure Component Liquid Viscosity (TRNSWT/1)/submodel 508.
92. M. L. V. Ramires, C. A. Nieto de Castro, Y. Nagasaki, A. Nagashima, M. J. Assael, W. A. Wakeham, *American Institute of Physics and American Chemical Society*, 1995.
93. www.wika.co.za/cth6500_cth650i0_en.WIKA.
94. ATAGO refractometer calibration record.
95. http://www.wika.co.za/cpc8000_en_co.WIKA.
96. http://www.wika.us/upload/DS_PE_S_10_en_us_16325.pdf
97. Handbook of Chemistry and Physics, David R. Lide (Editor), 84th Edition, *Boca Raton, Fla: CRC Press*, 2003.

Appendix A

Experimental fluid: De-Ionized water

De-ionized water source: Laboratory

Table 1.1: Purity of De-ionized water data

	Refractive index (25°C)	Density g/ml (20 °C)
Pure	1.3327	0.99789
Calorimeter discharge	1.3328	0.99802
Literature ⁹⁷	1.3325	0.998

Temperature calibration correction factors: $T_4 - T_3 = 0.03^\circ C$

: $T_7 - T_4 = 0.00^\circ C$

: $T_7 - T_3 = 0.03^\circ C$

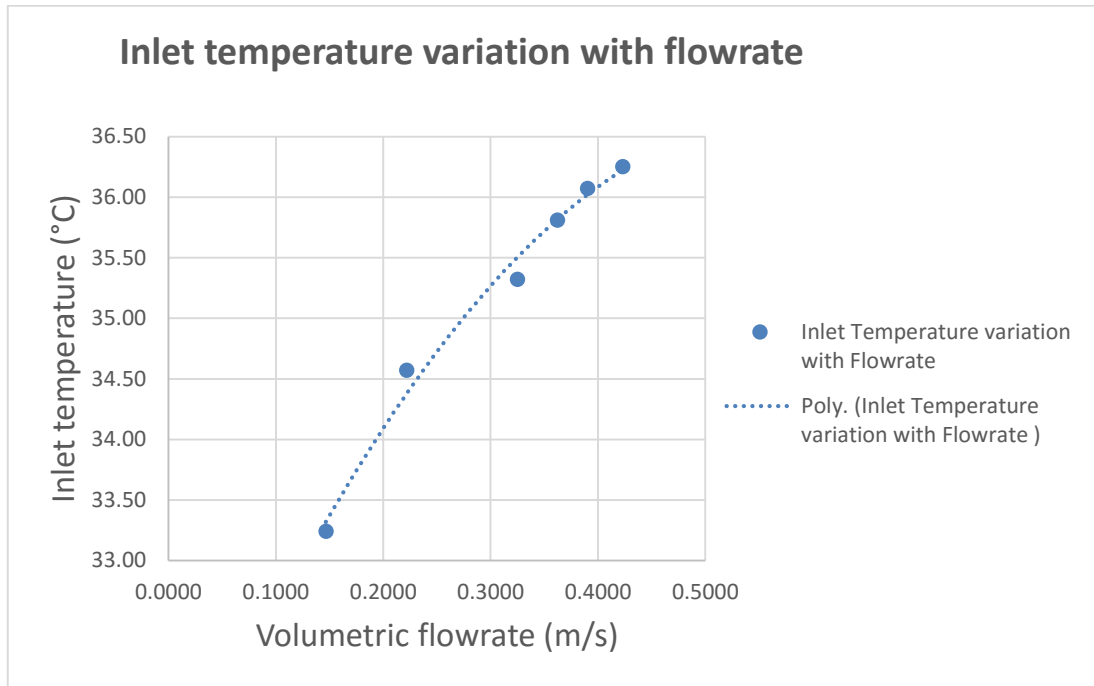


Figure 14 (a): Variation of De-ionized water inlet temperature with flowrate (lower temperature feed) during $U_i A_i$ experiments

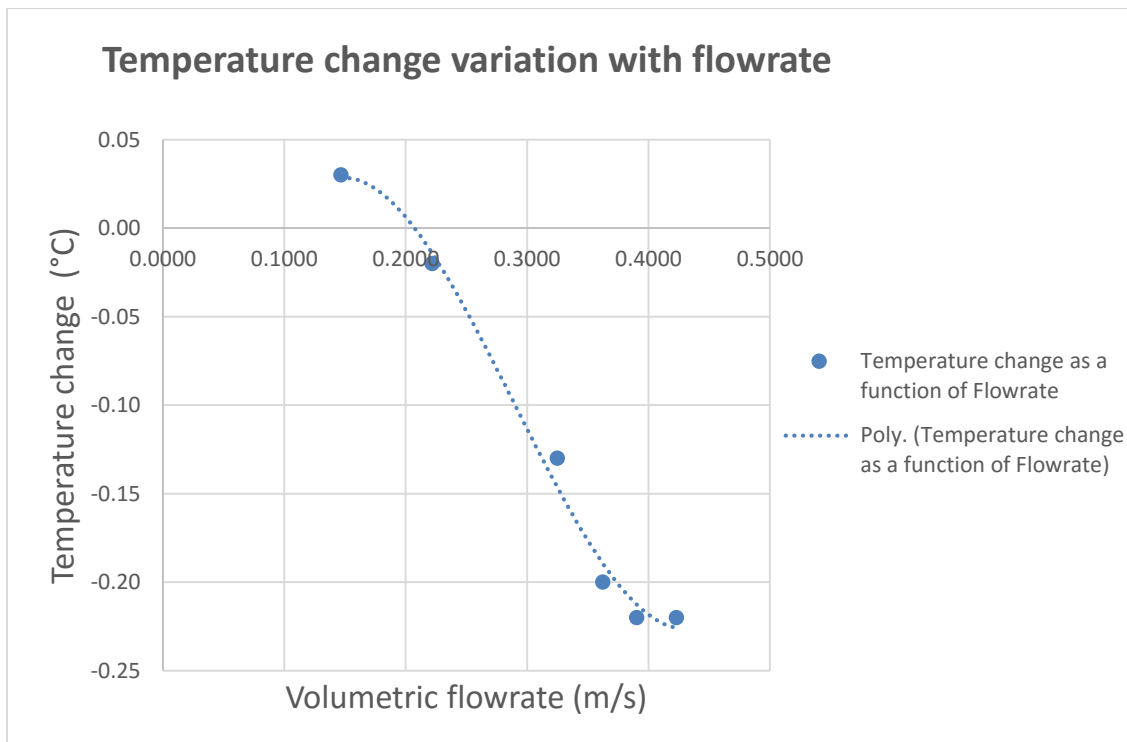


Figure 14 (b): De-ionized water temperature change variation with flowrate (lower temperature feed) during $U_i A_i$ measurements

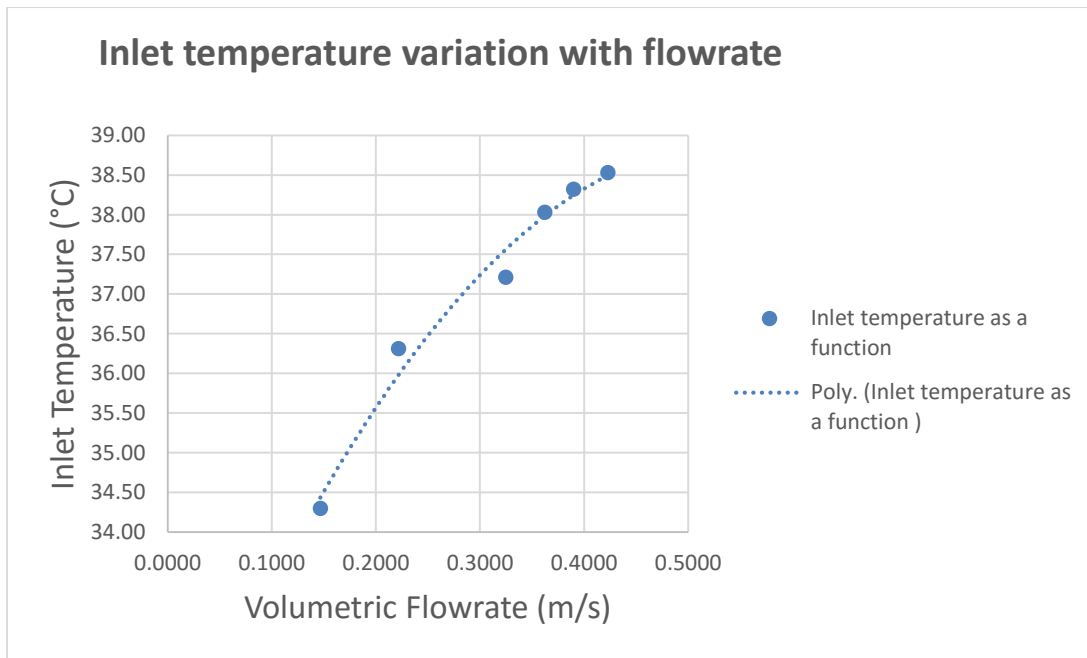


Figure 14(c): De-ionized water inlet temperature variation with flowrate (higher temperature feed) during $U_i A_i$ measurements

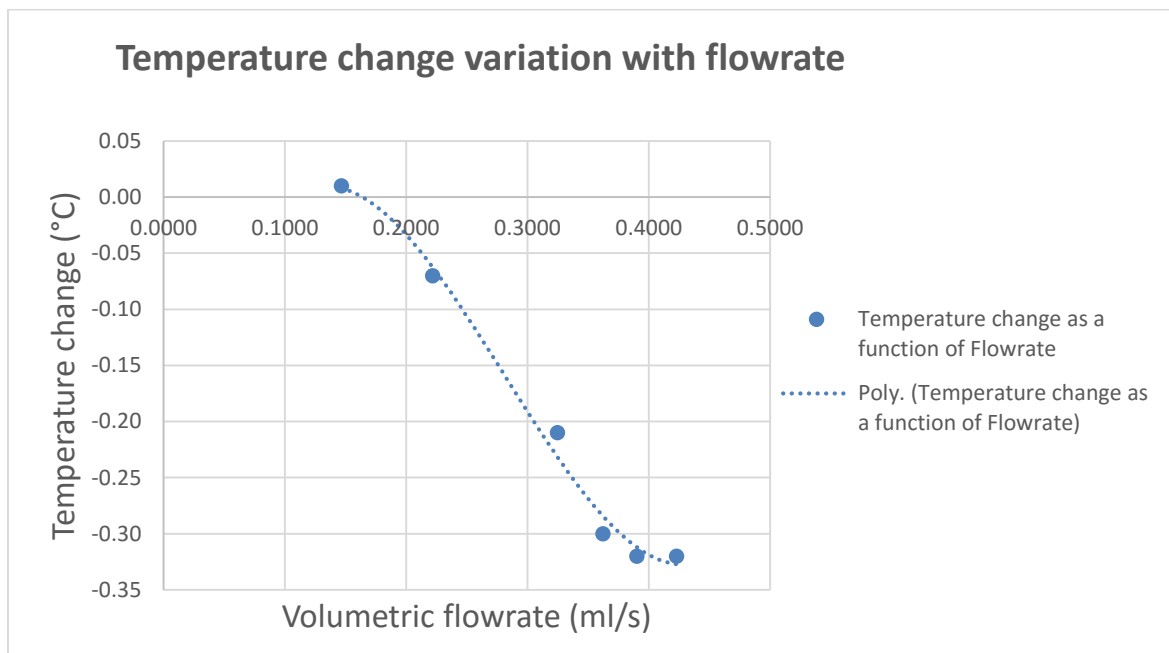


Figure 14 (d): De-ionized water temperature change variation with flowrate (higher temperature feed) during $U_i A_i$ measurements

Table 1.3.1: Measurement of De-ionized water conductive heat leaks at pump setting 6

\dot{V} (ml/s)	T_7 (°C)	T_6 (°C)	T_4 (°C)	T_3 (°C)	Corrected $T_4 - T_3$ (°C)	T_{mean} (°C)	$(\Delta T)_{LM}$ (°C)	μ_{wat}^* (mPa.s)	μ_{tol}^* (mPa.s)
0.1466	29.96	31.42	31.24	29.95	1.27	30.60	-0.2617	0.7884	0.5184
0.1466	29.96	31.42	31.43	29.95	1.46	30.69	-0.2926	0.7868	0.5178
0.1466	29.96	31.42	31.63	29.96	1.65	30.80	-0.3729	0.7851	0.5172
0.1466	29.96	31.42	32.09	29.97	2.10	31.03	-0.4926	0.7812	0.5158
0.1466	29.96	31.42	32.60	29.99	2.59	31.30	-0.6530	0.7768	0.5143

ρ (g/ml)	\dot{n} (mol/s)	C_p' (J/mol°C)	$U_i A_i$ (W/°C)
0.9956	0.0081	75.2340	0.0116
0.9956	0.0081	75.2340	0.0116
0.9956	0.0081	75.2340	0.0116
0.9956	0.0081	75.2340	0.0116
0.9956	0.0081	75.2340	0.0116

k^{**} (W/mK)	q_{CV} (W)	$\frac{\dot{V}}{\alpha L_t}$	Q_{ideal} (W)	Q (W)	q_{total} (W)	q_{HL} (W)	$\frac{q_{HL}\%}{Q}$
0.6152	-0.0030	2.4772	0.7748	1.0114	0.2366	0.2336	23.0935
0.6153	-0.0034	2.4766	0.8907	1.1610	0.2703	0.2669	22.9915
0.6154	-0.0043	2.4759	1.0066	1.3210	0.3144	0.3100	23.4715
0.6156	-0.0057	2.4744	1.2811	1.6718	0.3907	0.3850	23.0295
0.6158	-0.0076	2.4728	1.5800	2.0640	0.4840	0.4764	23.0809

$\ln q_{HL}$	π'_1	$\ln \pi'_1$	π'_4	$\ln \pi'_4$	$\ln \lambda$	Average $\ln \lambda$
-1.4543	1.5537	0.4406	0.0331	-3.4095	1.5220	1.5163
-1.3208	1.5540	0.4409	0.0378	-3.2747	1.5137	
-1.1710	1.5544	0.4411	0.0429	-3.1490	1.5311	
-0.9545	1.5553	0.4417	0.0539	-2.9210	1.5075	
-0.7415	1.5563	0.4423	0.0660	-2.7188	1.5072	

Table 1.3.2: Measurement of De-ionized water conductive heat leaks at pump setting 9

\dot{V} (ml/s)	T_7 (°C)	T_6 (°C)	T_4 (°C)	T_3 (°C)	Corrected $T_4 - T_3$ (°C)	T_{mean} (°C)	$(\Delta T)_{LM}$ (°C)	μ_{wat}^* (mPa.s)	μ_{tol}^* (mPa.s)
0.2218	29.96	31.03	30.86	29.98	0.86	30.42	-0.2762	0.7913	0.5194
0.2218	29.96	31.02	31.00	29.99	0.99	30.50	-0.3262	0.7901	0.5190
0.2218	29.96	30.92	31.13	29.99	1.12	30.56	-0.3552	0.7890	0.5186
0.2218	29.96	30.92	31.44	30.00	1.42	30.72	-0.4430	0.7863	0.5176
0.2218	29.96	30.92	31.79	30.01	1.76	30.90	-0.5393	0.7833	0.5166

ρ (g/ml)	\dot{n} (mol/s)	C_p' (J/mol°C)	$U_i A_i$ (W/°C)
0.9956	0.0123	75.2340	0.0277
0.9956	0.0123	75.2340	0.0277
0.9956	0.0123	75.2340	0.0277
0.9956	0.0123	75.2340	0.0277
0.9956	0.0123	75.2340	0.0277

k^{**} (W/mK)	q_{CV} (W)	$\frac{\dot{V}}{\alpha L_t}$	Q_{ideal} (W)	Q (W)	q_{total} (W)	q_{HL} (W)	$\frac{q_{HL}}{Q}\%$
0.6154	-0.0076	3.7499	0.7938	1.0114	0.2176	0.2099	20.7243
0.6155	-0.0090	3.7491	0.9138	1.1610	0.2472	0.2382	20.5135
0.6156	-0.0098	3.7485	1.0338	1.3210	0.2872	0.2773	20.9940
0.6159	-0.0123	3.7469	1.3107	1.6718	0.3611	0.3489	20.8669
0.6161	-0.0149	3.7452	1.6245	2.0640	0.4395	0.4245	20.5680

$\ln q_{HL}$	π'_1	$\ln \pi'_1$	π'_4	$\ln \pi'_4$	$\ln \lambda$	Average $\ln \lambda$
-1.5611	1.0504	0.0491	0.0332	-3.4038	1.9456	1.9348
-1.4348	1.0506	0.0493	0.0381	-3.2683	1.9293	
-1.2826	1.0507	0.0495	0.0432	-3.1413	1.9480	
-1.0531	1.0511	0.0499	0.0544	-2.9110	1.9351	
-0.8568	1.0516	0.0503	0.0668	-2.7061	1.9157	

Table: 1.3.3: Measurement of De-ionized water conductive heat leaks at pump setting 12

\dot{V} (ml/s)	T_7 (°C)	T_6 (°C)	T_4 (°C)	T_3 (°C)	Corrected $T_4 - T_3$ (°C)	T_{mean} (°C)	$(\Delta T)_{LM}$ (°C)	μ_{wat}^* (mPa.s)	μ_{tol}^* (mPa.s)
0.3249	29.96	30.73	30.64	29.96	0.66	30.30	-0.1872	0.7933	0.5201
0.3249	29.96	30.73	30.76	29.98	0.76	30.37	-0.2537	0.7922	0.5197
0.3249	29.96	30.73	30.86	29.98	0.86	30.42	-0.2762	0.7913	0.5194
0.3249	29.96	30.73	31.10	29.99	1.09	30.55	-0.3486	0.7892	0.5187
0.3249	29.96	30.73	31.86	29.99	1.35	30.68	-0.4051	0.7871	0.5179

ρ (g/ml)	\dot{n} (mol/s)	C_p' (J/mol°C)	$U_i A_i$ (W/°C)
0.9956	0.0180	75.2340	0.0642
0.9956	0.0180	75.2340	0.0642
0.9956	0.0180	75.2340	0.0642
0.9956	0.0180	75.2340	0.0642
0.9956	0.0180	75.2340	0.0642

k^{**} (W/mK)	q_{cv} (W)	$\frac{\dot{V}}{\alpha L_t}$	Q_{ideal} (W)	Q (W)	q_{total} (W)	q_{HL} (W)	$\frac{q_{HL}\%}{Q}$
0.6152	-0.0120	5.4950	0.8924	1.0114	0.1189	0.1069	10.5708
0.6153	-0.0163	5.4940	1.0277	1.1610	0.1333	0.1171	10.0827
0.6154	-0.0177	5.4933	1.1629	1.3210	0.1581	0.1404	10.6254
0.6156	-0.0224	5.4915	1.4739	1.6718	0.1980	0.1756	10.5028
0.6158	-0.0260	5.4896	1.8254	2.0640	0.2386	0.2126	10.2982

$\ln q_{HL}$	π'_1	$\ln \pi'_1$	π'_4	$\ln \pi'_4$	$\ln \lambda$	Average $\ln \lambda$
-2.2358	0.7383	-0.3035	0.0334	-3.3999	1.7498	1.7237
-2.1451	0.7384	-0.3033	0.0382	-3.2642	1.6978	
-1.9636	0.7385	-0.3032	0.0434	-3.1367	1.7454	
-1.7396	0.7387	-0.3029	0.0547	-2.9053	1.7259	
-1.5486	0.7389	-0.3026	0.0673	-2.6988	1.6997	

Appendix B

Experimental fluid: n-Butanol

Butanol source: Merc

Assay: 99 % (minimum)

Table 2.1: Purity of n-Butanol data

	Refractive index (25°C)	Density g/ml (20 °C)
Pure	1.3973	1.8091
Calorimeter discharge	1.3969	1.8108
Literature ⁹⁷	1.397	1.8098

Temperature calibration correction factors: $T_4 - T_3 = 0.01^\circ C$

: $T_7 - T_4 = 0.00^\circ C$

: $T_7 - T_3 = 0.01^\circ C$

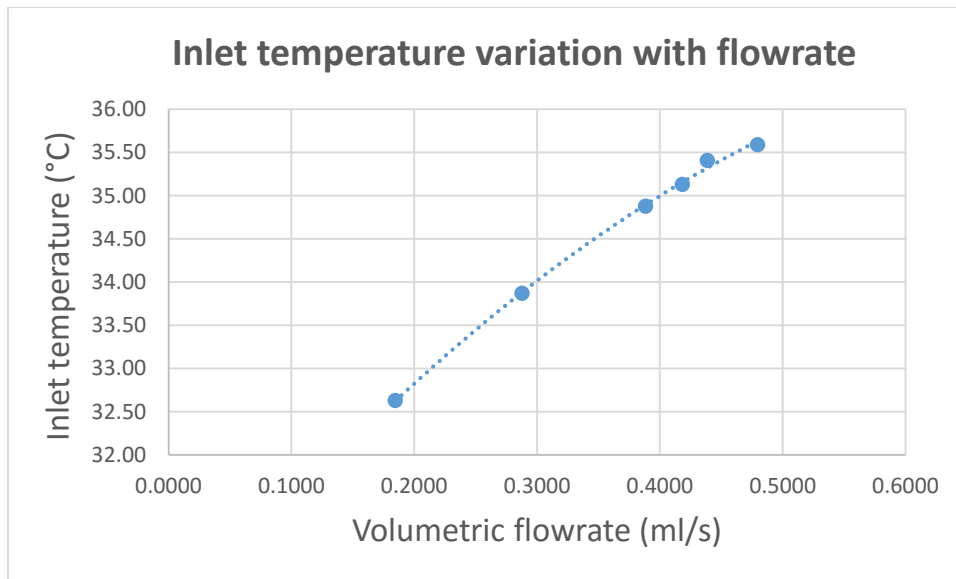


Figure 15 (a): 1-Butanol inlet temperature variation flowrate during $U_i A_i$ experiments

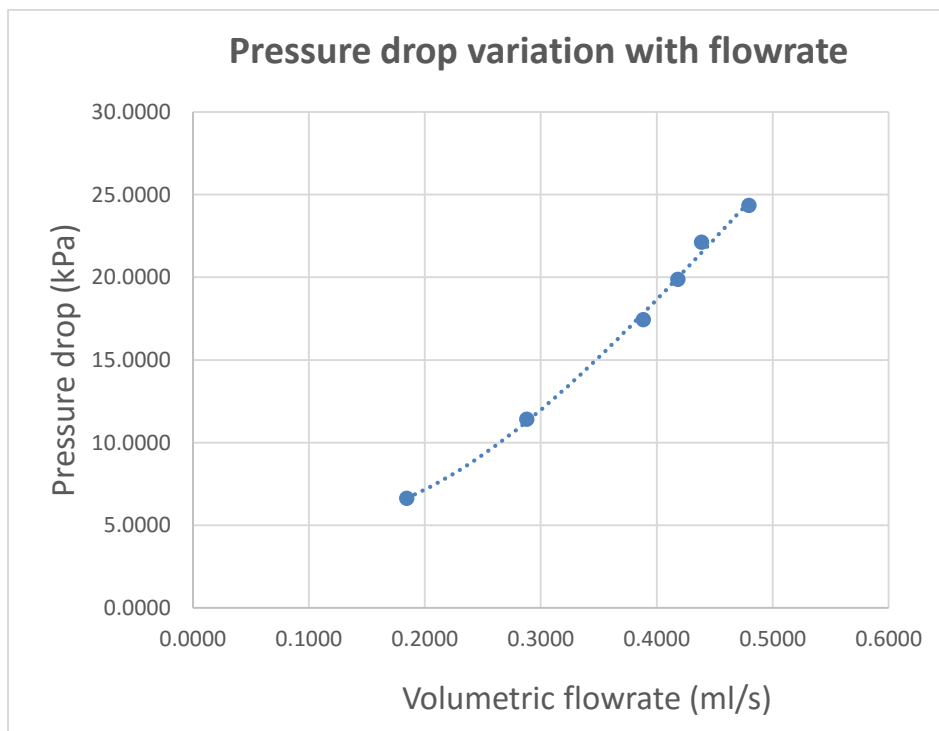


Figure 15 (b): Dependence of 1-Butanol pressure drop on flow rate during $U_i A_i$ experiments

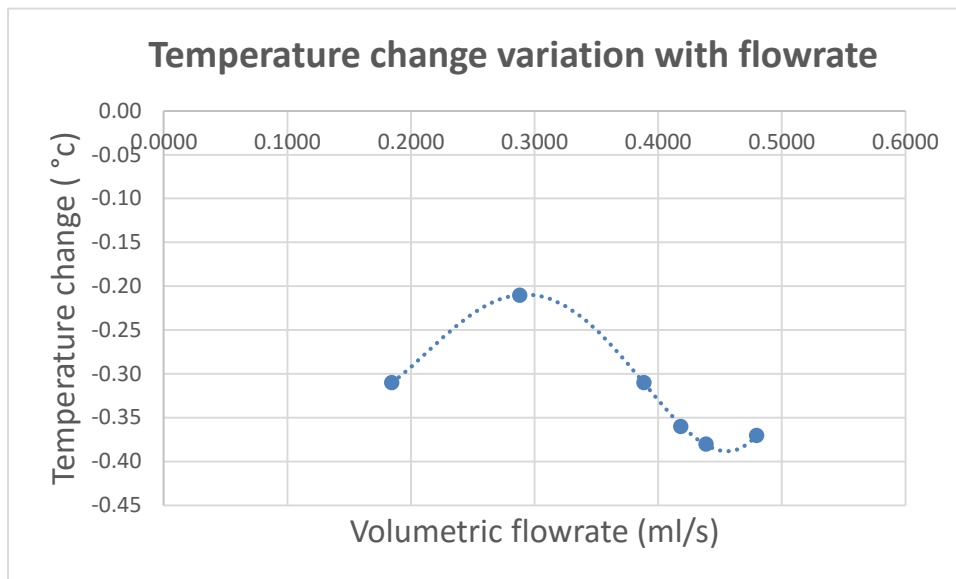


Figure 15 (c): 1-Butanol temperature variation with flowrate during $U_i A_i$ experiments

Table 2.3.1: Measurement of n-Butanol conductive heat leaks at pumps setting 6

\dot{V} (ml/s)	T_7 (°C)	T_6 (°C)	T_4 (°C)	T_3 (°C)	Corrected $T_4 - T_3$ (°C)	T_{mean} (°C)	$(\Delta T)_{LM}$ (°C)	μ_{but}^* (mPa.s)	μ_{tol}^* (mPa.s)
0.1846	29.97	31.64	30.74	30.00	0.73	30.37	-0.2468	2.3293	0.5197
0.1846	29.97	31.64	30.94	30.00	0.93	30.47	-0.2917	2.3232	0.5197
0.1846	29.97	31.64	31.26	30.13	1.12	30.70	-0.5527	2.3096	0.5178
0.1846	29.97	31.64	31.78	30.14	1.63	30.96	-0.7062	2.2935	0.5162
0.1846	29.97	31.64	32.36	30.14	2.21	31.25	-0.8546	2.2761	0.5145

ρ (g/ml)	\dot{n} (mol/s)	ΔP (kPa)	ΔP correction factor (kPa)	Corrected $\frac{\Delta P}{\rho}$		C_p' (J/mol°C)	$U_i A_i$ (W/°C)
				(J/kg)	(J/mol)		
0.8050	0.0020	3.6593	3.5000	8.8939	0.6592	181.0937	0.0456
0.8049	0.0020	2.7041	3.5000	7.7081	0.5713	181.1686	0.0456
0.8047	0.0020	3.3323	3.5000	8.4904	0.6293	181.3374	0.0456
0.8045	0.0020	3.3330	3.5000	8.4935	0.6295	181.5366	0.0456
0.8043	0.0020	3.4477	3.5000	8.6383	0.6403	181.7550	0.0456

k^{**} (W/m K)	q_{cv} (W)	$\frac{\dot{V}}{\alpha L_t}$	Q_{ideal} (W)	Q (W)	q_{total} (W)	q_{HL} (W)	$\frac{q_{HL}}{Q}\%$
0.1479	-0.0113	6.1365	0.2651	0.3302	0.0652	0.0552	16.7268
0.1479	-0.0133	6.1396	0.3378	0.4180	0.0802	0.0680	16.2716
0.1478	-0.0252	6.1465	0.4071	0.5160	0.1089	0.0850	16.4655
0.1478	-0.0322	6.1547	0.5930	0.7430	0.1501	0.1191	16.0318
0.1477	-0.0390	6.1636	0.8047	1.0114	0.2066	0.1690	16.7058

$\ln q_{HL}$	π'_1	$\ln \pi'_1$	π'_4	$\ln \pi'_4$	$\ln \lambda$	Average $\ln \lambda$
-2.8961	0.6679	-0.4036	0.0109	-4.5214	1.7342	1.7561
-2.6881	0.6676	-0.4040	0.0137	-4.2891	1.7219	
-2.4656	0.6670	-0.4050	0.0168	-4.0857	1.7521	
-2.1276	0.6662	-0.4062	0.0240	-3.7297	1.7528	
-1.7781	0.6653	-0.4076	0.0324	-3.4307	1.8193	

Table 2.3.2: Measurement of n-Butanol conductive heat leaks at pump setting 9

\dot{V} (ml/s)	T_7 (°C)	T_6 (°C)	T_4 (°C)	T_3 (°C)	Corrected $T_4 - T_3$ (°C)	T_{mean} (°C)	$(\Delta T)_{LM}$ (°C)	μ_{but}^* (mPa.s)	μ_{tol}^* (mPa.s)
0.2880	29.97	31.14	30.54	30.03	0.50	30.29	-0.2384	2.3345	0.5202
0.2880	29.97	31.14	30.7	30.06	0.63	30.38	-0.3169	2.3287	0.5197
0.2880	29.97	31.14	30.96	30.17	0.78	30.57	-0.5030	2.3175	0.5186
0.2880	29.97	31.14	31.26	30.12	1.13	30.69	-0.5414	2.3099	0.5178
0.2880	29.97	31.14	31.72	30.18	1.53	30.95	-0.7378	2.2941	0.5163

ρ (g/ml)	\dot{n} (mol/s)	ΔP (kPa)	ΔP correction factor (kPa)	Corrected $\frac{\Delta P}{\rho}$		C_p' (J/mol°C)	$U_i A_i$ (W/°C)
				(J/kg)	(J/mol)		
0.8050	0.0031	8.6341	3.5000	15.0730	1.1172	181.0301	0.0325
0.8050	0.0031	8.6092	3.5000	15.0434	1.1150	181.1012	0.0325
0.8048	0.0031	8.6327	3.5000	15.0754	1.1174	181.2398	0.0325
0.8047	0.0031	8.6692	3.5000	15.1223	1.1209	181.3336	0.0325
0.8045	0.0031	8.6348	3.5000	15.0833	1.1180	181.5290	0.0325

k^{**} (W/m K)	q_{cv} (W)	$\frac{\dot{V}}{\alpha L_t}$	Q_{ideal} (W)	Q (W)	q_{total} (W)	q_{HL} (W)	$\frac{q_{HL}}{Q}\%$
0.1480	-0.0077	9.5683	0.2831	0.3302	0.0471	0.0429	12.9793
0.1479	-0.0103	9.5729	0.3569	0.4180	0.0611	0.0543	12.9926
0.1479	-0.0163	9.5817	0.4421	0.5160	0.0739	0.0611	11.8382
0.1478	-0.0176	9.5878	0.6407	0.7430	0.1023	0.0883	11.8784
0.1478	-0.0240	9.6003	0.8682	1.0114	0.1431	0.1227	12.1299

$\ln q_{HL}$	π'_1	$\ln \pi'_1$	π'_4	$\ln \pi'_4$	$\ln \lambda$	Average $\ln \lambda$
-3.1497	0.4508	-0.7967	0.0109	-4.5186	-4.5186	1.7909
-2.9132	0.4506	-0.7971	0.0138	-4.2862	-4.2862	
-2.7955	0.4503	0.7979	0.0169	-4.0815	-4.0815	
-2.4274	0.4500	-0.7985	0.0242	-3.7209	-3.7209	
-2.0982	0.4495	-0.7996	0.0327	-3.4211	-3.4211	

Table 2.3.3: Measurement of n-Butanol conductive heat leaks at pump setting 12

\dot{V} (ml/s)		T_6 (°C)	T_4 (°C)	T_3 (°C)	Corrected $T_4 - T_3$ (°C)	T_{mean} (°C)	$(\Delta T)_{LM}$ (°C)	μ_{but}^* (mPa.s)	μ_{tol}^* (mPa.s)
0.3885	29.96	31.14	30.48	30.09	0.38	30.29	-0.2896	2.3345	0.5202
0.3885	29.96	31.14	30.60	30.11	0.49	30.35	-0.3437	2.3303	0.5198
0.3885	29.96	31.14	30.68	30.07	0.60	30.38	-0.3351	2.3290	0.5197
0.3885	29.96	31.14	30.99	30.12	0.87	30.56	-0.4754	2.3181	0.5186
0.3885	29.96	31.15	31.36	30.18	1.17	30.77	-0.6379	2.3052	0.5174

ρ (g/ml)	\dot{n} (mol/s)	ΔP (kPa)	ΔP correction factor (kPa)	Corrected $\Delta P / \rho$		C'_p (J/mol°C)	$U_i A_i$ (W/°C)
				(J/kg)	(J/mol)		
0.8057	0.0042	15.1919	3.5000	23.1997	1.7196	181.0301	0.0518
0.8057	0.0042	15.1422	3.5000	23.1393	1.7151	181.0818	0.0518
0.8056	0.0042	15.1454	3.5000	23.1439	1.7154	181.0982	0.0518
0.8055	0.0042	15.1166	3.5000	23.1121	1.7131	181.2324	0.0518
0.8053	0.0042	14.9456	3.5000	22.9045	1.6977	181.3914	0.0518

k^{**} (W/m K)	q_{cv} (W)	$\frac{\dot{V}}{\alpha L_r}$	Q_{ideal} (W)	Q (W)	q_{total} (W)	q_{HL} (W)	$\frac{q_{HL}\%}{Q}$
0.1480	-0.0150	12.9179	0.2905	0.3302	0.0397	0.0320	9.6844
0.1479	-0.0178	12.9225	0.3713	0.4180	0.0467	0.0361	8.6387
0.1479	-0.0174	12.9238	0.4610	0.5160	0.0550	0.0449	8.6978
0.1479	-0.0246	12.9354	0.6625	0.7430	0.0806	0.0631	8.4969
0.1478	-0.0331	12.9491	0.8976	1.0114	0.1138	0.0878	8.6862

$\ln q_{HL}$	π'_1	$\ln \pi'_1$	π'_4	$\ln \pi'_4$	$\ln \lambda$	Average $\ln \lambda$
-3.4426	0.3491	-1.0525	0.0109	-4.5189	1.7236	1.6638
-3.3213	0.3490	-1.0528	0.0138	-4.2853	1.6235	
-3.1038	0.3489	-1.0528	0.0170	-4.0753	1.6416	
-2.7625	0.3487	-1.0536	0.0243	-3.7165	1.6427	
-2.4321	0.3484	-1.0545	0.0329	-3.4151	1.6875	

Appendix C

Experimental fluid: Toluene

Toluene source: Sigma-Aldrich (puriss. p.a ACS reagent)

Assay: 99.7 % (minimum)

Table 4.1: Purity of Toluene data

	Refractive index (25°C)	Density g/ml (20 °C)
Pure	1.4938	0.86655
Calorimeter discharge	1.4936	0.86706
Literature ⁹⁷	1.494	0.8669

Temperature calibration correction factors: $T_4 - T_3 = 0.01^\circ\text{C}$

: $T_7 - T_3 = 0.00^\circ\text{C}$

: $T_7 - T_3 = 0.01^\circ\text{C}$

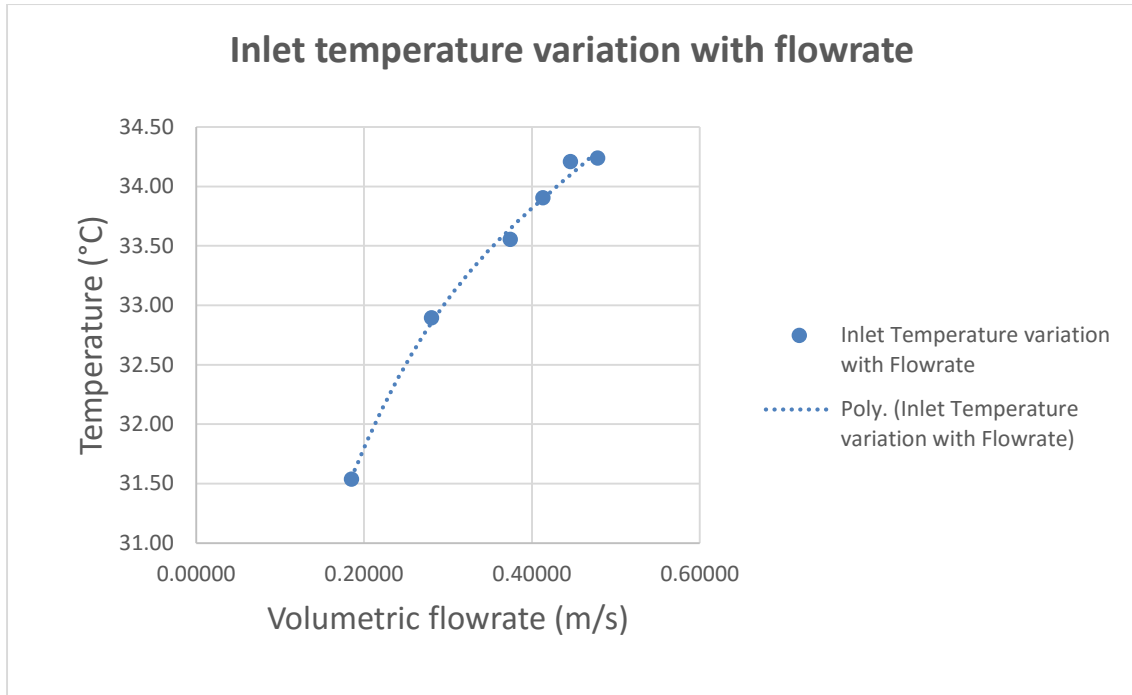


Figure 16 (a): Toluene variation of inlet temperature with flowrate during $U_i A_i$ measurements

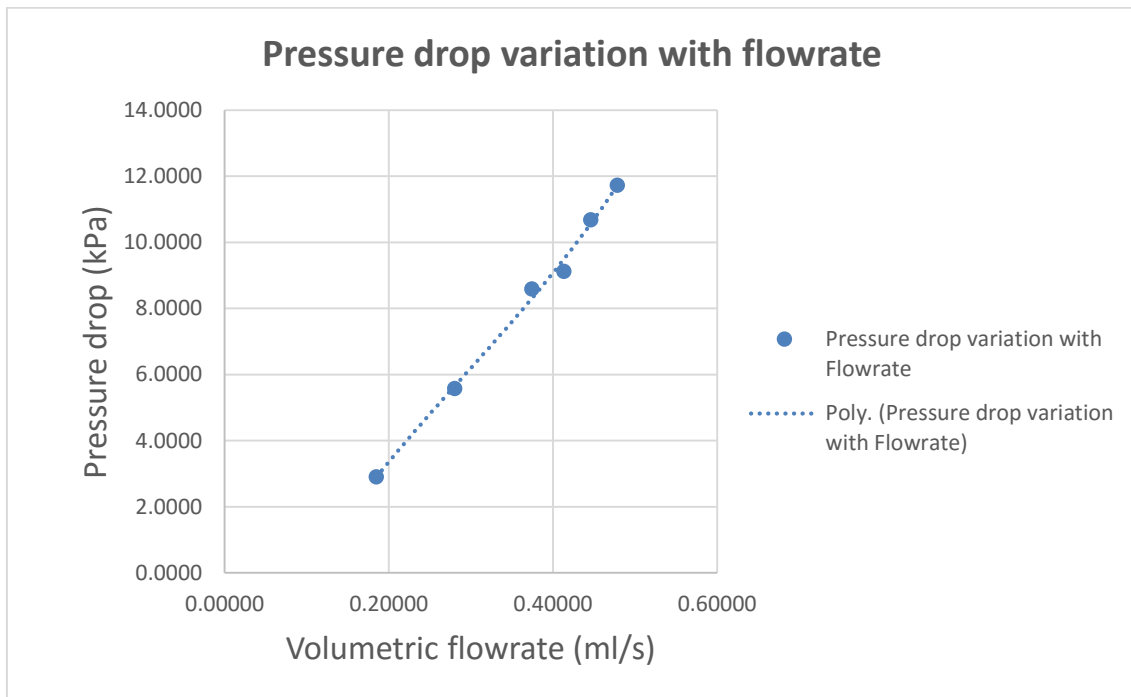


Figure 16 (b): Toluene pressure dependence on flowrate during $U_i A_i$ measurements

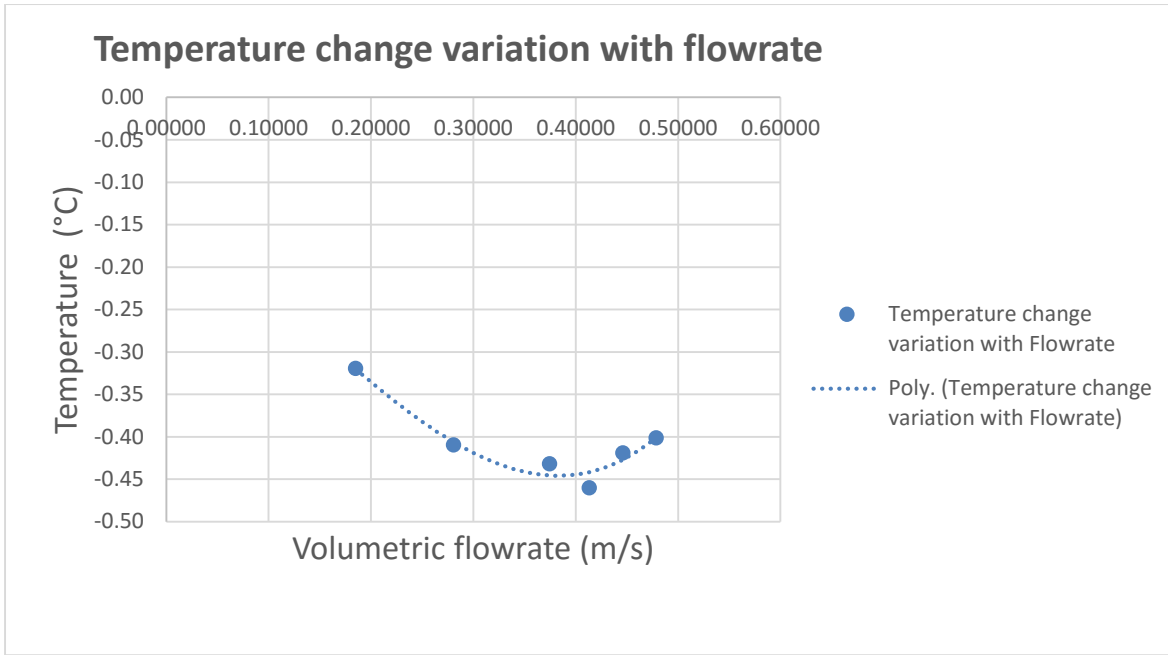


Figure 16 (c): Toluene temperature change variation with flowrate during $U_i A_i$ measurements

Table 3.3.1: Measurement of Toluene conductive heat leaks at pump setting 6

\dot{V} (ml/s)	T_7 (°C)	T_6 (°C)	T_4 (°C)	T_3 (°C)	Corrected $T_4 - T_3$ (°C)	T_{mean} (°C)	$(\Delta T)_{LM}$ (°C)	μ_{tol}^* (mPa.s)
0.1850	29.97	32.84	30.78	30.01	0.76	30.39	-0.2766	0.5196
0.1850	29.96	32.04	31.04	30.02	1.01	30.53	-0.3654	0.5188
0.1850	29.96	32.64	31.30	30.02	1.27	30.66	-0.4112	0.5180
0.1850	29.96	32.54	31.64	30.07	1.55	30.85	-0.5854	0.5169
0.1850	29.96	32.54	32.32	30.08	2.23	31.20	-0.7671	0.5148

ρ (g/ml)	\dot{n} (mol/s)	ΔP (kPa)	ΔP correction factor (kPa)	Corrected $\Delta P / \rho$		C'_p (J/mol°C)	$U_i A_i$ (W/°C)
				(J/kg)	(J/mol)		
0.8567	0.0017	-0.6894	3.5000	3.2809	0.3023	158.8501	0.0618
0.8565	0.0017	-0.7705	3.5000	3.1867	0.2936	158.8899	0.0618
0.8564	0.0017	-0.6107	3.5000	3.3737	0.3109	158.9261	0.0618
0.8562	0.0017	-0.9113	3.5000	3.0233	0.2786	158.9835	0.0618
0.8559	0.0017	-0.7350	3.5000	3.2304	0.2977	159.0846	0.0618

k^{**} (W/m K)	q_{cv} (W)	$\frac{\dot{V}}{\alpha L_f}$	Q_{ideal} (W)	Q (W)	q_{total} (W)	q_{HL} (W)	$\frac{q_{HL}\%}{Q}$
0.1291	-0.0171	158.8501	0.2071	0.2528	0.0457	0.0292	11.5313
0.1291	-0.0226	158.8899	0.2751	0.3302	0.0552	0.0331	10.0155
0.1291	-0.0254	158.9261	0.3470	0.4180	0.0710	0.0461	11.0226
0.1290	-0.0362	158.9835	0.4245	0.5160	0.0915	0.0558	10.8100
0.1289	-0.0474	159.0846	0.6088	0.7430	0.1342	0.0873	11.7466

$\ln q_{HL}$	π'_1	$\ln \pi'_1$	π'_4	$\ln \pi'_4$	$\ln \lambda$	Average $\ln \lambda$
-3.5351	0.7609	-0.2733	0.0083	-4.7892	1.6737	1.6343
-3.4090	0.7606	-0.2737	0.0108	-4.5266	1.5351	
-3.0776	0.7603	-0.2740	0.0136	-4.2952	1.6332	
-2.8863	0.7599	-0.2745	0.0167	-4.0909	1.61881	
-2.4386	0.7592	-0.2755	0.0238	-3.7375	1.7109	

Table 3.3.2: Measurement of Toluene conductive heat leaks at pump setting 9

\dot{V} (ml/s)	T_7 (°C)	T_6 (°C)	T_4 (°C)	T_3 (°C)	Corrected $T_4 - T_3$ (°C)	T_{mean} (°C)	$(\Delta T)_{LM}$ (°C)	μ_{tol}^* (mPa.s)
0.2805	27.97	31.84	30.52	29.98	30.25	30.25	-0.1674	0.5205
0.2805	29.97	32.05	30.72	30.01	30.36	30.36	-0.2608	0.5198
0.2805	29.97	32.14	30.90	30.02	30.46	30.46	-0.3280	0.5192
0.2805	29.97	32.15	31.20	30.13	30.67	30.67	-0.5393	0.5180
0.2805	29.97	32.15	31.71	30.15	30.93	30.93	-0.6089	0.5164

ρ (g/ml)	\dot{n} (mol/s)	ΔP (kPa)	ΔP correction factor (kPa)	Corrected $\Delta P / \rho$		C_p' (J/mol°C)	$U_i A_i$ (W/°C)
				(J/kg)	(J/mol)		
0.8568	0.0026	2.1243	3.5000	6.5643	0.6048	158.8086	0.0628
0.8567	0.0026	2.41999	3.5000	6.9101	0.6367	158.8418	0.0628
0.8566	0.0026	2.3280	3.5000	6.8036	0.6269	158.8702	0.0628
0.8564	0.0026	2.3382	3.5000	6.8170	0.6281	158.9293	0.0628
0.8562	0.0026	2.6182	3.5000	7.1460	0.6584	159.0047	0.0628

k^{**} (W/m K)	q_{cv} (W)	$\frac{\dot{V}}{\alpha L_f}$	Q_{ideal} (W)	Q (W)	q_{total} (W)	q_{HL} (W)	$\frac{q_{HL}\%}{Q}$
0.1292	-0.0105	8.0179	0.2191	0.2528	0.0338	0.0248	9.8176
0.1291	-0.0164	8.0207	0.2905	0.3302	0.0398	0.0251	7.5878
0.1291	-0.0206	8.0229	0.3594	0.4180	0.0586	0.0396	9.4791
0.1291	-0.0339	8.0275	0.4420	0.5160	0.0740	0.0417	8.0902
0.1290	-0.0439	8.0336	0.6434	0.7430	0.0997	0.0575	7.7327

$\ln q_{HL}$	π'_1	$\ln \pi'_1$	π'_4	$\ln \pi'_4$	$\ln \lambda$	Average $\ln \lambda$
-3.6960	0.5130	-0.6674	0.0084	-4.7844	2.0440	1.9044
-3.6866	0.5129	-0.6677	0.0109	-4.55212	1.7879	
-3.2285	0.5127	-0.6680	0.0137	-4.2888	2.0118	
-3.1762	0.5124	0.6686	0.0168	-4.0848	1.8587	
-2.8567	0.5121	-0.6693	0.0240	-3.7286	1.8194	

Table 3.3.3: Measurement of Toluene conductive heat leaks at pump setting 12

\dot{V} (ml/s)	T_7 (°C)	T_6 (°C)	T_4 (°C)	T_3 (°C)	Corrected $T_4 - T_3$ (°C)	T_{mean} (°C)	$(\Delta T)_{LM}$ (°C)	μ_{tol}^* (mPa.s)
0.3743	29.97	31.65	30.47	30.05	0.41	30.26	-0.2497	0.5204
0.3743	29.97	31.65	30.61	30.06	0.54	30.33	-0.2902	0.5200
0.3743	29.97	31.64	30.77	30.08	0.68	30.42	-0.3627	0.5194
0.3743	29.97	31.64	30.90	30.05	0.84	30.48	-0.3693	0.5191
0.3743	29.97	31.34	31.26	30.03	1.22	30.65	-0.4319	0.5181

ρ (g/ml)	\dot{n} (mol/s)	ΔP (kPa)	ΔP correction factor (kPa)	Corrected $\Delta P / \rho$		C'_p (J/mol°C)	$U_i A_i$ (W/°C)
				(J/kg)	(J/mol)		
0.8568	0.0035	4.7929	3.5000	9.6789	0.8918	158.8131	0.0718
0.8567	0.0035	4.7722	3.5000	9.6555	0.8897	158.8330	0.0718
0.8566	0.0035	4.1229	3.5000	8.8986	0.8199	158.8595	0.0718
0.8566	0.0035	4.1039	3.5000	8.8769	0.8179	158.8750	0.0718
0.8564	0.0035	4.7892	3.5000	9.6788	0.8918	158.9235	0.0718

k^{**} (W/m K)	q_{cv} (W)	$\frac{\dot{V}}{\alpha L_r}$	Q_{ideal} (W)	Q (W)	q_{total} (W)	q_{HL} (W)	$\frac{q_{HL\%}}{Q}$
0.1292	-0.0179	10.6994	0.2266	0.2528	0.0263	0.0114	4.5196
0.1292	-0.0208	10.7015	0.2993	0.3302	0.0310	0.0132	4.0044
0.1291	-0.0260	10.7043	0.3773	0.4180	0.0406	0.0175	4.1768
0.1291	-0.0265	10.7058	0.4654	0.5160	0.0506	0.0270	5.2243
0.1291	-0.0310	10.7110	0.6728	0.7430	0.0703	0.0424	5.7042

$\ln q_{HL}$	π'_1	$\ln \pi'_1$	π'_4	$\ln \pi'_4$	$\ln \lambda$	Average $\ln \lambda$
-4.4717	0.3874	-0.9482	0.0084	-4.7850	1.6507	1.6872
-4.3257	0.3874	-0.9484	0.0109	-4.5202	1.5295	
-4.0480	0.3873	-0.9487	0.0137	-4.2876	1.5727	
-3.6135	0.3872	-0.9488	0.0169	-4.0787	1.7963	
-3.1610	0.3870	-0.9493	0.0242	-3.7195	1.8868	

Appendix D

Equipment specifications

REGLO-Z gear pump head (Z-181) ⁷⁰

Pressure differential: 2.8 bar (maximum)

System pressure: 21 bar (maximum)

Swagelok non-return valves (SS-4CA-3) ⁷¹

Cracking pressure: adjustable (0.21-3.5 bar)

PolyScience immersion heater/circulator (7306) ⁶⁶

Temperature stability: ± 0.05 °C

Uncertainty: ± 0.5 °C

Built-in two-speed simplex circulator pump discharge 15 L/min (maximum)

WIKA Pt-100 sensors (Class A) ⁷³

Uncertainty: $\pm 0.15T$ °C (IEC 60751:2008)

Temperature coefficient of resistance: 0.385 % / °C

WIKA S-10 absolute pressure sensors ⁹⁶

Uncertainty: $\leq 0.25\%$ of the span

UNI-T (UT60B) digital multimeter ⁶⁹

Uncertainty in current measurement (near 400 mA): $\pm(1.2\% + 3)$

Resolution in current measurement: 0.1 mA

Uncertainty in resistance measurement ($< 400\Omega$): $\pm(1.2\% + 2)$

Resolution in resistance measurement: 0.1 Ω

Nichrome 80 mixer heater ribbon ⁶⁷

Nominal temperature coefficient of resistance (at 20 °C): 0.00011 $\Omega/\Omega/^\circ\text{C}$

NI cRIO 9073 chassis ^{74, 75}

Processor: 266 MHz

DRAM: 64 MB

Non-volatile memory: 128 MB

Connection to PC: single 10/100 Mb/s and RS 232 serial ports

NI C Series analogue modules ^{76,77}

Bandwidth decrease: 70.7% of the original amplitude

Noise contribution to measurement uncertainty (high resolution mode): $\pm 0.003^{\circ}\text{C}$

NI 9217 analog input module ^{77,78}

Resolution: 24 bit (2^{-24} of full scale)

Sampling rate: Variable (100S/s/ch maximum)

Uncertainty in temperature measurement (including noise contribution):

$\pm 0.15^{\circ}\text{C}$ (4 wire RTD connections)

$\pm 0.2^{\circ}\text{C}$ (3 wire RTD connections)

NI 9203 Analog input module ⁷⁹

Resolution: 16 Bit (2^{-16} of full scale)

Sampling rate: 200kS/s (maximum)

Unipolar gain uncertainty (at $25 \pm 5^{\circ}\text{C}$): 0.04 %

Pr electronics transmitter isolator (3186 AI) ⁸⁰

Uncertainty: ± 0.1 % of span

NI DC Power Supply (NI PS-15)

Input: 115/230 VAC

Output: 24-28 VDC, 5 A

Host PC (Proline Pentium 4)

Processor: Intel Celeron (1.1 GHz)

RAM: 2.00 GB

HDD: 500 GB

KERN Analytical balance (ABT 100-5 M) ⁸¹

Reproducibility: 0.05 mg

Linearity: ± 0.15 mg

Anton Paar Density meter (DMA 5000) ⁸²

Uncertainty: $5 * 10^{-5}$ gcm⁻³

WIKA Temperature standard (CTH 6500) ⁹³

Full scale uncertainty: ± 0.03 K

WIKA Mensor pressure controller (CPC 8000) ⁹⁵

Measurement uncertainty: 0.008 % IS

Atago Refractometer (RX-7000 α) ⁹⁴

Measurement uncertainty: ± 0.0001

Repeatability: ± 0.00005

Appendix E

Pump 1 calibrations experimental data

Table 7.1: Pump 1 calibration data with De-ionized water as reference liquid

Pump setting		6	9	12	13	14	15
Mass of beaker	g	35.079	35.079	45.618	45.618	45.618	45.618
Average mass of beaker + water	g	43.8483	48.3341	65.0553	67.2892	68.9558	70.9243
Water mass	g	8.7693	13.2551	19.4373	21.6712	23.3378	25.3063
t	s	60	60	60	60	60	60
\dot{m}_{wat}	g/s	0.1462	0.2209	0.3240	0.3612	0.3890	0.4218
T	°C	26.44	27.7	24.54	25.50	25.30	25.93
ρ_{wat}	g/ml	0.9967	0.9963	0.9972	0.9970	0.9970	0.9970
\dot{V}_{wat}	ml/s	0.1466	0.2218	0.3249	0.3623	0.3901	0.4230

Table 7.2: Pump 1 calibration data with n-Butanol as reference liquid

Pump setting		6	9	12	13	14	15
Mass of beaker	g	34.997	34.997	34.997	34.997	34.997	34.997
Average mass of beaker + n-butanol	g	43.9212	48.9180	53.7756	55.2196	56.2052	58.1808
n-Butanol mass	g	8.9242	13.9210	18.7786	20.2226	21.2082	23.1838
t	s	60	60	60	60	60	60
\dot{m}_{but}	g/s	0.1487	0.2320	0.3130	0.3370	0.3535	0.386
T	°C	27.00	27.00	27.02	27.01	26.99	27.00
ρ_{but}	g/ml	0.8056	0.8056	0.8056	0.8056	0.8056	0.8056
\dot{V}_{but}	ml/s	0.1846	0.2880	0.3885	0.4184	0.4388	0.4796

Table 7.3: Pump 1 calibration data with Toluene as reference liquid

Pump setting		6	9	12	13	14	15
Mass of beaker	g	34.997	34.997	34.997	34.997	34.997	34.997
Average mass of beaker + Toluene	g	44.5354	49.449	54.2702	56.2752	57.9658	59.6262
Toluene mass	g	9.5384	14.4520	19.2732	21.2782	22.9688	24.6292
t	s	60	60	60	60	60	60
\dot{m}_{tol}	g/s	0.4105	0.3828	0.3546	0.3212	0.2409	0.1590
T	°C	27.77	28.65	29.18	29.04	29.20	29.40
ρ_{tol}	g/ml	0.8594	0.8586	0.8581	0.8582	0.8581	0.8579
\dot{V}_{tol}	ml/s	0.1850	0.2805	0.3743	0.4132	0.4461	0.4785

Appendix F

Pt-100 sensor calibrations

Table 8.1.1: Test calibration sensor resistance values (Ω)

Reference probe temperature ($^{\circ}\text{C}$)	0.01	5.04	10.03	15.00	19.99	24.98
Sensor 1	99.9620	101.9248	103.8708	105.8005	107.7387	109.6715
Sensor 2	100.0496	102.0169	103.9673	105.9017	107.8442	109.7800
Sensor 3	100.0077	101.9765	103.8907	105.8605	107.8021	109.7376
Sensor 4	99.9745	101.9409	103.9429	105.8233	107.7643	109.6986
Sensor 5	100.0255	101.9927	103.9429	105.8769	107.8192	109.7554
Sensor 6	99.9859	101.9472	103.8915	105.8207	107.7581	109.6930
Sensor 7	100.0030	101.9542	103.8890	105.8116	107.7409	109.6729

Reference probe temperature ($^{\circ}\text{C}$)	30.04	35.03	40.00	44.99	49.98	54.97
Sensor 1	111.6292	113.5580	115.4753	117.3964	119.3159	121.2335
Sensor 2	111.7417	113.6735	115.5946	117.5191	119.4434	121.3650
Sensor 3	111.6995	113.6324	115.5529	117.4780	119.4024	121.3235
Sensor 4	111.6594	113.5918	115.5117	117.4351	119.3566	121.2754
Sensor 5	111.7186	113.6520	115.5739	117.4991	119.4222	121.3425
Sensor 6	111.6537	113.5841	115.5039	117.4272	119.3491	121.2691
Sensor 7	111.6301	113.5553	115.4740	117.3944	119.3131	121.2300

Table 8.1.2: Calibration parameters from test calibration

	$R_0 A * 10$	$R_0 B * 10^5$	R_0 / Ω	$A * 10^3 / ^{\circ}\text{C}$	$B * 10^7 / ^{\circ}\text{C}^2$
Sensor 1	3.9033	-6.0677	99.9594	3.9048	-6.0702
Sensor 2	3.9118	-6.2023	100.0475	3.9099	-6.1993
Sensor 3	3.9113	-6.1193	100.0066	3.9110	-6.1189
Sensor 4	3.9101	-6.3332	99.9722	3.9112	-6.3350
Sensor 5	3.9122	-6.1514	100.0226	3.9114	-6.1500
Sensor 6	3.9005	-5.1085	99.9825	3.9012	-5.1094
Sensor 7	3.8825	-3.5596	99.9978	3.8826	-3.5596

Table 8.2.1: Second calibration sensor resistance values (Ω)

Reference probe temperature ($^{\circ}\text{C}$)	0.04	5.04	10.02	15.01	19.99	24.98
Sensor 1	100.0246	101.9759	103.9155	105.8558	107.7895	109.7268
Sensor 2	100.1129	102.0636	104.0021	105.9422	107.8753	109.8123
Sensor 3	100.0369	101.9866	103.9244	105.8639	107.7966	109.7333
Sensor 4	100.0728	102.0267	103.9688	105.9122	107.8487	109.7888
Sensor 6	100.0111	101.9581	103.8928	105.8292	107.7593	109.6945
Sensor 7	100.0218	101.9623	103.8897	105.8185	107.7421	109.6725

Reference probe temperature ($^{\circ}\text{C}$)	29.94	35.03	40.00	44.96	49.94	55.05
Sensor 1	111.6462	113.6130	115.5320	117.4428	119.3584	121.3220
Sensor 2	111.7314	113.6878	115.6163	117.5264	119.4417	121.4047
Sensor 3	111.6521	113.6185	115.5371	117.4475	119.3633	121.3252
Sensor 4	111.7111	113.6809	115.6027	117.5164	119.4351	121.4013
Sensor 6	111.6119	113.5775	115.4963	117.4064	119.3215	121.2849
Sensor 7	111.5855	113.5486	115.4656	117.3749	119.2889	121.2510

Table 8.2.2: Sensor parameters from second calibration

Sensor	$R_0 A * 10$	$R_0 B * 10^5$	R_0 / Ω	$A * 10^3 / ^{\circ}\text{C}$	$B * 10^7 / ^{\circ}\text{C}^2$
1	3.9048	-6.0494	100.0090	3.9045	-6.0489
2	3.9904	-6.0186	100.0971	3.9865	-6.0128
3	3.9022	-5.8232	100.0208	3.9014	-5.8220
4	3.9104	-6.0139	100.0570	3.9081	-6.0105
6	3.8947	-4.9630	99.9954	3.8949	-4.9632
7	3.8771	-3.2381	100.0071	3.8769	-3.2379

Appendix G

Pt-100 sensor tolerance testing

Table 9.1: Sensor temperature deviation for standard probe reading after test calibration

Reference probe temperature (°C)	0.05	4.94	9.93	15.00	20.00	24.95
Sensor 1	-0.01	-0.01	-0.02	-0.01	-0.01	0.01
Sensor 2	0.02	0.01	0.02	0.02	0.01	0.01
Sensor 3	0.02	0.01	0.01	0.00	-0.01	-0.02
Sensor 4	0.04	0.03	0.02	0.02	0.01	0.01
Sensor 5	0.00	0.00	-0.01	0.00	-0.01	0.01
Sensor 6	0.02	0.02	0.02	0.01	0.00	0.00
Sensor 7	0.03	0.04	0.02	0.00	0.00	0.00

Reference probe temperature (°C)	30.03	35.00	40.07	45.08	50.08	55.01
Sensor 1	0	0	0.01	0.01	0.03	0.04
Sensor 2	0.01	0.01	0.01	0.01	0.02	0.02
Sensor 3	-0.02	-0.03	-0.04	-0.05	-0.05	-0.06
Sensor 4	0.00	0.00	-0.01	-0.01	-0.01	-0.01
Sensor 5	0.01	0.01	0.01	0.02	0.03	0.04
Sensor 6	0.00	0.00	-0.01	-0.01	-0.01	-0.02
Sensor 7	0.00	0.00	0.00	0.00	0.00	0.00

Table 9.2: Sensor temperature deviation from standard probe reading after second calibration

Reference probe temperature (°C)	0.08	5.04	9.93	15.00	19.99	24.98
Sensor 1	0.00	0.01	0.00	0.00	0.00	0.00
Sensor 2	-0.22	0.12	0.09	0.05	0.02	0.01
Sensor 3	-0.01	0.00	0.00	0.00	0.00	0.00
Sensor 4	0.00	0.01	0.01	0.01	0.01	0.01
Sensor 6	0.00	0.00	0.00	0.00	0.00	0.00
Sensor 7	0.02	0.00	0.00	-0.01	-0.01	0.00

Reference probe temperature (°C)	29.95	35.02	40.00	45.00	49.98	55.01
Sensor 1	0.00	0.00	0.00	-0.01	-0.01	-0.01
Sensor 2	0.00	0.00	0.00	-0.01	-0.01	-0.02
Sensor 3	0.00	0.00	0.00	0.00	0.00	0.00
Sensor 4	0.01	0.01	0.00	0.00	0.00	0.01
Sensor 6	0.00	0.01	0.01	0.00	0.00	0.00
Sensor 7	0.01	0.02	0.02	0.02	0.02	0.01

Appendix H

Pressure transmitter calibration

Table 10.1: Pressure transmitter output current (mA)

Calibrator pressure (kPa)	20	40	60	80	100	150	200
Pressure transmitter 1	4.1998	4.3967	4.5916	4.7931	4.9952	5.4929	5.9933
Pressure transmitter 2	4.3512	4.6679	4.9807	5.3028	5.6265	6.4222	7.2236

Calibrator pressure (kPa)	250	300	350	400	450	500
Pressure transmitter 1	6.4926	6.9913	7.4937	7.9932	8.4914	8.9905
Pressure transmitter 2	8.0248	8.8243	9.6288	10.4288	11.2298	12.0290

Table 10.2: Table Calibration parameters for pressure transmitters

	Gain (g)	Offset (k)
Pressure transmitter 1	100097.8942	-399.9579
Pressure transmitter 2	62469.0466	-251.4021

Appendix I

Pressure transmitter tolerance testing

Table 11.0: Pressure transmitter deviations (kPa) from the calibrator readings

Calibrator pressure (kPa)	20	40	60	80	100	150	200
Pressure transmitter 1	-0.28	-0.47	-0.61	-0.73	-0.54	-0.48	-0.26
Pressure transmitter 2	2.01	2.07	2.29	2.49	2.92	3.66	4.54

Calibrator pressure (kPa)	250	300	350	400	450	500
Pressure transmitter 1	0.33	0.34	0.45	0.49	0.72	0.84
Pressure transmitter 2	5.17	5.99	6.65	7.29	7.71	8.45

